

คาร์บอนไฟเบอร์เซนเซอร์ชนิดใหม่ เพื่อการวิเคราะห์ทางเคมีไฟฟ้าสำหรับสาร
ปริมาณน้อยและการใช้เป็นขั้วสำหรับสแกนนิ่งโพรบไมโครสโกปี และการ
วิเคราะห์โวลทามเมตรีในระบบปริมาณระดับไมโครลิตรอย่างง่าย



วิทยานิพนธ์นี้เป็นส่วนหนึ่งของการศึกษาตามหลักสูตรปริญญาวิทยาศาสตรดุษฎีบัณฑิต
สาขาวิชาเคมี
มหาวิทยาลัยเทคโนโลยีสุรนารี
ปีการศึกษา 2556

**CARBON FIBER-BASED SENSORS FOR TRACE
ELECTROANALYSIS AND SCANNING PROBE
MICROSCOPY, AND A NOVEL SYSTEM FOR SIMPLE
SMALL-VOLUME VOLTAMMETRY**

Jiyapa Sripirom

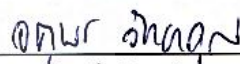


**A Thesis Submitted in Partial Fulfillment of the Requirements for the
Degree of Doctor of Philosophy in Chemistry
Suranaree University of Technology
Academic Year 2013**

**CARBON FIBER-BASED SENSORS FOR TRACE
ELECTROANALYSIS AND SCANNING PROBE MICROSCOPY,
AND A NOVEL SYSTEM FOR SIMPLE SMALL-VOLUME
VOLTAMMETRY**

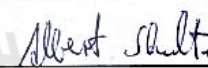
Suranaree University of Technology has approved this thesis submitted in
partial fulfillment of the requirements for the Degree of Doctor of Philosophy

Thesis Examining Committee



(Assoc. Prof. Dr. Jatuporn Wittayakun)

Chairperson



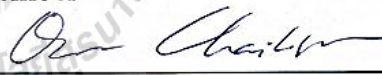
(Assoc. Prof. Dr. Albert Schulte)

Member (Thesis Advisor)



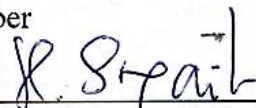
(Assoc. Prof. Dr. Malee Tangsathitkulchai)

Member



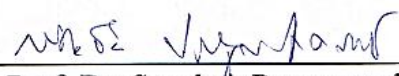
(Prof. Dr. Orawan Chailapakul)

Member



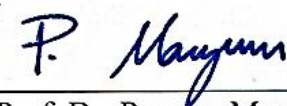
(Prof. Dr. Kritsana Sagarik)

Member



(Asst. Prof. Dr. Sanchai Prayoonpokarach)

Member



(Assoc. Prof. Dr. Prapun Manyum)



(Prof. Dr. Sukit Limpijumnong)

Vice Rector for Academic Affairs
and Innovation

Dean of Institute of Science

จิตยาภา ศรีภิรมย์ : คาร์บอนไฟเบอร์เซนเซอร์ชนิดใหม่ เพื่อการวิเคราะห์ทางเคมีไฟฟ้าสำหรับสารปริมาณน้อยและการใช้เป็นขั้วสำหรับสแกนนิ่งโพรบไมโครสโกปี และการวิเคราะห์โวลแทมเมตรีในระบบปริมาณระดับไมโครลิตรอย่างง่าย (CARBON FIBER-BASED SENSORS FOR TRACE ELECTROANALYSIS AND SCANNING PROBE MICROSCOPY, AND A NOVEL SYSTEM FOR SIMPLE SMALL-VOLUME VOLTAMMETRY) อาจารย์ที่ปรึกษา : รองศาสตราจารย์ ดร.อัลแบรต ชูลเทอร์, 167 หน้า

การย่อขนาดเครื่องมือตรวจวัดทางเคมีไฟฟ้าให้เล็กลงได้รับการพัฒนาอย่างต่อเนื่องในปัจจุบัน เพื่อการตรวจวิเคราะห์ทางเคมีไฟฟ้าสมัยใหม่ และวิทยาการการตรวจพื้นผิวด้วยเครื่องสแกนนิ่งโพรบไมโครสโกปีในระบบเคมีไฟฟ้า ซึ่งในวิทยานิพนธ์นี้ได้อธิบายถึง (i) การสร้างกระบวนการอย่างง่ายสำหรับการเตรียมคาร์บอนไฟเบอร์อัลตราไมโครอิเล็กทรอนิกส์ที่เคลือบด้วยคาร์บอนไฟเบอร์ส่วนที่เผยออกมามีลักษณะรูปร่างกรวย และ (ii) การพัฒนาของเซลล์ไฟฟ้าเคมีสามอิเล็กโทรดปริมาณน้อยใหม่ โดยใช้งานกับการวิเคราะห์โวลแทมเมตรีเพื่อหาสารจำนวนเล็กน้อยปริมาณ 15 ไมโครลิตร

(i) คาร์บอนไฟเบอร์อิเล็กทรอนิกส์ที่เคลือบด้วยคาร์บอนไฟเบอร์ได้รับการพัฒนาด้วยวิธีการกัดกร่อนด้วยไฟฟ้า กระแสตรงอย่างง่ายในสารละลายโซเดียมไฮดรอกไซด์เป็นขั้นตอนแรก เพื่อให้ปลายด้านหนึ่งของคาร์บอนไฟเบอร์แคบลงจนเกิดเป็นปลายเข็มแหลม จากนั้นคาร์บอนไฟเบอร์ปลายเข็มถูกเคลือบบางส่วน ยกเว้นส่วนปลายเข็มไว้ ด้วยวิธีการหุ้มด้วยกระแสไฟฟ้า (อีดีพี) การหุ้มด้วยกระแสไฟฟ้างดกล่าว เป็นการจำกัดขนาดของพื้นที่การนำไฟฟ้าและการเกิดปฏิกิริยารีดอกซ์ที่คาร์บอนไฟเบอร์ส่วนปลายเข็ม ผลที่ได้จากการตรวจสอบด้วยโวลแทมเมตรีของคาร์บอนไฟเบอร์รูปร่างกรวยอัลตราไมโครอิเล็กทรอนิกส์แสดงลักษณะของโวลแทมโกรมของสารละลายเฮกซะเอมีนรูทีเนียมคลอไรด์แบบซิกมอยด์ ซึ่งพิสูจน์ถึงคุณภาพของการหุ้มคาร์บอนไฟเบอร์อิเล็กทรอนิกส์ สำหรับการประยุกต์ใช้อิเล็กโทรดปลายเข็มเพื่อเป็นโพรบในเครื่องสแกนนิ่งเทิลเนลลิงไมโครสโกปี คาร์บอนไฟเบอร์ที่จุดปลายสุดเปลือย ถูกใช้จำลองภาพพื้นผิวซิลิคอน (111) ความละเอียดระดับอะตอมในสภาวะสูญญากาศ ส่วนคาร์บอนไฟเบอร์อัลตราไมโครอิเล็กทรอนิกส์ที่เคลือบด้วยคาร์บอนไฟเบอร์ส่วนปลายเข็มที่มีความสามารถวิเคราะห์เหมือนโพรบของสแกนนิ่งเทิลเนลลิงไมโครสโกปีในระบบเคมีไฟฟ้า เพื่อวิเคราะห์โครงสร้างอะตอมพื้นผิวทอง (111) นอกจากนี้ยังสามารถจำลองภาพชั้นโมเลกุลเดี่ยวของสารอินทรีย์บนพื้นผิวทอง (111) ความละเอียดระดับโมเลกุลในสภาวะแวดล้อมอิเล็กโทรไลต์ได้ การจำลองภาพของสแกนนิ่งเทิลเนลลิงไมโครสโกปีความละเอียดระดับ

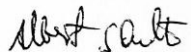
อะตอมด้วยคาร์บอนโพรบเป็นความสำเร็จใหม่ ซึ่งเปิดโอกาสสำหรับการทดลองทางวิทยาการพื้นผิวในระบบเคมีไฟฟ้าที่โพรบชนิดโลหะมีตระกูลไม่สามารถดำเนินการได้

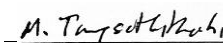
(ii) เซลล์เคมีไฟฟ้าปริมาณน้อยใหม่ได้ถูกออกแบบมาให้ใช้งานง่ายและรวดเร็ว อีกทั้งยังสามารถใช้ได้กับอิเล็กโทรดขั้วขนาดทั้งวัสดุคาร์บอนและโลหะมีตระกูลสำหรับการวิเคราะห์โวลแทมเมตรี เช่น ในวิธีการตรวจวิเคราะห์แบบเดิมสารละลายมาตรฐาน ระดับความสามารถของการวิเคราะห์เคมีไฟฟ้าปริมาตร 15 ไมโครลิตรใหม่นี้ ถูกประเมินผลผ่านการทดสอบวิเคราะห์ด้วยขั้วระงับอาการปวดพาราเซตามอล ซึ่งถูกทดสอบกับตัวอย่างจำลองพบว่ามีความเบี่ยงเบนมาตรฐานน้อยกว่า 5% หลังจากนั้นจึงประยุกต์กับการตรวจหาปริมาณพาราเซตามอลในซีรัมของมนุษย์ ซึ่งแสดงผลของช่วงที่ไม่มีอยู่ ช่วงปรากฏในซีรัม และช่วงหมดไปของยาในตัวอย่างซีรัมจากอาสาสมัคร ผู้ซึ่งรับประทานยา 1,000 มิลลิกรัม การตรวจวัดหาปริมาณในซีรัมตัวอย่างหลังจากรับประทานไปหนึ่งชั่วโมง และสี่ชั่วโมง และเลือดที่ไม่มีพาราเซตามอล ซึ่งผลออกมาสอดคล้องกับข้อมูลที่ได้รับการตีพิมพ์แล้ว โดยสรุปเซลล์เคมีขั้วขนาดไฟฟ้าสามารถใช้งานง่าย รวดเร็ว และสามารถวิเคราะห์เชิงปริมาณ โดยให้ผลที่ถูกต้อง และแม่นยำ

สาขาวิชาเคมี

ปีการศึกษา 2556

ลายมือชื่อนักศึกษา _____ 

ลายมือชื่ออาจารย์ที่ปรึกษา _____ 

ลายมือชื่ออาจารย์ที่ปรึกษาร่วม _____ 

JIYAPA SRIPROM : CARBON FIBER-BASED SENSORS FOR TRACE
ELECTROANALYSIS AND SCANNING PROBE MICROSCOPY, AND A
NOVEL SYSTEM FOR SIMPLE SMALL-VOLUME VOLTAMMETRY.

THESIS ADVISOR : ASSOC. PROF. ALBERT SCHULTE, Ph.D. 167 PP.

CARBON FIBER/ELECTROCHEMICAL ETCHING/ SCANNING TUNNELING
MICROSCOPY/SMALL-VOLUME CELL/VOLTAMMETRY

Miniaturized electrochemical tools are nowadays routinely used for modern electroanalysis and surface science with electrochemical probe microscopes. The contributions of this dissertation to these subjects were (i) the establishment of a novel procedure for the preparation of needle-type carbon ultramicroelectrodes (UMEs) with conical geometry of the exposed conductive carbon surface and (ii) the development of a novel small-volume three-electrode electrochemical cell that works with the full spectra of powerful voltammetric trace analysis available for normal sized cell configurations, in only 15 μL of measuring buffer.

(i) The desired needle-type carbon UMEs were prepared by a simple DC etching procedure in NaOH solution to provide, in a first step, narrowed single carbon fibers (CF) with very well-formed nanocones at their bottom. Coating the stems but not the ends of the tips of the carbon cones effectively with electrodeposition paint (EDP) layers limited the bare carbon to the foremost end and restricted the faradaic current response due to interfacial redox activity to exactly this area. The resulting conical carbon UMEs adequately displayed well-shaped sigmoidal voltammograms of dissolved $\text{Ru}(\text{NH}_3)_6\text{Cl}_3$, which proved the quality of the tapered carbon tips in terms of redox activity as well as insulation stability. At duty as STM probes, bare CF-tips imaged a Si (111) surface with atomic resolution in UHV. With a tip-sparing

insulation in place, tapered UMEs were gained that had the capacity to resolve as electrochemical scanning tunneling microscopy (EC-STM) tips the atomic fine structure of a Au(111) surface reconstruction. Also, individual molecules of an organic monolayer on Au(111) could be imaged with molecular resolution in an electrolyte environment. Atomic resolution STM imaging with carbon-based scanning probes is a world-wide novel achievement that opens up opportunities for exciting electrochemical surface science experiments that cannot be carried out with common noble metal EC-STM tips.

(ii) The novel small-volume electrochemical cell was designed to be simple and rapid in use, and meant to be compatible with miniaturized carbon and noble metal working electrodes for common voltammetry, e.g. in the standard addition mode. The performance level of 15 μL electroanalysis in the novel cell was evaluated through analytical trials with the common analgesic paracetamol (ACMP). Adjusted ACMP levels in model samples were well recovered with the deviations from true values being less than $\pm 5\%$. Applied to human serum ACMP detection, the strategy revealed nicely the absence, appearance and clearance of the drug in samples coming from a volunteer who did not or did ingest a 1000 mg dose of the medicine. Quantitative measurements on a serum sample taken 1 hour past tablet uptake revealed a free blood ACMP level that was in good accordance with published data. In conclusion a miniaturized electrochemical cell has been accomplished that can accurately handle 15 μL sample volumes for voltammetric quantification.

School of Chemistry

Academic Year 2013

Student's Signature _____ 

Advisor's Signature _____ 

Co-advisor's Signature _____ 

ACKNOWLEDGMENTS

My time here at the Suranaree University of Technology had a great influence on me as a person and a scholar. I have learned a lot about myself in addition to the scientific skills that I have acquired. As my graduate studies come to an end, I wish to give thanks to those who took part in this stage of my life.

To my advisor, Assoc. Prof. Dr. Albert Schulte, I am grateful for the support that he has supplied throughout my graduate career. Dr. Albert was always there to provide guidance and support. His counsel was always insightful and often presented a way to approach a problem that I had not previously considered. I could tell that he always wanted to see me succeed.

I am thankful to the Office of the Higher Education Commission, Thailand for financial support through a Ph.D. scholarship for 4 years. And also I sincerely thank Udon Thani Rajabhat University for giving me the time to improve my knowledge and technical skills for my career.

Special thanks go to my committee members. I appreciate the time and effort they spent to evaluate my thesis. I am grateful for the advice and support that I have received from them.

Thanks also to collaborators at Ruhr Universität Bochum, Prof. Dr. Wolfgang Schuhmann and his Analytische Chemie - Elektroanalytik & Sensorik members. I appreciate the provision of a good opportunity and experience to work in an international environment and I have gotten valuable suggestions and guidance to reach to my research aim. And I would like to thank Prof. Dr. Ulrich Köhler, his

student Sani Noor and other members of the Surface Science group for helping me to achieve atomic-resolution imaging with carbon fiber tips from UHV-STM and thus my first publication. And of course I am grateful Prof. Dr. Olaf Magnussen, Sonja Kuhn, Ulrich Jung, and all members in Interface Physics Group, Institute of Experimental and Applied Physics, Christian-Albrechts-Universität zu Kiel for their joint effort on carbon fiber based EC-STM and my second work.

I would be truly ungrateful if I did not acknowledge my all group members in Biochemical-Electrochemistry Research Unit, especially, the group leaders, Assoc. Prof. Dr. Wipa Suginta, Dr. Panida Khunkaewla, and Dr. Chutima Talabnin. They were the forces behind a functional facility and always there for guidance of my work, if necessary. Moreover, I would like to thank Pooi, Pook, and Mam for their help during my learning and doing experiment. And special thanks go to “The Gang”. I have gained a lot effort, warmth and merriness at same time. And also I would like to thank the rest of the group members that have been wonderful companions. In addition, I appreciate encouragement of all fellow in SUT-Science Park.

Finally, I would like to honestly thank my parents for their endless love and encouragement for my educational pursuits and goals. My sister Pla, brother-in-law Tum and Bond were there with me through the ups and downs, and stressful burdens that accompany graduate school and they took good care of me. My family love and kindness gave me strength to persevere. I could not have completed my education without the support and encouragement of all of those who stood with me, thank you.

Jiyapa Sripirom

CONTENTS

	Page
ABSTRACT IN THAI.....	I
ABSTRACT IN ENGLISH.....	III
ACKNOWLEDGEMENTS.....	V
CONTENTS.....	VII
LIST OF TABLES.....	XI
LIST OF FIGURES.....	XII
LIST OF ABBRIVIATION.....	XVII
CHAPTER	
I INTRODUCTION.....	1
1.1 Rationale of the study.....	1
1.2 Research objectives.....	3
II LITERATURE REVIEW.....	5
2.1 Ultramicroelectrodes (UMEs).....	5
2.1.1 General remarks and benefits of UMEs.....	6
2.1.2 UME applications and designs.....	10
2.2 UME function as probe tip for electrochemically assisted STM.....	17
2.2.1 Scanning probe microscopy, SPM.....	17
2.2.2 The development of STM.....	19

CONTENTS (Continued)

	Page
2.2.3 Electrochemical scanning tunneling microscopy (EC-STM).....	29
2.2.4 Carbon-based material STM probe tip and ultramicroelectrodes.....	32
2.3 Small-volume voltammetry.....	43
2.4 References.....	49
III CONICAL CARBON FIBER ULTRAMICRO ELECTRODES AS IMAGING TOOL FOR SCANNING TUNNELING MICROSCOPY AND SENSORS FOR VOLTAMMETRY	69
Abstract.....	69
3.1 Introduction.....	71
3.2 Experimental and methods.....	72
3.2.1 Conical CF UMEs: Fabrication and characterization.....	72
3.2.2 Tapered CFs as probe tip for atomic resolution STM in the UHV and electrolyte environments.....	79
3.3 Results and discussion.....	82
3.3.1 The formation of tapered carbon fiber tips with nanometric tip radii.....	82
3.3.2 Scanning tunneling microscopic imaging with etched carbon fiber tips.....	89
3.3.3 Etched carbon fiber tip insulation – Fabrication of conical carbon UMEs/EC-STM tips.....	95

CONTENTS (Continued)

	Page
3.3.4 The insulation of the etched carbon fiber/metal wire junction with a silicone elastomer	102
3.3.5 Proof of the beneficial potential window of CF-UME for the target application “EC-STM”	108
3.3.6 STM imaging with carbon fiber EC-STM tip	112
3.4 Conclusion	116
3.5 References	116
IV A NOVEL SYSTEM FOR SIMPLE SMALL-VOLUME VOLTAMMETRY	120
Abstract	120
4.1 Introduction	122
4.2 Experimental and methods	125
4.2.1 Working electrode preparation procedures	125
4.2.2 Voltammetric measurements	127
4.3 Results and discussion	130
4.3.1 The 15- μ L-three-electrode cell design	130
4.3.2 15- μ L volume electroanalysis of acetaminophen (ACMP)	135
4.3.3 15- μ L volume electroanalysis of ACMP in drug tablets	139
4.3.4 15- μ L volume electroanalysis of ACMP in spiked human blood serum (HBS)	140
4.3.5 Detection of ACMP in human blood serum (HBS) sampled before and after oral medication	142

CONTENTS (Continued)

	Page
4.4 Conclusion.....	146
4.5 References.....	146
V CONCLUSION AND RECOMMENDATION.....	151
5.1 Conical Carbon Fiber Ultramicroelectrodes as Imaging Tool for Scanning Tunneling Microscopy and Sensors for Voltammetry.....	151
5.1.1 Electrochemical tip etching.....	151
5.1.2 Carbon fiber tip insulation.....	151
5.1.3 Application of tapered carbon fiber as novel scanned probe tips for STM.....	152
5.2 A novel system for simple small-volume voltammetry.....	152
5.2.1 15- μ L-volume-electroanalysis of acetaminophen (ACMP).....	153
APPENDICES.....	154
APPENDIX A ELECTROCHEMICAL METHODS.....	155
APPENDIX B ELECTROACTIVE AREA OF CONICAL ULTRAMICROELECTRODE.....	160
APPENDIX C REFERENCE ELECTRODE FABRICATION.....	162
APPENDIX D QUANTITATIVE DETERMINATION OF ACETAMINOPHEN.....	164
CURRICULUM VITAE.....	167

LIST OF TABLE

Table	Page
2.1 Comparison of properties between carbon fiber and steel.....	36



LIST OF FIGURES

Figure	Page
2.1 Electrochemical microsystem technologies in materials, engineering, and life science.....	6
2.2 Flow chart demonstrating the properties of UMEs that are gained because of their very small electrode surface areas.....	8
2.3 The diffusion profiles at a macroelectrode and an UME.....	9
2.4 Graphical representation of the most common UME geometries.....	11
2.5 The example of three-dimensional STM image of graphite surface.....	19
2.6 A schematic of a typical Scanning Tunneling Microscope.....	21
2.7 Schematic of STM tips in close distance to a surface.....	23
2.8 Schematic diagram of imaging process with a single atom acting as a tip.....	26
2.9 Schematic the electrochemical etching of metal wire and the etching process at air/electrolyte interface.....	27
2.10 Comparison of SEM image of electrochemically etched tungsten tip and a cutted platinum tip.....	28
2.11 Schematic diagram of an EC-STM setup.....	30
2.12 The SEM images of the microstructure of PAN- and pitch-based fibers.....	37
2.13 The preparation of carbon nanoelectrodes with effective radii of only a few nanometers and its voltammograms.....	37
2.14 Electrical spark etched carbon fiber based UME.....	38

LIST OF FIGURES (Continued)

Figure	Page
2.15	Preparation of the carbon microelectrode for voltammetry inside of living cells.....39
2.16	Scanning electron micrographs (SEM) of a flamed-etched carbon coated with an insulating layer of poly(oxyphenylene)..... 39
2.17	A SEM image of an electro-painted 10- μ m-diameter carbon fiber, insulated by anodic EDP at 20 V for 4 min, and cut with the scalpel.....40
2.18	A partially insulated carbon-nanotube ultramicroelectrode.....42
2.19	Experimental arrangement for manipulating microelectrodes in nanoscopic domains 44
2.20	Example of a microcell for voltammetric measurements46
2.21	Cross-section of a microcavity and the procedure for anodic stripping voltammetry in small volumes of silver drop47
2.22	Schematic drawing of the carbon screen printed electrode.....48
3.1	Illustration of a single carbon fiber / tungsten wire assembly as used as precursor for conical CF UME fabrication73
3.2	Setup used for the electrochemical etching of carbon fibers with the aim of tip formation.....74
3.3	Photograph of the rolled up Pt foil with a “o” shaped cross section that was used as counter electrode and trough for the EDP paint application to CFs.....75
3.4	The two SEM instruments used for CF tip characterization.....77

LIST OF FIGURES (Continued)

Figure	Page
3.5	Scheme of voltammetric CF tip characterization in 1 mM Ru(NH ₃) ₆ Cl ₃ in 0.1 M KCl.....78
3.6	The (7 x 7) structure of the (111) surface of silicon.....80
3.7	Chemical structure of self-assembled monolayer of the octyl-TATA molecule on the Au(111) substrate.....81
3.8	A scanning electron micrograph of a 7 μm diameter electrochemically etched carbon fiber electron emitter.....82
3.9	Scanning electron micrographs of electrochemically etched CFs and a schematic of the selection procedure of high quality.....83
3.10	High-speed flash photographs of an oscillating 520 μm-long and 5-μm- diameter CF.....85
3.11	Procedure for controlled carbon fiber etching and establishment of an etched CF/metal holding wire assembly.....86
3.12	Scanning electron micrographs of electrochemically etched CFs.....88
3.13	Scanning electron micrograph of electrochemically etched CFs (E/XAS).....89
3.14	Constant-current scanning tunneling microscopy images of a thinly gold-coated optical grating.....91
3.15	Test of a CF tip in a UHV scanning tunneling microscope for Si(111)-7x7 surface imaging.....93

LIST OF FIGURES (Continued)

Figure	Page
3.16	A representative published example of an atomically resolved STM image of a Si(111), 7×7-reconstructed surface obtained by a tungsten STM tip in UHV-STM.....94
3.17	Principle of the operation of STM tips in electrolytes.....95
3.18	Schematic of CF tip insulation by electrodeposition paint solution in a Ω-shaped Pt trough.....97
3.19	Scanning electron micrographs of carbon fiber microelectrode of various geometry. And cyclic voltammograms of then in 1 mM Ru(NH ₃) ₆ Cl ₃ in 0.1 M KCl.....98
3.20	Etched carbon fibers shielded with electrodeposition paint except at the top of the taper.....101
3.21	Application of an insulating silicone rubber coating to the carbon fiber/metal wire junction of EDP insulated CF UMEs.....104
3.22	Cyclic voltammograms (CVs) of a conical CF-based UME.....106
3.23	Insulation stability test for an EDP-insulated conical CF-UME.....107
3.24	Potential window assessment for a EDP insulated conical CF-UME.....109
3.25	Cyclic voltammograms recorded for a conical CF-based UME and a tungsten EC-STM in the electrochemical cell of an EC-STM setup.....111
3.26	In situ STM images of a clean Au(111) electrode surface in 0.1 M HClO ₄113

LIST OF FIGURES (Continued)

Figure	Page
3.27	In situ STM images of an octyl-TATA adlayer on Au(111) in 0.1 M HClO ₄115
4.1	Schematic illustration of a cylindrical carbon fiber UME.....126
4.2	The stereomicroscope/micromanipulation platform for voltammetry in 15 μ L samples.....130
4.3	Cyclic voltammograms of 1 mM Ru(NH ₃) ₆ Cl ₃ in 0.1 M KCl at carbon and noble metal UMEs.....133
4.4	Influence of solvent evaporation on the voltammetry of in a 15- μ L small-volume electrochemical cell.....135
4.5	ACMP cyclic voltammogram at a cylindrical CF UME.....136
4.6	Acetaminophen calibration measurement in the 15- μ L three electrode electrochemical cell.....137
4.7	Voltammetric quantification of ACMP in the 15- μ L three-electrode small-volume electrochemical cell by means of the standard addition method.....138
4.8	Voltammetric quantification of ACMP in a paracetamol tablet with a listed content of 500 mg active compound.....139
4.9	Small volume voltammetric quantification of ACMP in human blood serum (HBS).....141
4.10	Application of the small-volume voltammetry for studying the pharmacokinetics of ACMP in HBS before and after paracetamol ingestion.....143

LIST OF FIGURES (Continued)

Figure	Page
4.11	Determination of the ACMP quantity in HBS 1 h after ingestion of a paracetamol tablet.....145
A.1	The typical cyclic voltammogram for a reversible charge transfer reaction.....155
A.2	Potential wave forms and voltammogram shape for normal pulse, differential pulse and square wave voltammetry.....157
B.1	Cyclic voltammograms of 1mM Ru(NH ₃) ₆ Cl ₃ in 0.1 M KCl at needle-type CF-UMEs of different size.....160
C.1	Photographs of homemade Ag/AgCl reference electrode.....162
D.1	Small volume voltammetric quantification of ACMP in HBS before and after ingestion of a paracetamol tablet and measured in 15- μ L-three-electrode cell by means of the standard addition method.....165

LIST OF ABBREVIATIONS

ACMP	N-acetyl-p-aminophenol or Acetaminophen
AFM	Atomic force microscopy
Ag/AgCl	Silver/Silver chloride
ASV	Anodic stripping voltammetry
C	Capacitance
CE	Counter electrode or auxiliary electrode
CF	Carbon fiber
CNT	Carbon nanotube
CR	Carbon rod or pencil-lead
CV	Cyclic voltammetry
DC	Directing current
DI	Deionized
DOS	Density of states
DPV	Differential pulse voltammetry
EC	Electrochemistry
EC-STM	Electrochemical scanning tunneling microscopy
EDP	Electrodeposition paint
I_C	Capacitive current
I_{DC}	Directing current
I_F	Faradaic current
I_P	Peak current

LIST OF ABBREVIATIONS (Continued)

I_T	Tunneling current
LOD	Limit of detection
NAPQI	N-acetyl-p-benzoquinoneimine
NMR	Nuclear magnetic resonance
octyl-TATA	Octyl-triazatriangulenium
PAN	Polyacrylonitrile
PB	Phosphate buffer
R	Resistance
RE	Reference electrode
S/N	Signal-to-noise ratio
SAM	Self-assembled monolayer
SECM	Scanning electrochemical microscopy
SEM	Scanning electron microscope
SPM	Scanning probe microscopy
STM	Scanning tunneling microscopy
STS	Scanning tunneling spectroscopy
SWV	Square wave voltammetry
TEM	Transmission electron microscopy
UHV	Ultrahigh vacuum
UME	Ultramicroelectrode
$V_{\text{bias}}/U_{\text{bias}}$	Bias voltage
WE	Working electrode

CHAPTER I

INTRODUCTION

1.1 Rationale of the study

Systematic electrochemical science and analysis have their origin in the 19th century and the past more than 200 years saw a continuous trend towards more sophistication of the techniques in this field as well as an immense widening of the scopes of applications. As the entire field of science and engineering also modern electrochemical instrumentation took in more recent time great advantage of the many improvements in electronics and particularly beneficial was the boom in printed circuitry and computer hard- and software technology. As a valuable result modern electroanalysis is now able to work with compact and easy to handle computer-controlled electrochemical workstation that in best case reach femtoampere current and microsecond time resolution. The more powerful instrumentation led to advanced versions of the already existing traditional electrochemical detection schemes and gave them a well lowered detection limit and great sensitivity, selectivity and linear range. Targets of highly sensitive state-of-the-art electroanalysis, and amperometry and voltammetry in the main modes are a variety of important analytes and representative examples are environmental heavy metal and insecticide pollutants, pharmaceutical drugs, food ingredients and biomolecules that act in the human body as physiological messengers. And advanced electrochemical micro- and nanosensors found an intensive use as valuable probes for non-optical microscopes and

scanning electrochemical microscopy (SECM) and scanning tunneling microscopy (STM) are prominent examples in surface science.

In general electroanalysis is competitive in terms of precision, accuracy, and sensitivity when compared with other analytical methods. Moreover, electrochemical instrumentation is cheaper and less complex than, for instance, the apparatus for the different variants of spectroscopy which are the prominent alternatives for trace analysis. Based on the excellent cost-to-performance ratio electrochemical analysis has become a very active area of research and routes are found in battery and fuel cell development, prevention of the corrosion of metals, environmental pollutant assessment, water quality and industrial process control, pharmaceutical drug screening and chemical synthesis via electrolysis and electrophoresis). Among others, two important streams of recent and current research in the electroanalysis field are continuous efforts on further miniaturization of electrodes and/or electrochemical cells and the advancement of the performance level of needle-type electrochemical sensors in scanning probe microscope settings for a high-resolution inspection of the local properties of solid/electrolyte interfaces. Within this topical framework the dissertation here was designed to have two main parts which are (1) the development of a simple and reproducible procedure for the fabrication of conical carbon fiber UMEs with the special potential to be used as probe tips for electrochemical STM (EC-STM) and (2) the development of a novel miniaturized electrochemical cell that is able to work in easy but efficient fashion with sample volumes of not more than about 15 microliters for environmental pollutant and medical drug analysis. The full spectrum of advantages of ultramicroelectrodes (UMEs), the principles and possible applications of scanning probe microscopy electrolytic media, and the pros and cons

of small volume electrochemical cells will be presented in the section dealing with state of the art of the two subjects of this dissertation before the outcome of own laboratory work will be portrayed and discussed in terms of value for specific analytical purposes.

1.2 Research objectives

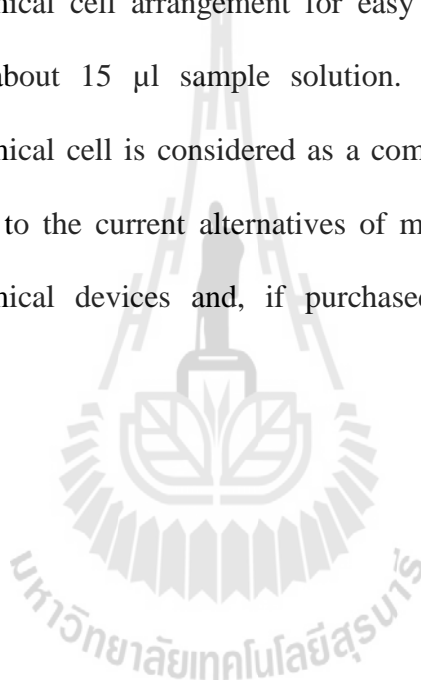
Though UME fabrication reached a good level of standard, there is still a lot of room to improve the procedures and explore novel electrode materials, at least for certain electrode geometries. Good examples are needle-type tapered carbon UMEs. As outlined in more detail in the following section of the literature review, existing procedures for the fabrication of these “conically-shaped” voltammetric sensors suffer from a poor reproducibility and/or an extreme difficulty in the steps of execution. For that reason, the fabrication of well-working conical carbon nano- and microelectrodes is limited to a few laboratories, and a routine application has not been reached yet. On the other hand, there is a high demand for this particular type of sensors as they offer unique opportunities for local EC-STM and SECM measurements, and for a voltammetry at small redox-active objects or in small volumes.

In the light of the above the objectives of this research study have been set as:

1. The establishment of a reproducible electrochemical etching procedure for high-modulus carbon fibers. Result of the etching should be well-shaped nanometric carbon cones at the endings of otherwise unaffected and at thus stable carbon fiber stems.
2. The development of easy-to-perform reproducible and effective procedures for the “regioselective” insulation of all but not the very tip of

etched carbon fiber nanocones to produce conical carbon micro- or nanoelectrodes. The novel type of carbon sensors will be evaluated for their performance as EC-STM probes and as voltammetric sensors for analysis of trace heavy metals and other environmental pollutants.

3. The establishment of a technically undemanding and cheap option for trace electroanalysis in μl -volume sample. The goal here is a specific electrochemical cell arrangement for easy measurements in volumes as small as about 15 μl sample solution. The target microliter-volume electrochemical cell is considered as a complementary cheap and easy to use option to the current alternatives of more complicated flow-through electrochemical devices and, if purchased, costly screen printed cell systems.



CHAPTER II

LITERATURE REVIEW

Significant importance in the miniaturization of the electrochemical instrument have been made over the few decades for electroanalysis and scanning probe microscopy (SPM); in addition, the hardware and software technologies were progressing to support this development. Efforts led to the appearance of ultramicroelectrodes (UMEs) and ultrasmall-volume electrochemical cells and both became routine tools for powerful voltammetry. In this work, the main focus was on the development of a reproducible method for fabricating needle-like conical carbon fiber (CF) UMEs. Also aimed at is the establishment of a technically undemanding and cheap option for trace electroanalysis in μl -volume sample. This chapter will thus review the state-of-the-art of UME preparation and their application as improved sensors for voltammetry and as scanned tips of electrochemical SPMs. Furthermore, the current status of an electroanalysis in ultrasmall electrochemical cells will be provided.

2.1 Ultramicroelectrodes (UMEs)

UMEs have played an important role in the movement of electroanalytical chemistry toward small-volume measurements as well as real time and spatially resolved electrochemical screening. The advantages of UMEs are exploited in many areas of electroanalysis. It is now possible to obtain electrochemical information at

length scales ranging from centimeters to micrometers and even nanometers. As illustrated in Figure 2.1, electrochemical microsystem technology, often also named microelectrochemistry, is rapidly developing field that forms interdisciplinary bridges between fundamental science and medicine, corrosion research, microelectronics and biology.

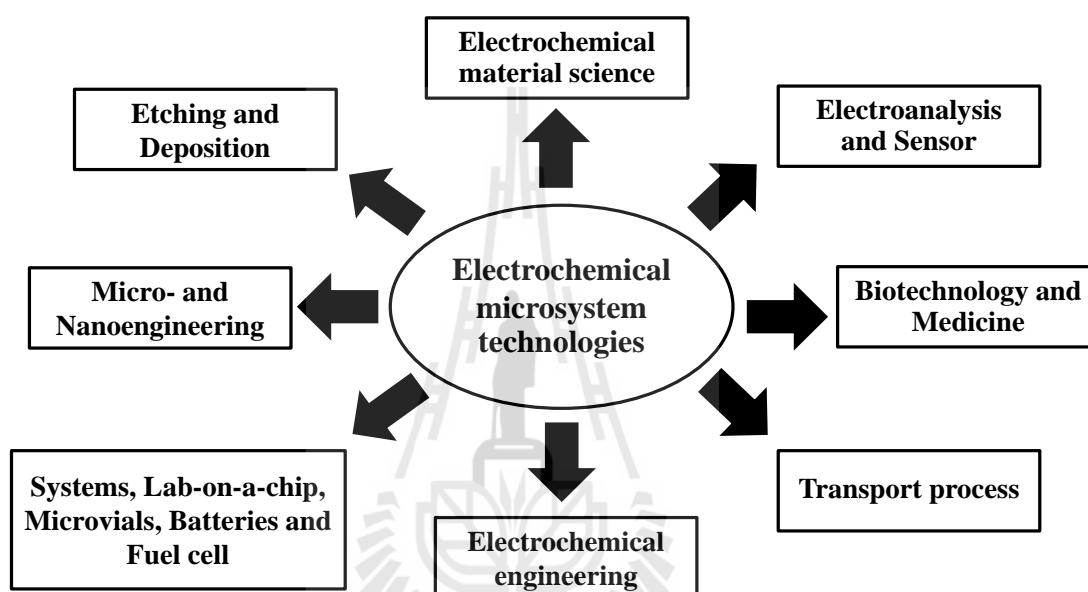


Figure 2.1 Electrochemical microsystem technologies in materials, engineering, and life science.

Electrochemical microsystem technologies with connections to and applications in electrochemical materials science, microengineering, electrochemical engineering, and biology and medicine (Zoski and Vanysek, 1996).

2.1.1 General remarks and benefits of UMEs

An UME is defined as an electrode that has at least one of its characteristic dimension (such as the radius of a disk, the radius of sphere, or the width of a band) in the order of a few nm to about 25 μm (Wightman and Wipf, 1989). UMEs offer remarkable advantages when employed in electrochemical studies

and applications. UMEs benefit from the fact that their critical dimension controls the electrochemical response.

The significant reduction of the electroactive area of a working electrode leads to a few impressive behavioral changes. If not only the electrode itself but also its physical support is kept small, the UME may be well suited for immersions as need-like sensor in small electrolyte containers or placements at small objects such as living cell. The small electroactive area is also associated with a change in the geometry of the different profile from planar to spherical diffusion and, due to enhanced mass transport to the small consumer of reduce species, with an improved faradaic response. At the same time the capacitance of UME is small since it is proportional to the effective area, which for a 10 μm disk microelectrode, for instance, is only 78.54 μm^2 as compared to 7068.58 μm^2 for a conventional 3 mm disk macroelectrode. Of course, the enhanced redox current (I_F) and decreased capacitive current (I_C) together will grant a superb signal to noise ratio (I_F/I_C) to miniaturized voltammetric electrodes. And finally, the iR drop is favorable for UME because of their tiny total currents, which are usually in the low nano- or even picoscopic range. A current of 1 nA in an electrolyte of 1 k Ω resistance will be reduced to an ohmic drop of 1 μV , which is insignificant when dealing with normal electroanalysis. Figure 2.2 is summarizing the above statements on UME properties and benefits in an illustrated flow chart presentation.

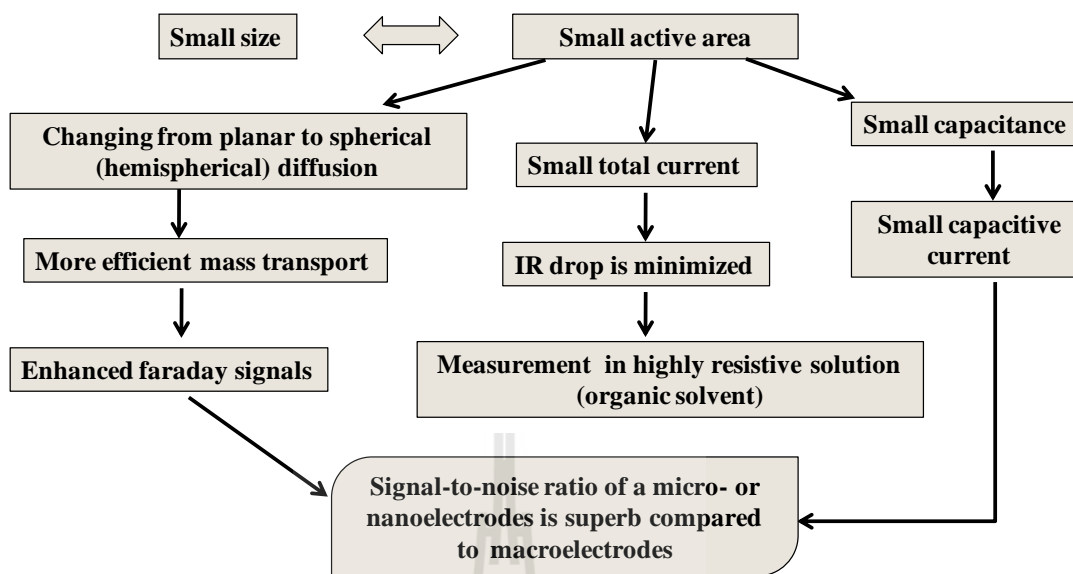


Figure 2.2 Flow chart demonstrating the properties of UMEs that are gained because of their very small electrode surface areas.

The already mentioned change in the geometry of the diffusion profile has an effect on the appearance of I vs. E curves (Voltammograms) of UMEs (Wightman and Wipf, 1989). Radial diffusion becomes dominant and result is a more efficient mass transport and delivery of redox species to the electrode. Accordingly, the voltammogram is not anymore peak shaped due to the influence of restricted supply of redox compound but sigmoidal with a diffusion-limited steady-state current at voltages significantly exceeding the formal potential of the redox couples. Figure 2.3 is a display of the situation and shows the different voltammograms for macro- and ultramicroelectrodes (Bard and Faulkner, 2001; Mirkin, Fan and Bard, 1992; Penner, Heben and Lewis, 1989; Zoski and Mirkin, 2002).

An area in which UMEs are of great importance is the study of redox systems in highly resistive solvents. Electrochemical currents at UMEs are much

smaller than those seen at electrodes of conventional size. The iR drop distortion is thus reduced due to the small total currents that are measured at an UME (working electrode). This advanced feature allows that electrochemistry without correction for iR effects is applied even in solutions with very high resistance (Morris, Franta and White, 1987; Norton, White and Feldberg, 1990).

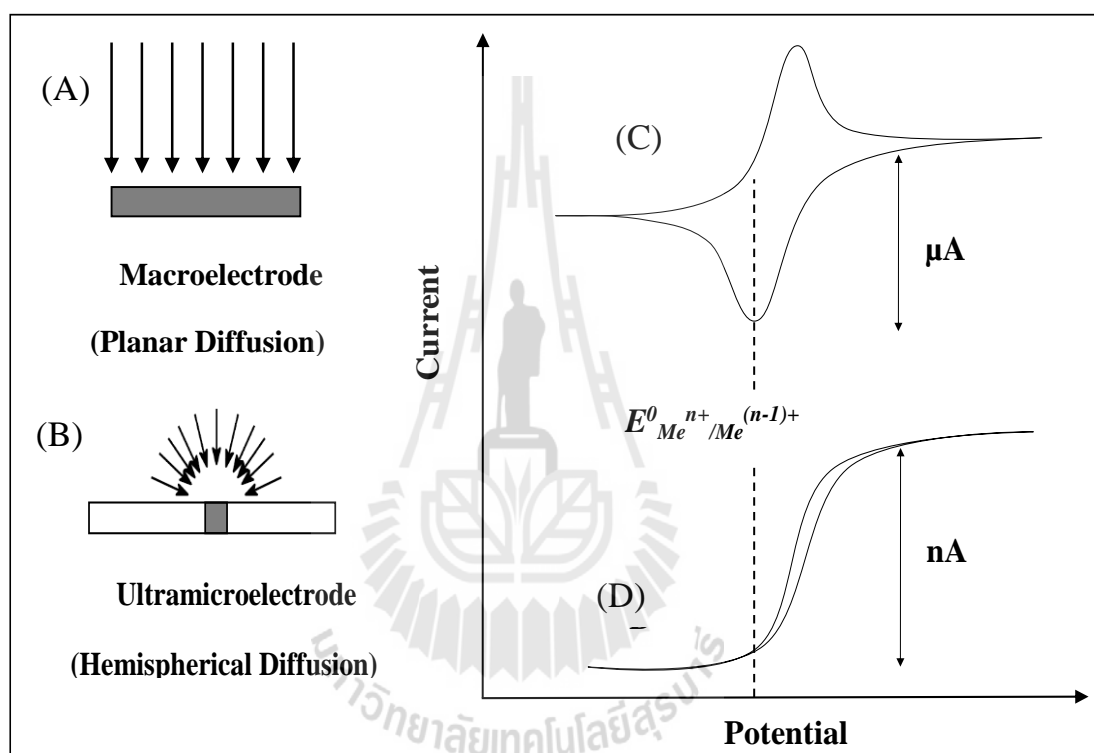


Figure 2.3 The diffusion profiles at a macroelectrode and an UME.

The left panel shows the diffusion profiles at macroelectrode and ultramicroelectrode.

(A) a macroelectrode and (B) an UME (e.g. a disk-shaped UME); the right panel shows an illustration of the CVs of a redox species ($\text{Me}^{(n)+} + \bar{e} \leftrightarrow \text{Me}^{(n-1)+}$) at either (C) a macroelectrode or (D) a microelectrode.

Moreover, the reduction in the area of the capacitive double layer at the tiny electrodes must be considered. The double-layer charging current is decreasing exponentially with a decrease of the area. Thus, the charging current density is

favorably reduced at an UME. Due to this property, very rapid time-dependent measurements of chemical concentration changes of redox-active species can be monitored and nanosecond time resolution has been demonstrated feasible (Wipf, Kristensen, Deakin and Wightman, 1988).

If the overall size of an UME is small, measurements at the tiny objects or restricted microscopic areas become possible. Required then are needle-type UMEs and an UME positioning with precise micro- or nanomanipulators.

2.1.2 UME designs and applications

Since the UME introduction to electroanalytical chemistry about 30 years ago, they enabled immense advances in electrochemistry. Initially developed by physiologists (Loeb, Peck and Martyniuk, 1995) UME access to electroanalytical chemistry occurred through pioneer's work of several laboratories. Since that time, these tools have extended electrochemical methodology into broad new domains of space (e.g. single cells), time (fast sweep), chemical medium (nanoaqueous solvents, unsupported electrolyte, ice, air), and methodology (kinetics, single molecule studies). Overviews of UME developments are provided in many reviews that have been dedicated to the theory and practice of UME and their use (Amatore, 1995; Clark, Zerby and Ewing, 1998; Denault, Nagy and Toth, 2001; Fleischmann, 1987; Forster, 1994; Heinze, 1993; Kawagoe, Zimmerman and Wightman, 1993; Koudelka-Hep and Wal, 2000; Michael and Wightman, 1996; Pletcher, 1991; Pons and Fleischmann, 1987; Slevin, Ryley, Walton and Unwin, 1998; Smith, Haydon, Hengstenberg and Jung, 2001; Stulik et al., 2000; Wightman, 1981; Wightman and Wipf, 1989; Zoski and Vanysek, 1996). The most popular UME geometries are those which reach a

voltammetric steady-state fast. Typical micro- and nanoelectrode geometries include inlaid disks, inlaid rings, inlaid ring- disks, hemispherical and spherical electrodes, and finally conical shapes (see Figure 2.4). Cylindrical and microband (line) electrodes exist (Amatore, 1995; Fleischmann, 1987) and they enjoyed some popularity in the 1980's because they provided relatively large currents as the electrode are small in one but long in the other dimension, which is different as compared to the disk electrode geometry, for example. At the time as microelectrodes appeared, they were also easier to fabricate than, for instant, an inlaid disk electrode. Currently, however, cylindrical and band-like microelectrodes are much less popular than the other UME geometries because they do not reach as fast real steady state and they are not as useful in eliminating iR drops as for instance disk-shaped micro- and nanoelectrodes.

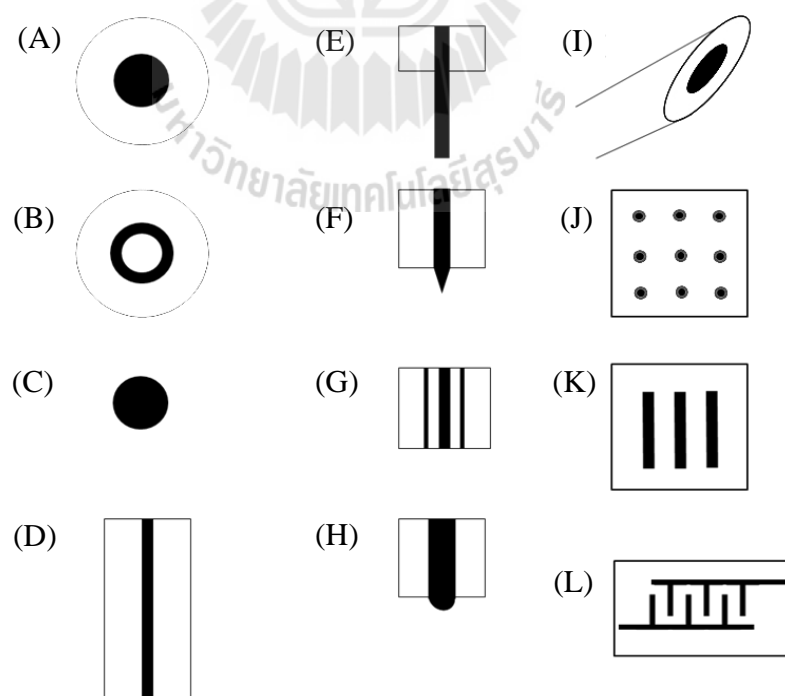


Figure 2.4 Graphical representation of the most common UME geometries.

(A) disk, (B) ring, (C) sphere, (D) band, (E) cylinder, (F) finite cone, (G) ring-disk, (H) hemisphere, (I) beveled ellipse, (J) disk array, (K) band array, and (L) interdigitated array.

Materials used for micro- and nanoelectrode fabrications include small-diameter metal (e.g. Au, Pt, Pt/Ir etc.) wires and carbon filaments (e.g. CFs, CNTs, etc.). These structures have to be embedded appropriately in an insulating shield in order to establish the desired UME geometry. Glass- or polymer embedments have been demonstrated equally successful for the insulation purpose; the choice depends actually on the experimental application. Glass, for instance, is needed when the UME's are to be operated in an organic electrolyte that would dissolve a polymeric insulation layer. The properties and applications of UMEs have been the subject of a number of comprehensive review articles (Collinson and Wightman, 1995; Barker, Gonsalves, Macpherson, Slevin, and Unwin, 1999; Basha and Rajendran, 2006; Bond, 1994; Clark and Ewing, 1998; Cox and Zhang, 2012; Feeney and Kounaves, 2000; Fleischmann, 1987; Forster, 1994; Gewirth, Craston and Bard, 1989; Kashyap and Gratzl, 1998; Liu, He, Zhang, and Chen, 2010; Pletcher, 1991; Stulik, Amatoe, Holab, Marecek, and Kunter, 2000; Zoski and Vanysek, 1996; Zoski, 2002). The work with microelectrodes in this thesis is focusing on the realization of a new procedure for establishing the conical carbon electrode geometry. The prime target application for the novel type of sensor is use as functional probe tip for electrochemical scanning tunneling microscopy. However, the potential for other application is also seen.

As already mentioned, the key property of individual UMEs is a characteristic dimension in the micrometer to nanometer range. Motivations for the

trend towards sensor miniaturization were interests in small-volume and small object inspection as well as the aim to improved time and space resolution of electrode measurements. UME studies therefore exploded in number during the last two decades. Microelectrodes are now applied in many different areas of electroanalysis, with environmental, biomedical and surface application probably being the most active fields. As illustrated in Figure 2.1, micro- and nanoelectrochemistry is still a continuously developing field that forms interdisciplinary bridges from fundamental science to medicine, corrosion research, microelectronics and biology. The small physical size of needle-type UME's allows the dimension of the electrochemical cell to be dramatically reduced to enable direct measurements in nanolitre and even picolitre volumes. The actual details of small-volume electroanalysis will be discussed in 2.3, e.g. advantages and applications of the strategy will be outlined.

Electrochemical experiments using a standard reduction-oxidation couple, ferrocene-carboxylic acid, have been performed in volumes as small as 1 pl. It is perhaps important to note that irrespective of the sample volume the amount of sample probed in an electrochemical experiment depends on the timescale. This sensitivity arises because for solution phase reactants, diffusion is typically the dominant mode of mass transport and when the response is under semi-infinite linear diffusion control, the thickness of the diffusion layer. This approach can be exploited to monitor reactions involving single molecules. For example, Wightman and co-workers investigated electrochemiluminescent reactions involving individual reactant pairs (Collinson and Wightman, 1995). Their approach was to use 50 μ s potential steps at a 5 μ m radius UME to electrolyze a few femtolitres of 9,10-diphenylanthracene so as to generate a small population of radical anions. Because of

the low concentrations involved, these reactions are seen as individual light producing events. Moreover, UMEs have been used in combination with classical analytical techniques such as Anodic stripping voltammetry (ASV) to determine the concentration of a wide range of analytes especially metal ions (Daniele and Mazzocchin, 1993; Tercier and Buffle, 1993; Vitre et al., 1991) and more contemporary approaches that modify the surface of the microelectrode to produce sensors (Devadoss and Burgess, 2004).

In biological systems, the chemical events of interest are often restricted to the interior or exterior surfaces of single cells and they are fast. Therefore, to provide useful information about *in vivo* biochemistry, measurements, whether optical or electrochemical must be performed with a high spatial and temporal resolution as well as a suitable sensitivity and selectivity (Wightman, Runnels and Troyer, 1999). UME voltammetry is offering superb sensitivity and very good spatial and time resolution. Wightman and co-workers, for example, took advantage of cyclic voltammetry with fast-scan rates, for resolving neurochemical release on sub-second timescale. (Heien, Johnson and Wightman, 2004). Xin and Wightman demonstrated the exquisite performance of UMEs by detecting fast cellular catecholamine exocytosis and calcium ion uptake by single bovine chromaffin cells with a dual amperometric /calcium selective dye-bound fluorescence sensor and they could show that catecholamine release and calcium uptake were temporally and spatially highly correlated (Xin and Wightman, 1998). And Amatore and co-workers used assemblies of paired microband electrodes as functional electronic model of a neuronal synapse (Amatore, Thouin and Warkocz, 1999). More information about applications of UME's in the area of single-cell microelectrochemistry can be found in a series of

recent review comprehensive articles (Amatore, Arbault, Guille, and Lemaitre, 2008; Amemiya, Guo, Xiong, and Gross, 2006; Borges, Camacho, and Gillis, 2008; Hayashi and Niwa, 2002; Mellander, Cans, and Ewing, 2010; Mirkin, Liu, and Rotenberg, 2002; Schulte, Nebel, and Schuhmann, 2010; Schulte and Schumann, 2007; Wang, 2009).

As earlier discussed, one of the major uses of UMEs is for studying redox systems in highly resistive solvents, where electrochemistry without correction for iR effects is feasible with UMEs (Morris, Fischer, and White, 1987; Norton, White, and Feldberg, 1990). Voltammetry in pure aqueous solution without added electrolyte became possible (Bond and Thomas, 1988; Nyholm and Wikmark, 1993; Wang and Zadeii, 1988; Widera, Steinecker, Pacey and Cox, 2003; Wong and Ewing, 1990). The ability to perform voltammetric stripping analysis of ultratrace level metals without the need of potentially contaminating supporting electrolyte is a particularly important application of UMEs (Widera, Steinecker, Pacey and Cox, 2003). White and co-workers pioneered the use of UMEs in neat organic liquids (Li and White, 1995; Malmsten, Smith and White, 1986; Malmsten and White, 1986; Morris, Fischer and White, 1988; Norton, Anderson and White, 1992; Paulson, Okerlund and White, 1996; Ragsdale and White, 1997; Stevenson and White, 1996). The ability to perform electrochemical measurements without deliberately adding supporting electrolyte was shown to have the potential to extend the range of analyte that can be measured (Myland and Oldham, 1993; Palys, Sokolowska and Stojek, 2004; Pałys, Stojek, Bos and Linden, 1997).

Many significant interfacial electrochemical events, such as electron and proton transfers, ligand exchanges, isomerizations, and ejection of leaving groups,

occur at electrode surface on the low microsecond and even nanosecond time domains. To achieve a meaningful insight into these redox processes, it must be possible to measure rate constants under a wide range of experimental conditions, such as driving force, temperature etc. The use of UMEs with critical dimensions in the micron and nanometer range has opened new possibilities for fast kinetic studies because of the greatly diminished capacitance of these ultras small probes. The RC time constant is typically hundreds of microseconds for a conventional millimeter sized electrode placing a lower limit on the useful timescale of the order of several milliseconds. Electrochemistry has several advantages over spectroscopy in that it provides direct information about electron transfer and coupled chemical reactions. An example of the use of UME for ultrafast electroanalysis is the elucidation of rapid homogeneous chemical reactions (Amatore, Jutand and Pflüger, 1987). Howell and Wightman (Howell and Wightman, 1984) have studied electrode reactions and electrochemical redox mechanisms using cyclic voltammetry at scan rates up to 10^5 $\text{V}\cdot\text{s}^{-1}$ and good agreement between the predictions of the Nicholson and Shain theory and experiment (Michael and Wightman, 1996) was found after correcting for the non-spherical nature of the microdisk UME in use.

Finally, a variety of techniques have been used to fabricate micro- and nanometer scale electrodes for applications as probes for electrochemical probe microscopy. Good example are electrochemical (in situ) scanning tunneling microscopy (EC-STM) and scanning electrochemical microscopy (SECM) (Gewirth, Craston, and Bard, 1989; Slevin, Gray, Macpherson, Webb, and Unwin, 1999).

Usually, in SECM the UMEs are attached to precise micromanipulator devices for accurate x, y, and z movements. For imaging, the SECM probe is scanned

at close distance to sample surface and the UME faradaic current is measured as function of position. Plots of the UME signal vs. x-y location provide then the maps of the electrochemical activity with a spatially resolution that is defined by the probe size (e.g. the disk diameter of the SECM probe tip) (Amemiya, Bard, Fan, Mirkin, and Unwin, 2008). Main emphasis of this dissertation, however, is the use of conical UMEs as probing tip of scanning tunneling microscopes. EC-STM and insights in the instrumental layout and function of EC-STM will be discussed and introduced in the following section.

2.2 UME function as probe tip for electrochemically assisted STM

2.2.1 Scanning probe microscopy, SPM

The term scanning probe microscopy (SPM) comprises a whole class of techniques that measure surface properties of materials on an extremely confined local scale. SPM produces the high-resolution, high-magnification images of sample surfaces by scanning a sharp probe back and forth over a specimen and recording a distance-dependent probe signal as function of probe x, y location. Although initially only topography could be examined, further advances in methodology extended the measurement capabilities to other surface properties, such as friction, adhesion, electric and magnetic forces or specific interactions between molecules. Good examples of SPM approaches are STM (scanning tunneling microscopy), AFM (atomic force microscopy), MFM (magnetic force microscopy), SCM (scanning capacitance microscopy), SECM (scanning electrochemical microscopy) SICM (scanning ion-conductance microscopy), SThM (scanning thermal microscopy) and NSOM (Near-Field Scanning Optical Microscopy) (Paredes, Martinez and Tascón,

2002). Since their invention in the 1980s, STM and AFM have provided scientists with exquisitely detailed snapshots of a wide variety of structural and chemical phenomena occurring on surfaces. An understanding of surface chemistry and physics an atomic and molecular level is immense important and the great potential STM on this subject was foreseen already at early stage. Gerd Binnig and Heinrich Rohrer were awarded the Nobel Prize for their invention of the STM only 5 years after first publication. The success of STM and AFM has led to the proliferation of scanning probe technology in all aspects of science and industry. New scanning probe microscopies followed Binnig and Rohrer's STM/AFM gave access to high-resolution imaging of a large spectrum of sample characteristics in addition to topography, including frictional properties, local electric and magnetic domains, thermal behavior, optical absorption, fluorescence, and birefringence. SPMs are now valued not just as common imaging instruments, but also as important analysis and metrology tools for examining a range of material properties on nanometer length scales and for confined surface modification. Novel scanning probe techniques continue to be developed and/or existing ones get improved. They have an impact on virtually every area of technology ranging from molecular biology to semiconductors, surface chemistry, catalysis, and nanofabrication. In this dissertation focus is on STM and the tuning of the STM scanning probe for imaging work in electrochemical environments, which in contrast to STM in air and UHV need special design of the scanned probe tip to allow recognition of tunneling current on top of faradaic background signals.

2.2.2 The development of STM

Binnig and Rohrer have invented STM in 1982 as the first true scanning probe microscope in IBM's research laboratory in Zurich, Switzerland (Binnig, Rohrer, Gerber and Weibel, 1982). A scanning tunneling microscope utilizes electron tunneling between the further most atom of a sharp metal tip and atoms on the surface of a sample and because of the atomic scale of probe-sample interaction it creates images with atomic resolution. STM is earliest performed in controlled or ambient atmosphere, or in vacuum. A fundamental limitation of STM is that samples must be conductive in order to facilitate the process of electron tunneling. This generally restricts STM to characterization of metal, graphite, and semiconductor surfaces (Bobrov, Mayne and Dujardin, 2001; Bobrov et al., 2002). As long as a sample is conductive, however, STM can provide three-dimensional (3D) real space images of the atomic surface layout along with spatially localized measurements electronic structures (Figure 2.5).

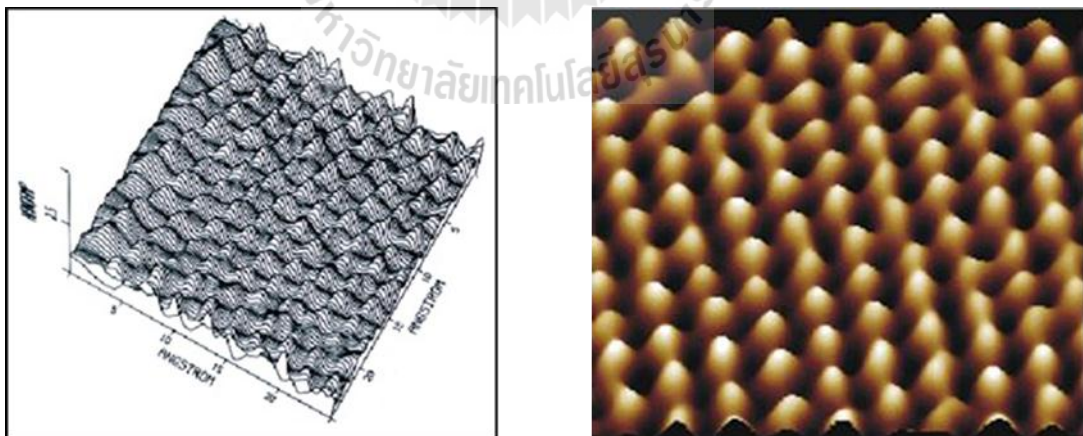


Figure 2.5 The example of a three-dimensional STM image of a graphite surface.

Each bump in the plot of the right and left corresponds to a single carbon atom. The size of the image to the left is only 3 nm x 3 nm; a processed perspective color view of the graphite surface is shown to the right (Joost, 2004).

An STM instrument takes advantage of multiple piezoelectric drivers to control the vertical and horizontal STM tip location and allow movements in close proximity to a sample surface. During tip motion, the tunneling current is measured between the conductive sample and the metallic STM probe tip and displayed as function of tip position in order to generate a topographic STM image of the sample surface. The two physically non-interacting “electrodes” in an STM arrangement differ in their electronic work functions and closeness may or may not support electron tunneling current, dependent on the presence or absence of a driving bias potential. (Chen, 1993; Tersoff and Lang, 1993; Wiesendanger and Güntherodt, 1994). As the probe of a scanning tunneling microscope is a conductive needle that tapers down to a single atom at the end and as this atom is interactive with sample surfaces on the level of atoms, a reconstruction of surface topography is gained at the resolution of angstroms (Å) and imaging resolves in best case atomic or molecular surface features. Figure 2.6 is a simple schematic of the technical arrangement of a common STM device.

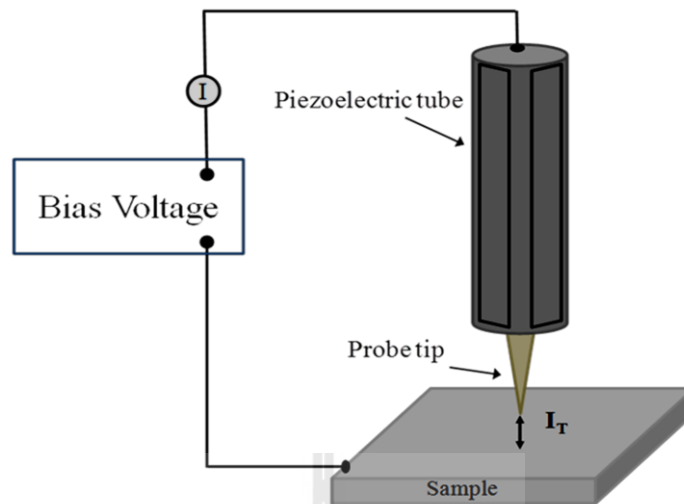


Figure 2.6 A schematic of a typical Scanning Tunneling Microscope.

A voltage is applied between tip and sample, while the tip height and lateral position are controlled by the piezoelectric tube. Plots of tip current vs. tip position lead to topographic images, which variations of the tunneling current (I_T) representing surface features at the atomic scale.

STM imaging

STM relies on the highly localized interaction between the STM probe and surface atom achieve to surface imaging. STM tip position control gained through specially adapted may be a feedback system in which the tip-to-sample distance is manipulated by the control electronics. The measured current interaction may be kept at a constant, user-defined, value to establish setpoint “**constant current mode**” where the tip is approached to maintain constant distance and thus constant current. Alternatively, the z-position of the tip may be kept constant with “**constant height mode**” (Chen, 1993; Tersoff and Lang, 1993; Wiesendanger and Güntherodt, 1994). Generally, the arrangements of the atoms on the tip that are closest to sample surface

determine the stability and resolution of the tunneling contact to sample. The current variations caused by atomic up and downs on the scanned surface produce atomic-resolution topographical images and of course is the imaging quality thus depending on the quality of the STM probe. The position of the probe in a modern STM is controlled by a cylindrical piezoelectric crystal that can deform in three dimensions. A bias voltage is applied between the tip and sample, which causes electrons to tunnel from the tip to the sample or vice versa (depending on the polarity of the bias) (Bonnell, 1993). In the most common mode of imaging this tunneling current is selected via the STM control electronics (Figure 2.7 Top). The tip is then rastered over the surface by applying a voltage to the piezoelectric crystal. As the tip travels over the sample the feedback electronics of the STM maintain the tunneling current at the selected value. When the relative height of the sample changes the tip must move in the z-direction (i.e., in the plane containing the sample normal) in order to keep the tunneling current constant for the selected bias. The voltage applied to the piezoelectric cylinder is then recorded, providing a three dimensional map of the surface. This mode of imaging is the most common and is quite useful for imaging surfaces that are not atomically flat. However, it requires that the tip be raster-scanned relatively slowly due to the finite response time of the piezoelectric crystal. Alternatively, the STM can be operated in constant height mode (Figure 2.7 Bottom). Here, the z-position of the tip is held constant as the tip is scanned rapidly over the surface and the variations in tunneling current are recorded. This method has the benefit of imaging the surface much more quickly, which greatly reduces thermal drift and hysteresis due to the piezoelectric cylinder. The obvious drawback is that the sample surface needs to be virtually atomically flat or else the tip will come into

physical contact with surface (Chen, 1993; Heben, 1990; Julian, 1993; Wiesendanger and Güntherodt, 1994).

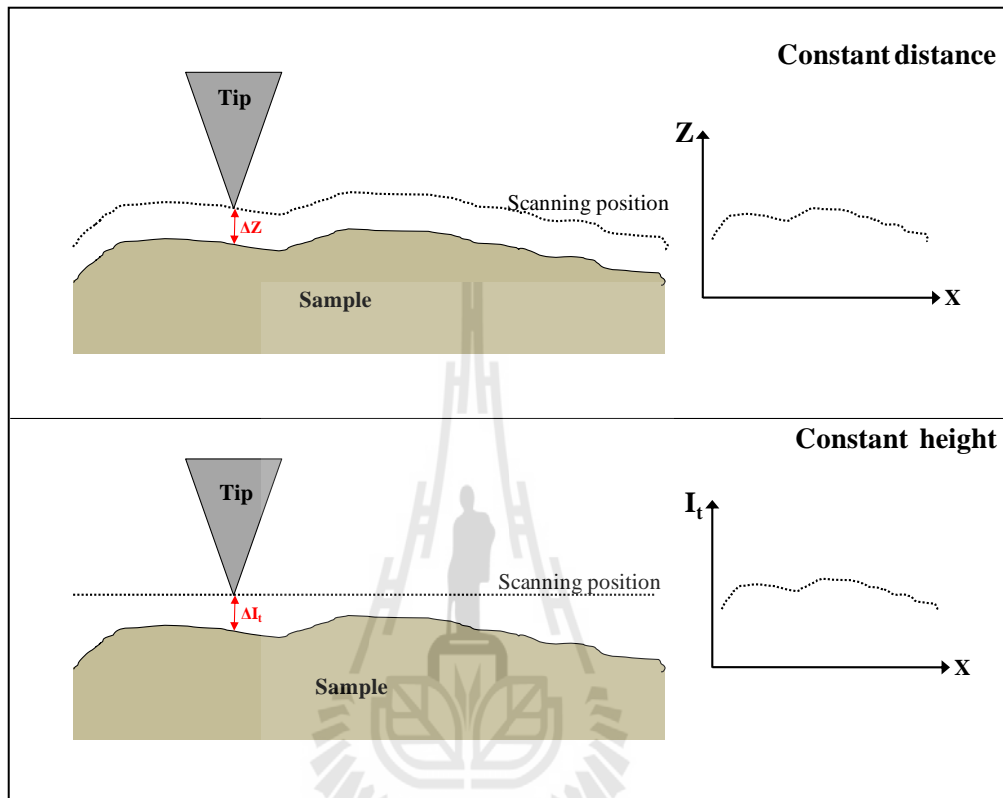


Figure 2.7 Schematic of STM tips in close distance to a surface.

(Top) Illustration of the constant current mode: the tip is rastered over the surface and moves up or down over surface features in order to maintain a selected tunneling current. Changes in the vertical position are translated into topography of surface in the STM image. (Bottom) Illustration of the constant height mode, where the STM is guided at constant height above the surface and the change in tunneling current due to distance variation is translated into an image of the vertical features of the sample surface.

STM Applications

1. Atomic resolution topography and imaging surface modification

The STM has provided a variety of new physical visions in the fields of semiconductor, metallic, superconducting, and magnetic surfaces. Due to the spatially confined tip-sample interaction, atomic resolution on metallic surfaces is possible, even though the intrinsic corrugation of the surfaces is supposed to be too low for being atomically resolved by STM, for example, on reconstructed semiconductor surfaces of Si(111)-7x7-surfaces (Avouris and Wolkow, 1989). Moreover, STM, when performed in an electrochemical cell, may facilitate deposition of atomic-sized metallic cluster on the surface sample by tip-induced deposition of dissolved metal ions (Schindler, Hofmann and Kirschner, 2001; Kolb, Engelmann and Ziegler, 2000) or support local sample etching via tip-induced anodic dissolution of sample surface atoms (Zhang and Stimming, 1990).

2. Imaging of electronic state properties of conductors

Since the STM in first place is imaging electronic states of the sample surface, the technique can also be used for imaging the electronic fine structure at atomic scale (Li, Schneider, Crampin and Berndt, 1999). Images of molecular layers can, for instance, reveal the orbital structure in the LUMO or HOMO states (lowest-unoccupied/highest-occupied molecular orbital), depending on the polarity of the bias voltage used during image acquisition (Qiu et al., 2000).

3. Imaging of magnetic properties at atomic scale

A special application of STM is its use for spin-polarized tunneling experiments with magnetic STM tips that, in ideal, have at their an atomic magnetic monopole for local interaction with magnetic sites on the sample surface (Heinze et

al., 2000). This type of investigation is capable to give very valuable insights into the principles of magnetism, information that ultimately may support the future development of new magnetic storage devices.

4. Scanning tunneling spectroscopy (STS)

Combining atomic-scale STM imaging with measurements of current–voltage (I–V) characteristics at similar resolution makes it possible to obtain a detailed map of the electronic structure of a surface. While interrupting the feedback loop and keeping the tip-to-sample distance constant, a voltage ramp is applied to the tunneling junction and the tunneling current monitored as a function of tip bias; the signal provides information about the convolution of the tip density of states (DOS) (Binnig and Rohrer, 1987). Performed at different grid points, the tunneling junction voltage scans allow to create a map of tunneling spectra. The origins of STS are already laid in some of the earliest STM work of the inventor Gerd Binnig and Heinrich Rohrer (Binnig and Rohrer, 1987), as they observed changes in the appearance of some atoms in the (7 x 7) unit cell of the Si(111) – (7 x 7) surface with varied tip-sample bias (Hamers and Padowitz, 2001). STS is applicable to metals, semiconductors, and thin insulators and capable to provide electronic structure on a scale unobtainable with other spectroscopic methods. The spectroscopic data can be recorded together with atomic resolution topographic images for better interpretation.

For all STM applications, the geometry of the top of the STM tip apex is of critical importance for the quality of measurement. Next, thus will be discussed the procedures for the preparations of the suitable, needle-like STM tips.

Tip fabrication

As mentioned earlier, the feedback-controlled tip positioning during scanning is crucial for the imaging quality, but the key factor for good STM surface inspection is the quality of the STM tip itself. Therefore, proper STM tip preparation is an important step in an STM experiment. Improper sharpness of an STM tip may cause a distortion of imaging, certainly on rough surfaces. Ideally, an STM tip should be extremely sharp, possibly terminating in a single atom, in order to resolve sample details at the atomic or molecular level.

The chemical identity and arrangement of the atoms on the tip at closest to sample surface are in control of the stability and resolution of the tunneling tip; however, these two parameters are extremely difficult to control or quantify (Rohrer, 1993). The theory describes the tip shape in ideal as a spherical potential well with no atomic features, as a small cluster of three or four atoms, or as a single atom (Figure 2.8).

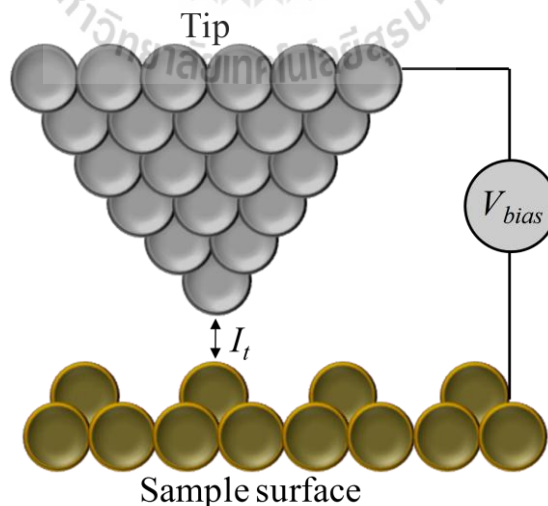


Figure 2.8 Schematic diagram of imaging process with a single atom acting as a tip.

Ideal, the tunneling contact is made by a single atom at the very end of the STM tip and a single atom on the sample surfaces.

STM tips are usually made of thin W, Pt, Pt-Ir or Au wires. The tips are fabricated by several different methods such as mechanical forming (clipping the end of the wire at an angle with wire cutters or by pulling) (Binnig, Rohrer, Gerber and Weibel, 1982, Feestra and Fein, 1985), or electrochemical etching (Nakamura, Mera, and Maeda, 1999). Obviously, mechanically cutting a metal wire is difficult to control in terms of tip shapening and thus not very reproducible. Non-manual electrochemical etching has here clear advantages.

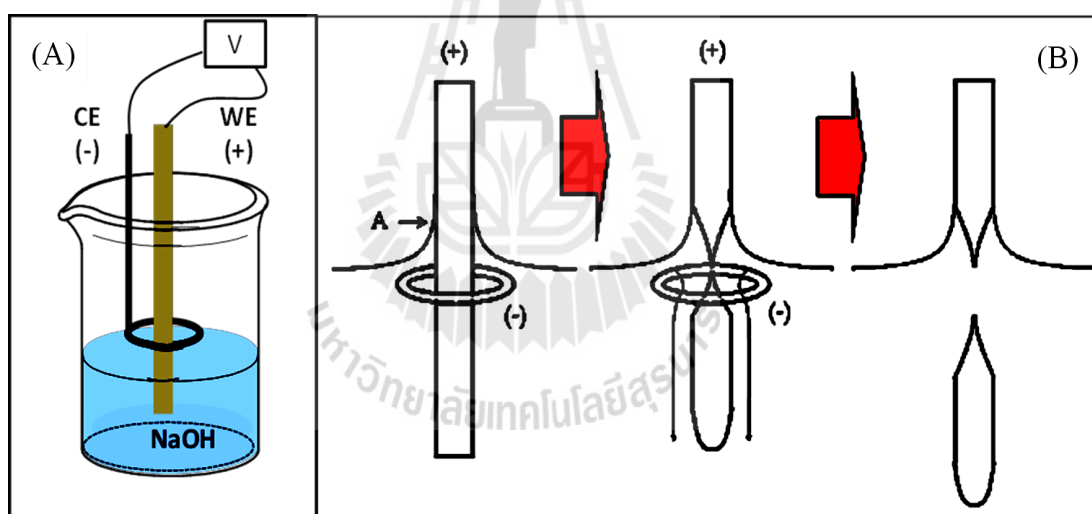


Figure 2.9 Schematic the electrochemical etching of metal wire and the etching process at air/electrolyte interface.

(A) Schematic diagram of the experimental setup for the electrochemical etching of metal wire. (B) Schematic drawing of the etching process at air/electrolyte interface (Kim et al., 2006).

Figure 2.9(A) shows a typical experimental arrangement for the electrochemical etching of STM tip. The setup includes an inert counter-electrode (e.g. a Pt-ring electrode etc.) the etching solution (e.g. 2 M of NaOH) and the metal wire to be etched. Local corrosion dissolution of metal ions from the metal wire leads finally to the narrowing of the filament at the air/electrolyte interface and at very end of the process to an electrochemical cut through and taper formation (Figure 2.9(B)). Detailed information on the electrochemical STM tip etching can be found in the original literature where type of electrolytes, type of potential profiles for the anodic etching process and the type of treated metal wire are listed and resulting tip shapes are described and discussed (Kim et al., 2006). An interesting option for electrochemical etching of STM tips is a technical arrangement that allows to turn automatically off the etching voltage at the moment of full cut-through, an effect that protects the end of the produced tip for further inspect, which leads to better reproducibility and in “good” tip fabrication (Figure 2.10).

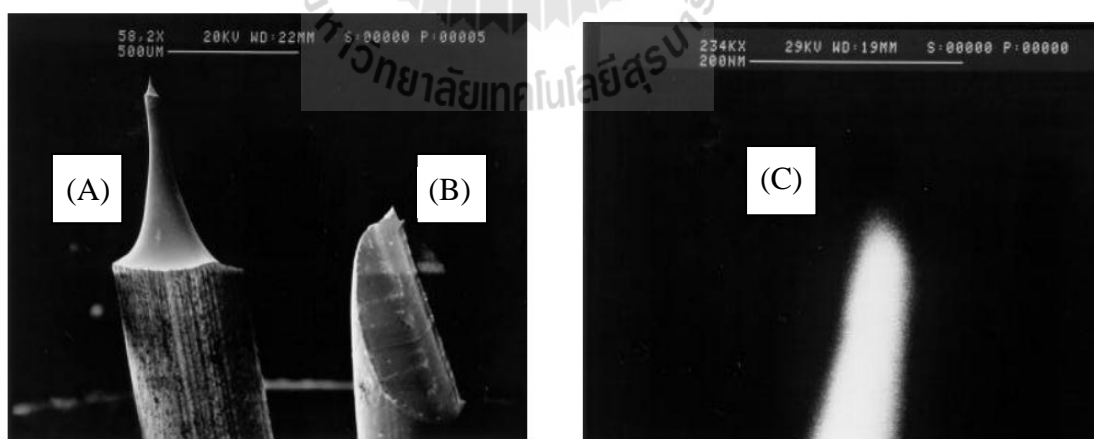


Figure 2.10 Comparison of SEM image of electrochemically etched tungsten tip and a cut platinum tip.

Electrochemically etched tungsten tip (A) compared to a cutted platinum tip (B), (C) high resolution SEM image of tungsten tip with a tip radius of 16 nm (Rickart and Bauer, 1998).

If W is tip material, however, etching may form an unwanted oxide layer on the tip surface or the oxide coverage may be result of slow oxidation due to air exposure (Biegelson, Ponce, Tramontana and Koch, 1987; Garnaes, Krangh, Morch and Tholen, 1990). The oxide layer at the end of a W tip may hide the tunneling signal. Oxide removal is thus needed and may be achieved by an acid etching, ion milling, or heating in vacuum (annealing) (Biegelson, Ponce, Tramontana, and Koch, 1987).

To conclude STM is a unique local probing microscope that can be operated in vacuum, air and in aqueous environments. The technique has revolutionized the study of surfaces under various conditions and become rapidly a key analytical tool in surface-related scheme. At very attractive form of STM is electrochemical STM (EC-STM) or *in situ* STM because of relation to electrodeposition, corrosion, metal crystallization, absorbate formation and catalysis. The technical details and principles of EC-STM will be presented in the next section.

2.2.3 Electrochemical scanning tunneling microscopy (EC-STM)

The STM is an interesting tool for a number of attractive electrochemical applications, including atomic scale topographic and spectroscopic studies of solid/liquid interfaces and extremely high resolution electrochemically-induced lithography. Additionally, the STM's capability to control the tip/sample spacing

facilitates space- and time-resolved inspections of diffusion layer profiles in front of active electrodes. Since STM was first applied for studies in electrolyte solutions in 1986 (Sonnenfeld and Hansma, 1986), it has become a popular in situ technique for studies of the electrode-electrolyte interfaces. In situ STM is also called electrochemical STM (EC-STM). In EC-STM, a bipotentiostat has to be employed to independently control the potentials of the substrate (which is also the working electrode, WE) and the tunneling tip (the scanning probe), both with respect to a common reference electrode (RE). The Faradaic current flowing through the substrate and the counter electrode (CE) is collected by a current follower, while the tunneling current is measured by a tunneling current amplifier (Figure 2.11). Employment of a bipotentiostat successfully support interference free acquisition of the faradaic current and the tunneling current, which was a problem in the concept of early EC-STM system (Chen, 2004).

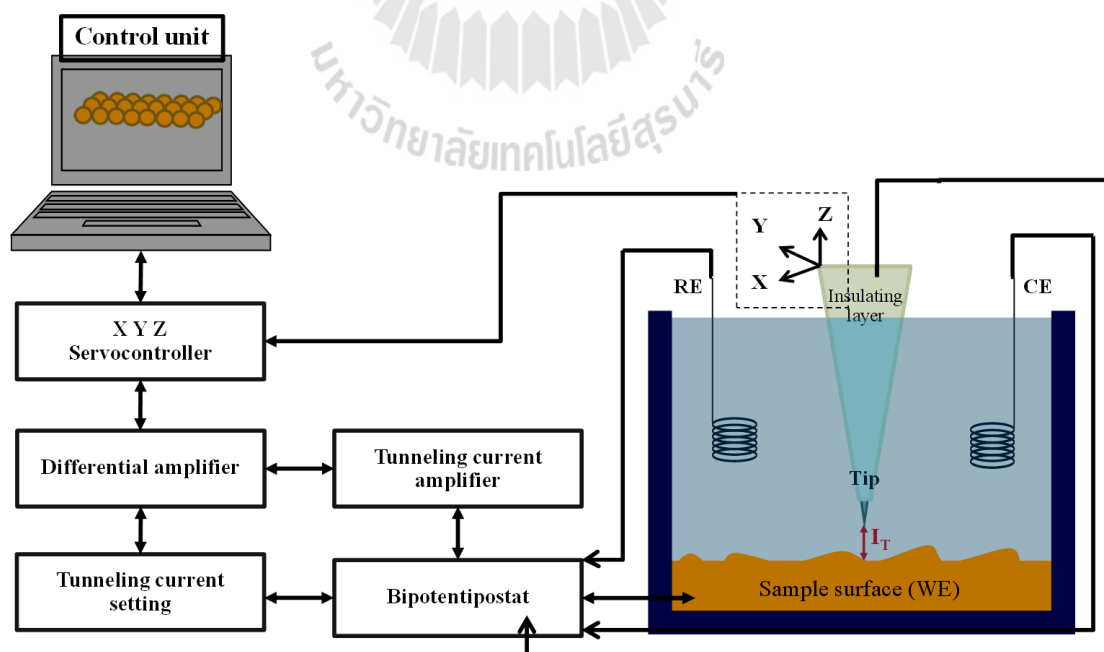


Figure 2.11 Schematic diagram of an EC-STM setup.

Schematic diagram of a setup for electrochemical scanning tunnelling microscopy (EC-STM, in situ STM). The potentials of the tip and sample are controlled vs. RE; the bias voltage inducing electron tunneling (E_{Bias}) is the difference between sample and tip potential ($E_{\text{Bias}} = E_{\text{sample}} - E_{\text{tip}}$).

To induce the tunneling current, the STM tip is exposed potential to a small anodic (+) or cathodic (-) potential and as it is immersed in electrolyte solution, there is a risk that a Faraday current flows through the tip large enough to disturb the tunneling current that is the signal for STM imaging.

To minimize the faradaic current (I_f), the exposed electroactive area of the STM tip is reduced by a coating with an insulator. The ideal EC-STM tip would have a single exposed atom of the tip apex with all the remainder of the tapered metal wire electrochemically insulated. The required partial tip insulation can be obtained by a selective coating with glass or polymers (e.g. Wax, Teflon, Nafion, electrodeposition paint) that spare the tip front (Nagahara, Thundat, and Lindsay, 1989). Actually, an EC-STM tip is a tapered (“conical”) UME that may function as normal working electrode for conventional electroanalysis, as well. The reduction of the electroactive area of STM tips equal to the preparation of UMEs is discussed in the later UME section.

The conventional STM tips are usually made of noble metal (e.g. Pt, Pt-Ir alloy or Au) or from W. In particular true for W wire etching, the process of tip formation is likely to cause unwanted oxide layers (Biegelson, Ponce, Tramontana and Koch, 1987; Garnaes, Krangh, Morch and Tholen, 1990). The oxide layer at the end of W tip may hide the tunneling signal and removal by an acid etching, ion milling, or heating in vacuum (annealing) (Biegelson, Ponce, Tramontana, and Koch,

1987) may be addressed in an additional preparation step. On the other hand, carbon is known to be chemically a rather inert material and thus became an attractive alternating STM tip material. Carbon fiber tips with an apex radius of just a few nanometers are expected to be functional for STM imaging, and their fabrication and adaptation thus highly attractive. The most interesting application of CF-based probe tip in STM is the investigation of sample surfaces in electrolyte environment. For this type of measurement, the etched CF tip has to be coated with a tip-sparing insulating film to limit the faradaic current caused by electrooxidation/electroreduction of redox species in electrolyte. To the time of the start of this thesis nobody has been able to operate carbon STM tips successfully for electrochemical in situ surface imaging with atomic or molecular resolution. Realization of this approach would thus be a novelty and significant achievement.

2.2.4 Carbon-based STM probe tips and ultramicroelectrodes

Carbon is, as already mentioned before, an appreciated material of scanning probe microscopy (SPM) tips and macro- or microscopic voltammetric sensors as it has many properties that are constructive for these applications:

- In its various forms carbon is chemically inert enough to assure sound resistance against degradation during sensor storage and continuous use.
- If desired, carboxyl and other oxide moieties can efficiently be generated at carbon surfaces via simple chemical or electrochemical treatments and may then be used together with carefully chosen inorganic/organic coupling reactions for covalent modification and the establishment of

chemically modified SPM tips and nanoelectrodes with a chemically modified surface.

- Carbon surfaces are associated with high overpotentials for the anodic oxygen and cathodic hydrogen evolution. Inhibited water electrolysis is of course helpful when operating polarized sensors, and this are scanning tunneling microscopy (STM) tips or voltammetric electrodes, in an electrolytic milieu since it helps keeping faradaic background currents from unwanted gas formation low that otherwise would superimpose or in worst case even completely hide the analytically relevant tunneling current or voltammetric responses.
- Graphite-like carbon fibers and carbon-nanotubes offer ultrathin filaments that are flexible and mechanically highly stable.

Representative examples of carbon-based structures that in the past have been used for fabricating STM tips are:

- **Carbon Nanotubes (CNTs).** Equipped with unique aspect ratios, the same nanometric sections all along their length and highest strength, single- and multi-walled CNTs brought about STM tips of high quality in terms of spatial resolution, durability and good performance for the imaging of challenging surface features such as trenches, ridges and pikes (Dai et al., 1996).
- **Electron beam-deposited (EBD) carbon supertips.** The slender carbonaceous nanotowers that can be grown onto the apex of parental scanning probes by the pyrolyzing impact of the stationary electron beam of a scanning electron microscope (SEM) on residual hydrocarbon

molecules, also turned out to be practical as high aspect ratio STM imaging tool for hill-and-valley shapes (Akama, Nishimura, Sakai, and Murakami, 1990, Huebner et al., 1992).

- **Pointed graphite pencil leads and rods of carbon fiber/epoxy composites or pyrolytic graphite.** The nanometric protrusions that randomly appear at the front of mechanically or electrochemically sharpened graphite pencil leads and rods of carbon fiber/epoxy composites or pyrolytic graphite have been reported as functional STM tips (Ohmori, Nagahara, Hashimoto, and Fujishima, 1994, Rohlfing and Kuhn, 2007).

Ultra small carbon working electrodes with cylindrical, conical or disk-shaped geometries and prepared for voltammetry and amperometry applications, on the other hand, have been prepared from:

- **Carbon fibers.** Carbon fibers (CFs) represent a material in which little sheets of graphite are packed and folded tightly together to form thin round fibers as shown in Figure 2.12. Existing high performance CFs have diameters of about 4 to 12 μm and normally are used in manufacturing as mechanically strong and stringy filler components of the advanced reinforced polymer composites that are the base material of light and firm utensils as for instance modern tennis rackets, sailboats, gliders, bicycles, and fishing rods. But a small diameter, high electrical conductivity and good mechanical strength (see Table 2.1) made the high-tech graphitic filaments attractive also for electro- and analytical chemists who took prompt advantage out of the good blend of properties

for the design of cylindrical and disk-shaped carbon microelectrodes. Flame (Bailey, Malinski, and Kirchle, 1991, Bessenhard, Schulte, Schur, and Jannakoudakis, 1990, Schulte, 1994, Strein and Ewing, 1992) ion beam (Zhang, Zhang, Zhou, and Ogorevc, 1996) spark (Millar and Pelling, 2001) and electrochemical (Bailey, Malinski, and Kirchle, 1991, Bessenhard, Schulte, Schur, and Jannakoudakis, 1990, Schulte, 1994, Strein and Ewing, 1992, Armstrong-James, Fox, and Millar, 1980, Stamford, 1986, Meulemans et al., 1986, Mousa, 1996, Schulte and Chow, 1998, Chen and Kucernak, 2002, Tel-Vered, Walsh, Mehrgardi, and Bard, 2006, El-Giar and Wipf, 2006, Li et al., 2007) etching have been disclosed as procedures for thinning the ends of factory-made CFs. Attempts to convert unetched and etched carbon fiber versions into miniaturized voltammetric carbon micro- or nanoelectrodes was crowned with good success (Bailey, Malinski, and Kirchle, 1991, Strein and Ewing, 1992, Schulte, 1994, Zhang, Zhang, Zhou, and Ogorevc, 1996, Millar and Pelling, 2001, Armstrong-James, Fox, and Millar, 1980, Stamford, 1986, Meulemans et al., 1986, Mousa, 1996, Schulte and Chow, 1998, Chen and Kucernak, 2002, Tel-Vered, Walsh, Mehrgardi, and Bard, 2006, El-Giar and Wipf, 2006, Li et al., 2007, Armstrong-James and Millar, 1979, Golas, Osteryoung, 1986, Kelly and Wightman, 1986, Frenzel, 1987, Edmonds, Dean, and Latif, 1988, Wang, Creasy, and Shaw, 1991, Chow, Rueden, and Neher, 1992, Math and Marianneau, 1994, Zhao, Giolando, and Kirchhoff, 1995, Schulte and Chow, 1996, Swiergiel, Palamrchouk, and Dunn, 1997, Koh and

Hille, 1999). Figures 2.13-2.17 are showing, examples of particular cases of carbon micro- and nanoelectrodes: (1) is the schematic of the procedure for the fabrication of voltammetric carbon ultramicroelectrodes with effective radii as small as only a few nanometers (Figure 2.13) (Chena and Kucernak, 2002), (2) is a presentation of a flame-etched and poly-oxyphenylene-insulated carbon fiber ultramicro disk electrode for exocytosis measurements (Figure 2.14) (Budai and Molnár, 2001), (3) is a glass-insulated spark-etched carbon fiber microelectrode for electrophysiology applications (Figure 2.15), (Meulemans et al., 1986), (4) is an electrochemically etched carbon fiber that was sealed into a pulled glass pipette to form a submicron disk carbon ultramicroelectrode with capability to penetrate the lipid bilayer membrane of living cells and serve as sensor for intracellular voltammetry (Figure 2.16) (Strein and Ewing, 1992) and (5) is a SEM image of an electro-painted 10- μm -diameter carbon fiber that was insulated by an anodic electrodeposition paint and got is electroactive carbon disk via scalpel cutting perpendicular to the fiber axis (Figure 2.17) (Schulte and Chow, 1996).

Table 2.1 Comparison of the mechanical properties between carbon fiber and steel.

Material	Density (g cm^{-3})	Tensile Strength (GPa)	Tensile Modulus (GPa)	Specific Strength (GPa)
Carbon fiber	1.75	3.5	230.0	2.00
Steel	7.87	1.3	210.0	0.17

Remark (Donnet and Bansal, 1990, p. 26)

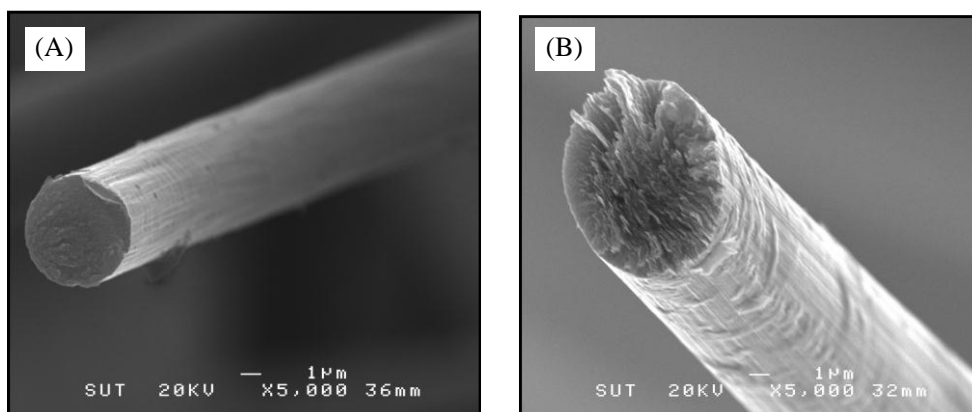


Figure 2.12 The SEM images of the microstructure of PAN- and pitch-based fibers.

(A) is the PAN-based fiber (T300) and (B) is the pitch-based fiber (P100).

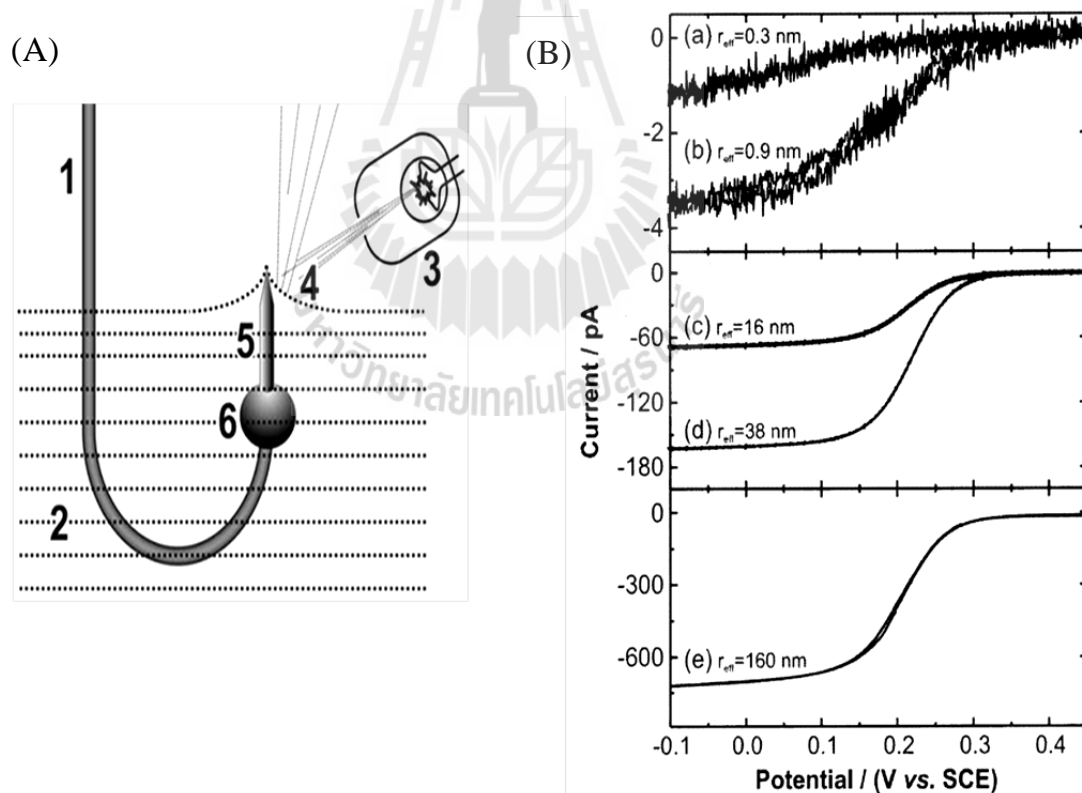


Figure 2.13 The inverted carbon fiber arrangement of insulating process with electrodeposition paint.

(A) Schematic of the preparation of carbon nanoelectrodes with effective radii of only a few nanometers. Used was an anodic deposition of electrodeposition paint in the inverted carbon fiber arrangement. The conically etched carbon fiber was immersed into the polymer deposition solution in upside-down position: carbon fiber tip up. Copper wire, 1; EDP solution, 2; light source, 3; meniscus, 4; etched carbon fiber tip, 5; carbon colloid contact, 6. (B) Steady-state voltammograms of the reduction of Fe(III) in 0.01M $K_3Fe(CN)_6/0.5M$ KCl at carbon nanoelectrodes made as in (A); scan speed was 10 mV/s. The effective radii were calculated from limiting currents. (Chen and Kucernak, 2002).



Figure 2.14 Electrical spark etched carbon fiber based UME.

Scanning electron micrograph (SEM) of the tapered tip of a carbon fiber UME protrudes from the insulating borosilicate glass capillary tubing. Conical carbon fiber sharpening was achieved by electrical spark etching. The tapered tip of the carbon fiber protrudes from the insulating borosilicate glass capillary tubing. The carbon tip is suitable for extracellular recording and for in vivo electrochemical measurements (Budai and Molnár, 2001).

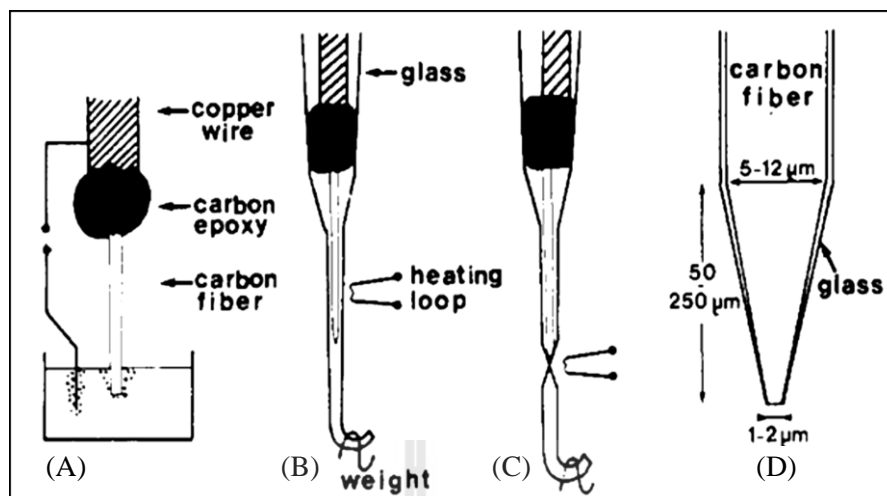


Figure 2.15 Preparation of the carbon microelectrode for voltammetry inside of living cells.

(A) electrochemical etching of the tapered carbon fiber tip; (B) Placement of the etched carbon fiber inside a glass capillary tube; (C) Application of a gentle pulling procedure that seals the carbon taper into a very thin glass coat; (D) complete carbon microelectrode after beveling and mechanical polishing (Meulemans et al., 1986).

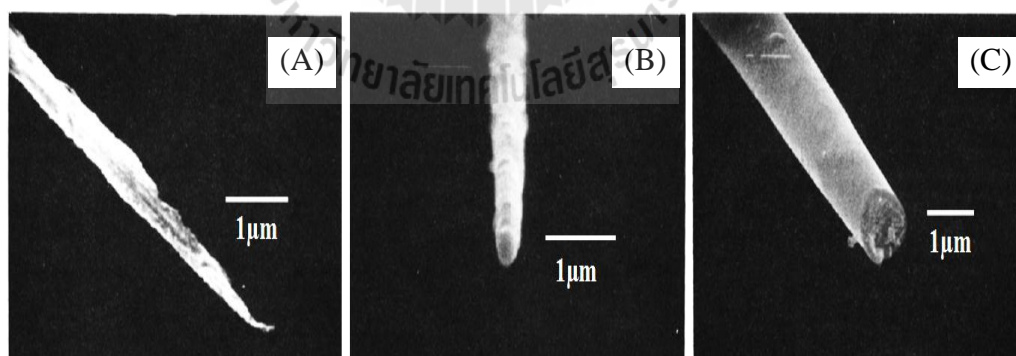


Figure 2.16 Scanning electron micrographs (SEM) of a flame-etched carbon coated with an insulating layer of poly(oxyphenylene).

Scanning electron micrographs (SEMs) of flame etched carbon fibers. (A) a carbon fiber which has been tapered through the burn in a hot oxygen/methane flame, (B) an flame-etched carbon fiber which has been later coated with an insulating thin film of

poly-oxyphenylene, and (C) a coated fiber which has been cut with a scalpel blade perpendicular to the fiber axes to expose the submicron disk-shaped carbon electroactive surface (Strein and Ewing, 1992).

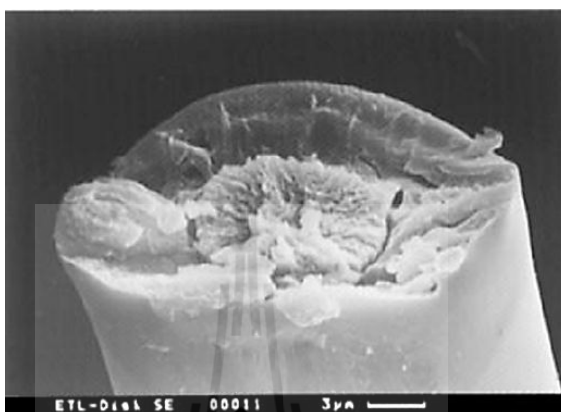


Figure 2.17 A SEM image of an electro-painted 10- μm -diameter carbon fiber, insulated by anodic EDP at 20 V for 4 min, and cut with the scalpel.

A SEM image of an electro-painted 10- μm -diameter carbon fiber. The central circular cross-section is surrounded by a tightly gripping polymer insulation forming a well-shaped carbon disk microelectrode surface (Schulte and Chow, 1996).

- **Pyrolyzed carbon.** An alternative pathway towards micron and sub- μm carbon disc electrodes has been reported with the pyrolysis of methane or acetylene at the heated inner walls of the nanometric tips of pulled quartz capillaries and the complete closure of the nanometric pipette openings with conductive carbonaceous products of combustion (MacNally and Wong, 2001, Wong and Xu, 1995). Coating the surface of etched tungsten tips with a photoresist, pyrolyzing the organic varnish and insulating the obtained carbon-coated tip with an epoxy resin except

at its tip has been described as another way to get to carbon microelectrodes through pyrolysis (Hermans and Wightman, 2006).

- **Carbon nanotubes.** Crooks and coworkers demonstrated already in 1999 as so far the only ones redox voltammetry at individual multiwalled CNTs (\O 80-200 nm) that could be movable carbon nanoelectrodes by an attachment to sharp platinum tips as conductive holder and maneuvering via an accurate micropositioning device (Campbell, Sun, and Crooks, 1999). The design and fabrication of the CNT nanoelectrodes is schematically illustrated in Figure 2.18. Dipped into electrolyte solution solutions containing electroactive species, CNTs behaved as cylindrical (“tubular”) nanoelectrodes and displayed in cyclic voltammograms the predictable spherical diffusion and limiting currents that scaled nicely with depth of immersion. Coating an attached CNT with thin but insulating polymer films and a subsequent vertical cut exposed nanometric carbon circles and restricted voltammetric current responses to the furthest tube tip.

Neither CNT-based nor carbon fiber- and pyrolyzed carbon-based sensors had been used successfully as hybrid bifunctional sensors in an STM microscope setting for attractive joint high resolution (STM) topography and electrochemistry studies at the start of this PhD thesis. In the case of the CNT-based probes, it was/is apparently the difficulty of the preparation, actually attachment to appropriate holding structures and/or subsequent proper partial insulation, which hindered their fruitful exploitation for in situ STM studies. For the carbon fiber- and pyrolyzed carbon-based alternatives, on the other hand, the structural design of the

bodies/stems of both types of sensors apparently was/is not in favor of an implementation into the scanning units of existing commercial or self-made AFM/STM instruments. As EC-STM with carbonaceous/graphitic scanning probes would open up novel opportunities for experiment design and reduce the limitation set by water electrolysis at the sensing tip the establishment of carbon-fiber based EC-STM tips was thus chosen as a prime goal of this thesis work.

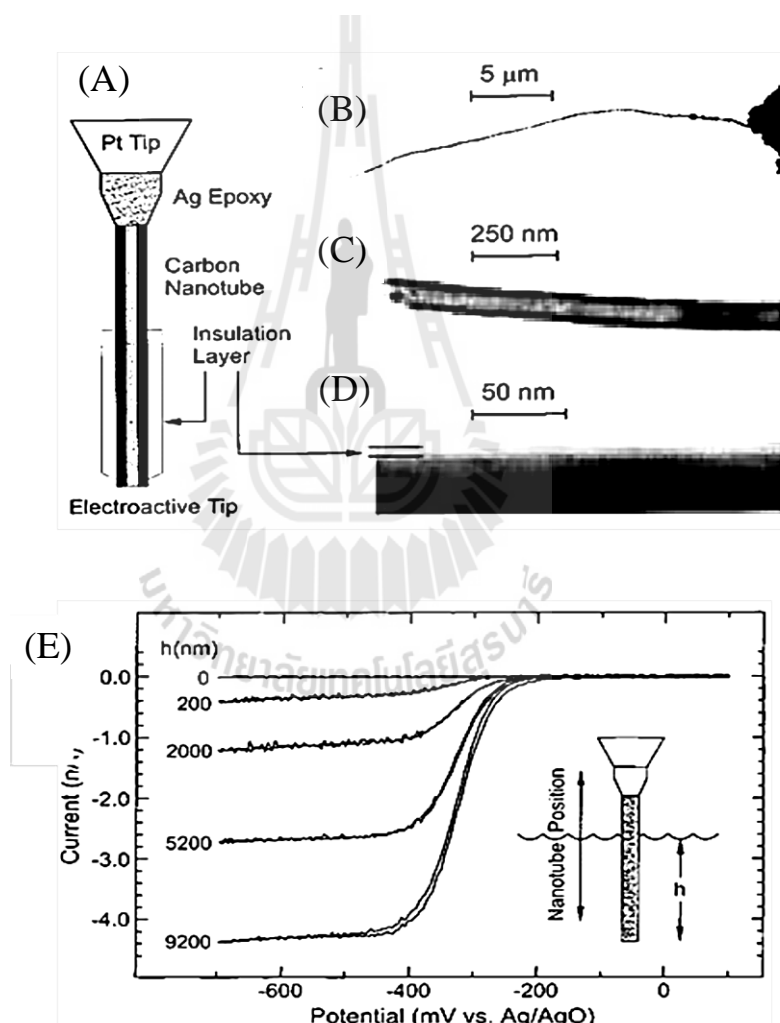


Figure 2.18 A partially insulated carbon-nanotube ultramicroelectrode.

(A) Schematic representation of a partially insulated carbon-nanotube electrode. (B-D) TEM images of mounted nanotubular electrodes showing (B) a 30-μm long

electrode; (C) the tip of a ~100-nm diameter uninsulated nanoelectrode; (D) a ~10-nm thick insulation layer of polyphenol on a ~220-nm diameter nanotube. (E) CVs from an uninsulated 150-nm diameter nanotubular electrode in 5 mM $\text{Ru}(\text{NH}_3)_6$ + 0.1M K_2SO_4 (V) 100 mV/s). CVs indicate near-ideal radial diffusion with limiting currents that scale with immersion depth, h . (Campbell et al., 1999).

2.3 Small-volume voltammetry

A popular direction in current electroanalytical research and development is the miniaturization of chemical analysis methods. Reducing the overall size of an analysis device has the advantage of using less material, generating less waste, and allowing smaller samples to be measured at a higher throughput. Currently, the strategies of working in nanoscopic volumes mainly fall into two categories: (i) positioning the top ends of microelectrodes into target domains (Figure 2.19 A and B); and (ii) preparing volume-limited structures with integrated functional electrodes (Figure 2.19 C and D) (Li and Hu, 2011).

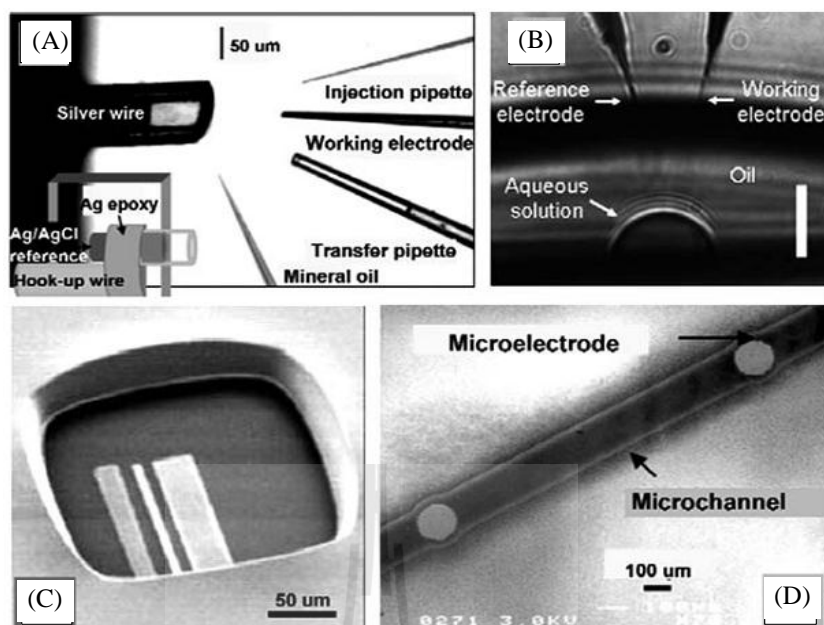


Figure 2.19 Representative ways of manipulating microelectrodes in nanoscopic domains (Li and Hu, 2011).

In the example in Figure 2.19, a manipulation of pipette and microelectrode into the open end of picolitre-volume vials. A mineral oil cap was placed on the vial to prevent solution evaporation (Troyer and Wightman, 2002). (B) Insertion of needle-type microelectrodes into micro-droplets with volumes down to a few picolitres. The scale bar is 10 μm (Yum, Cho, Hu and Yu, 2007). (C) Integration of micro-electrodes into microchambers fabricated by photolithographic method (Cai, Glidle and Cooper, 2000). (D) Microchannels with integrated micro-working, counter and reference electrodes prepared by plasma etching (Lion et al., 2003).

Small-volume detection has been motivated by the need for analysis of samples of limited availability. An organic/pharmaceutical micro-synthesis may, for instance, only yield very tiny amounts of high-molecular weight redox active products, redox active chemicals of interest may be extremely expensive or solutions with dissolved

electroactive analytes may only be available in small quantity (Ball et al., 2000). Electroanalysis for the mentioned situations would struggle because of the reduced material available for making substantial volumes of measuring electrolyte that contain levels of analyte species detectable for conventional voltammetric or amperometric assays. Existing technical arrangements for electrochemical measurements of small volume samples include miniaturized flow-based analytical devices with small flow-through electrochemical cells or miniaturized stand-alone electrochemical cells. Electrochemical cells with small volume capability are, for instance, based on the thin-layer principle (usually in a “sandwich type” configuration) (Wang and Freiha, 1982). Other cells or approaches include a microcell that suits a rotating disk electrode (Eggle, 1977; Miller and Bruckenstein, 1974), a capillary packed-bed electrode (Messner and Engstrom, 1981), a mercury drop electrode microcell (Huderová and Štulík, 1972), specially designed cells with a stationary carbon electrode (Karolczak, Dreiling, Adams, Felice, and Kissinger, 1976), and finally micro flow cells for liquid chromatography and flow injection analysis (Rucki, 1980). Wang and Freiha performed measurements in 50 μ l solution by using a carbon paste electrode in a microcell as shown in Figure 2.20 (Wang and Freiha, 1982).

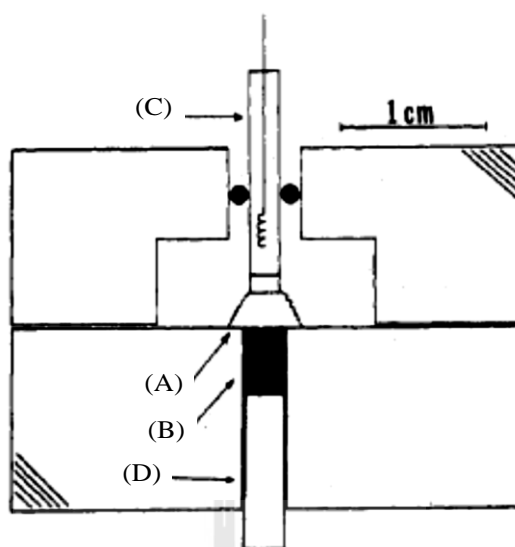


Figure 2.20 Example of a microcell for voltammetric measurements.

(A) sample solution; (B) carbon paste working electrode; (C) capillary silver-silver chloride reference electrode; (D) copper lead to working electrode (Wang and Freiha, 1982).

Walter and coworkers demonstrated the performance of small volume detection on volumes of ~ 1 nl with a self-contained microfabricated microcavity device (Figure 2.21) that contained multiple electrodes (Walter, Vandaveer, and Fritsch, 2002). Furthermore, the invention of screen printed electrodes led to tools that could be used with small sample volumes (Ball et al., 2000; Wang, Zhang, Huang, Zhang, and Zhou, 1998).

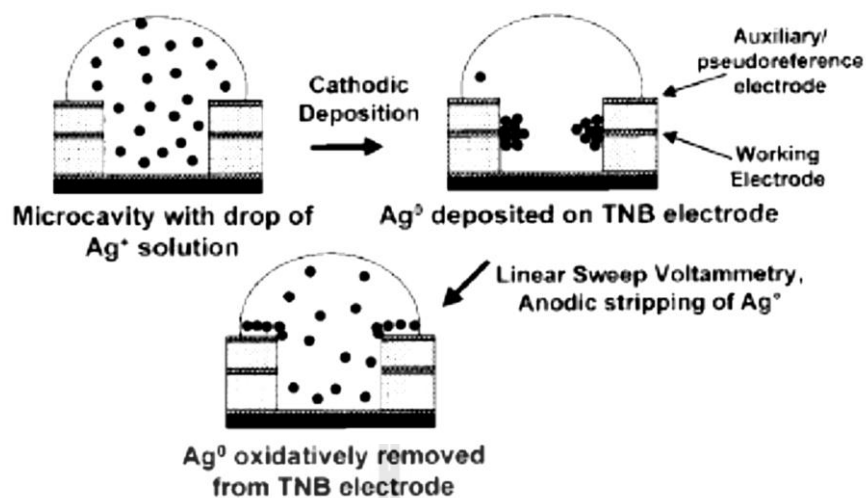


Figure 2.21 Cross-section of a microcavity and the procedure for anodic stripping voltammetry in small volumes of silver drop.

Cross-sectional diagram of the microcavity with incorporated electrodes. Cross-sectional diagram of the microcavity with incorporated electrodes at the side wall and bottom and schematic of the procedure for measurements of analyte in small volumes by anodic stripping voltammetry of cathodically deposited silver from the electrolyte drop (Walter, Vandaveer, and Fritsch, 2002).

Rievaj, Dovalovská and Bustin described the application of mercury-coated carbon screen printed electrode (see Figure 2.22) for performing anodic stripping voltammetry (ASV) in total sample volumes as small as 50 μl to detect, for instance, Pb in blood samples by the standard addition method (Rievaj, Dovalovská and Bustin, 2006).

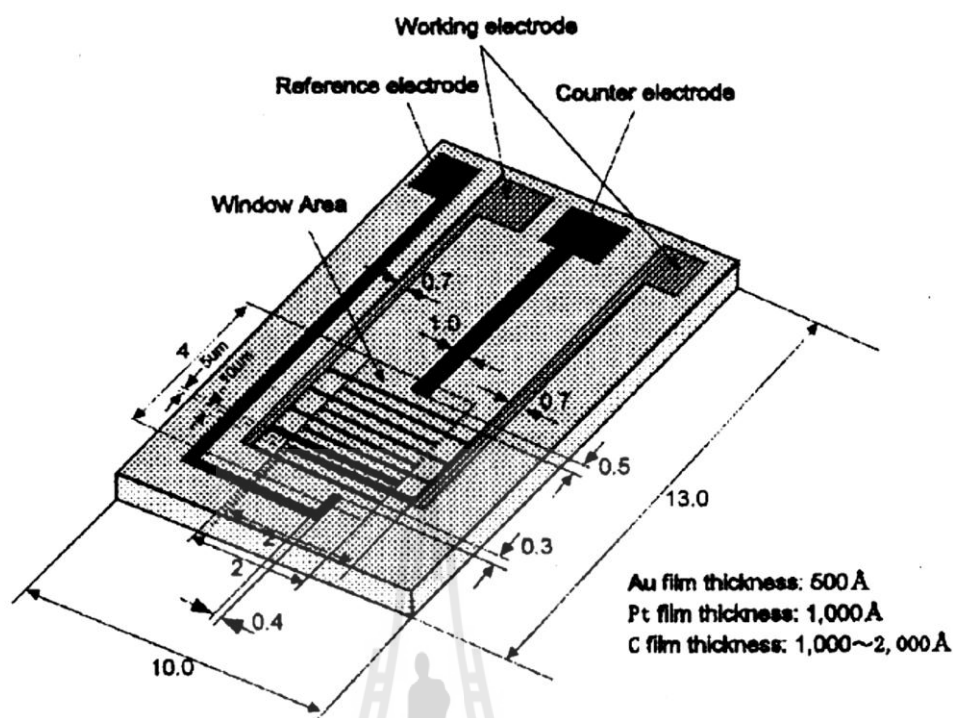


Figure 2.22 Schematic drawing of a carbon screen printed electrode (Rievaj, Dovalovská and Bustin, 2006).

When implementing microelectrodes into electrochemical microsystems all their beneficial properties such as enhanced mass transport, improved faradic-to-capacitive current, and decreased deleterious effects of solution resistance are of course available at the same time as small sample volumes can be traced (Wang and Freiha, 1982). The application of carbon fiber microelectrodes for small-volume voltammetry is an example of such an attempt (Troyer and Wightman, 2002). In this study the neurotransmitter dopamine is measured in a picoliter vial by means of voltammetry at the disc-shaped carbon fiber sensors. The vials were fabricated from fused-silica capillaries that provided a transparent small container suitable for the observation and manipulation of a biological cell, sample solutions, and electrodes.

As part of this thesis a novel small-volume electrochemical cell design was developed. The architecture of the own system will provide in Chapter IV.

2.4 References

- Akama, Y., Nishimura, E., Sakai, A. S., and Murakami, H. (1990). New scanning tunneling microscopy tip for measuring surface topography. **Journal of Vacuum Science & Technology A** 8(1): 429-433.
- Amatore, C. A., Jutand, A. and Pflüger, F. (1987). Nanosecond time resolved cyclic voltammetry: Direct observation of electrogenerated intermediates with bimolecular diffusion controlled decay using scan rates in the megavolt per second range. **Journal of Electroanalytical Chemistry and Interfacial Electrochemistry** 218(1-2): 361-365.
- Amatore, C. and Maisonhaute, E. (2005). When voltammetry reaches nanoseconds. **Analytical Chemistry** 77(15): 303A-311A.
- Amatore, C., Arbault, S., Guille, M., and Lemaitre, F. (2008). Electrochemical monitoring of single cell secretion: vesicular exocytosis and oxidative stress. **Chemical Reviews** 108(7): 2585-2621.
- Amatore, C., Thouin, L. and Warkocz, J. S. (1999). Artificial Neurons with Logical Properties Based on Paired-Band Microelectrode Assemblies. **Chemistry-A European Journal** 5(2): 456-465.
- Amemiya, S., Bard, A. J., Fan, F. F., Mirkin, M. V., and Unwin, P. R. (2008). Scanning electrochemical microscopy. **Annual Reviews of Analytical Chemistry** 1: 95-131.

- Amemiya, S., Guo, J., Xiong, H., and Gross, D. A. (2006). Biological applications of scanning electrochemical microscopy: chemical imaging of single living cells and beyond. **Analytical and Bioanalytical Chemistry** 386(3): 458-471.
- Armstrong-James M, Fox K, Millar J. (1980). A method for etching the tips of carbon fibre microelectrodes. **Journal of Neuroscience Methods** 2(4): 431-432.
- Armstrong-James, M. and Millar, J. (1979). Carbon fibre microelectrodes. **Journal of Neuroscience Methods** 1(3): 279-287.
- Avouris, P. and Wolkow, R. (1989). Atom-resolved surface chemistry studied by scanning tunneling microscopy and spectroscopy. **Physical Review B** 39(8): 5091.
- Bai, C. (1999). Scanning tunneling microscopy and its application. In G. Ertl, R. Gomer, H. Lüth, and D. L. Mills (eds.). **Surface Science** (2nd ed., pp. 1-32). Heidelberg: Springer.
- Bailey, F., Malinski, T., and Kiechle, F. (1991). Carbon-fiber ultramicroelectrodes modified with conductive polymeric tetrakis (3-methoxy-4-hydroxyphenyl) porphyrin for determination of nickel in single biological cells. **Analytical Chemistry** 63(4): 395-398.
- Ball, J. C., Scott, D. L., Lump, J. K., Daunert, S., Wang, J., and Bachas, L. G. (2000). Electrochemistry in nanovials fabricated by combining screen printing and laser micromachining. **Analytical Chemistry** 72(3): 497-501.
- Bard, A. J. and Faulkner, L. R. (2001). **Electrochemical Methods; Fundamentals and Application** (2nd ed.). New York: Chichester: John Wiley & Sons, Inc.

- Barker, A. L., Gonsalves, M., Macpherson, J. V., Slevin, C. J. and Unwin, P. R. (1999). Scanning electrochemical microscopy: beyond the solid/liquid interface. **Analytica Chimica Acta** 385(1): 223-240.
- Basha, C. A. and Rajendran, L. (2006). Theories of ultramicrodisc electrodes: review article. **International Journal of Electrochemical Science** 1: 268-282.
- Besenhard, J. O., Schulte, A., Schur, K., and Jannakoudakis, A. D. (1990). Preparation voltammetric and potentiometric carbon fibre microelectrode. In M. I. Montenegro, M. A. Queiros, and J. L. Daschbach (eds.). **Microelectrodes: Theory and Applications** (pp 189-204). Dordrecht, The Netherlands: Kluwer Academic Publishers.
- Biegelsen, D. K., Ponce, F. A., Tramontana, J. C., and Koch, S. M. (1987). Ion milled tips for scanning tunneling microscopy. **Applied Physics Letters** 50(11): 696-698.
- Biegelsen, D. K., Ponce, F. A., Tramontana, J. C., and Koch, S. M. (1987). Ion milled tips for scanning tunneling microscopy. **Applied Physics Letters** 50(11): 696-698.
- Binnig, G., Rohrer, H. Gerber, C., and Weibel E. (1982). Surface studies by scanning tunneling microscopy. **Physical Review Letters** 49: 57.
- Binnig, G., Rohrer, H. Gerber, C., and Weibel E. (1982). Tunneling through a controllable vacuum gap. **Applied Physics Letters** 40(2): 178.
- Bobrov, K., Mayne, A. J., and Dujardin, G. (2001). Atomic-scale imaging of insulating diamond through resonant electron injection. **Nature** 413: 616-619

- Bobrov, K., Soukiassian, L., Mayne, A. J., Dujardin, G., & Hoffman, A. (2002). Resonant electron injection as an atomic-scale tool for surface studies. **Physical Review B** 66(19), 195403.
- Bond, A. M. (1994). Past, present and future contributions of microelectrodes to analytical studies employing voltammetric detection. A review. **Analyst** 119(11): 1R-21R.
- Bond, A. M. and Thomas, F. G. (1988). Studies of adsorption processes in the absence of added electrolyte: phase changes in coumarin adsorbed at conventional and micro mercury electrodes. **Langmuir** 4(2): 341-345.
- Bonnell, D. A. (1993). Microscope Design and operation. In B. Dawn (ed.), **Scanning tunneling microscopy and Spectroscopy theory, techniques, and applications** (pp. 7-30). New York: VCH publisher, Inc.
- Borges, R., Camacho, M., and Gillis, K. D. (2008). Measuring secretion in chromaffin cells using electrophysiological and electrochemical methods. **Acta Physiologica** 192(2): 173-184.
- Cai, X., Glidle, A. and Cooper, J. M. (2000). Miniaturized electroanalytical sensor systems in micromachined structures. **Electroanalysis** 12(9): 631-639.
- Campbell, J. K., Sun, L., and Crooks, R. M. (1999). Electrochemistry using single carbon nanotubes. **Journal of the American Chemical Society** 121(15): 3779-3780.
- Chen, J. C. (1993). **Introduction to Scanning Tunneling Microscopy**. New York: Oxford University Press.
- Chen, S. and Kucernak, A. (2002). Fabrication of carbon microelectrodes with an effective radius of 1 nm. **Electrochemistry Communications** 4(1): 80-85.

- Chow, R. H., von Rüden, L., and Neher, E. (1992). Delay in vesicle fusion revealed by electrochemical monitoring of single secretory events in adrenal chromaffin cells. **Nature** 356: 60-63.
- Ciszkowska, M. and Stojek, Z. (2000). Peer Reviewed: Voltammetric and Amperometric Detection without Added Electrolyte. **Analytical Chemistry** 72(23): 754A-760A.
- Clark, R. A. and Ewing, A. G. (1998). Characterization of electrochemical responses in picoliter volumes. **Analytical Chemistry** 70(6): 1119-1125.
- Clark, R. A., Zerby, S. E. and Ewing, A. G. (1998). Electrochemistry in neuronal microenvironments. **Electroanalytical Chemistry** 20: 227-294.
- Collinson, M. M. and Wightman, R. M. (1995). Observation of individual chemical reactions in solution. **Science** 268(5219): 1883.
- Cox, J. T. and Zhang, B. (2012). Nanoelectrodes: recent advances and new directions. **Annual Review of Analytical Chemistry** 5: 253-272.
- Dai, H., Hafner, J. H., Rinzler, A. G., Colbert, D. T., and Smalley, R. E. (1996). Nanotubes as nanoprobes in scanning probe microscopy. **Nature** 384(6605): 147-150.
- Daniele, S. and Mazzocchin, G. A. (1993). Stripping analysis at mercury microelectrodes in the absence of supporting electrolyte. **Analytica Chimica Acta** 273(1): 3-11.
- Denault, G., Nagy, G. and Toth, K. (2001). **Scanning Electrochemical Microscopy** (2nd ed.). New York: Marcel Dekker.
- Devadoss, A. and Burgess, J. D. (2004). Steady-state detection of cholesterol contained in the plasma membrane of a single cell using lipid bilayer-modified

- microelectrodes incorporating cholesterol oxidase. **Journal of the American Chemical Society** 126(33): 10214-10215.
- Edmonds, T. E., Dean, J. R., and Latif, S. (1988). Potentiometric and voltammetric responses of carbon fibre electrodes. **Analytica Chimica Acta** 212: 23-30.
- Eggle, R. (1977). Anodic stripping coulometry at a thin-film mercury electrode. **Analytica Chimica Acta** 91(2): 129-138.
- El-Giar, E. E. D. M. and Wipf, D. O. (2006). Preparation of tip-protected poly(oxyphenylene) coated carbon-fiber ultramicroelectrodes. **Electroanalysis** 18(23): 2281-2289.
- Feeney, R. and Kounaves, S. P. (2000). Microfabricated ultramicroelectrode arrays: Developments, advances, and applications in environmental analysis. **Electroanalysis** 12(9): 677-684.
- Feenstra, R. M. and Fein, A. P. (1985). Surface morphology of GaAs(110) by scanning tunneling microscopy. **Physical Review B** 32: 1394.
- Feenstra, R. M. and Fein, A. P. (1985). Surface morphology of GaAs (110) by scanning tunneling microscopy. **Physical Review B** 32(2): 1394.
- Fleischmann, M., Pons, S., Rolinson, D. R. and Schmidt, P. P. (1988). **Ultramicroelectrodes**. Morganton, North Carolina: Datatech Systems
- Forster, R. J. (1994). Microelectrodes: new dimensions in electrochemistry. **Chemical Society Reviews** 23(4): 289-297.
- Frenzel, W. (1987). Electrochemical stripping with carbon fiber electrodes in a microliter-capacity cell. **Analytica Chimica Acta** 196: 141-152.

- Garnaes, J., Kragh, F., Mo, K. A., and Thölen, A. R. (1990). Transmission electron microscopy of scanning tunneling tips. **Journal of Vacuum Science & Technology A** 8(1): 441-444.
- Gewirth, A. A., Craston, D. H., and Bard, A. J. (1989). Fabrication and characterization of microtips for in situ scanning tunneling microscopy. **Journal of Electroanalytical Chemistry and Interfacial Electrochemistry** 261(2): 477-482.
- Golaś, J. and Osteryoung, J. (1986). Carbon-fiber micro-electrodes as substrates for mercury films. **Analytica Chimica Acta** 186: 1-9.
- Hamers, R. J. and Padowitz, D. F. (2001). Methods of tunneling spectroscopy with the STM. In D. A. Bonnell (ed.), **Scanning Probe Microscopy and Spectroscopy: Theory, Techniques, and Applications** (2nd ed.). New York: Wiley-VCH, Inc.
- Hayashi, K. and Niwa O.(2002). Measurement of biomolecules in the brain and neurotransmitters released from cells using electrochemical sensing systems. **Bunseki Kagaku** 51(1): 1-12.
- Heben, M. J. (1990). **Scanning tunneling microscopy in electrochemical environments**. California California Institute of Technology.
- Heckl, W. M. (1993). Scanning tunneling microscopy and spectroscopy. theory, techniques, and applications. In D. A. Bonnell (ed.). **Angewandte Chemie International Edition in English** (pp. 2226-2227). New York: VCH Publishers, Inc.
- Heien, M. L. A. V., Johnson, M. A. and Wightman, R. M. (2004). Resolving neurotransmitters detected by fast-scan cyclic voltammetry. **Analytical Chemistry** 76(19): 5697-5704.

- Heinze, J. (1993). Ultramicroelectrodes in electrochemistry. **Angewandte Chemie International Edition in English** 32(9): 1268-1288.
- Heinze, J. (1993). Ultramicroelectrodes in electrochemistry. **Angewandte Chemie International Edition in English** 32(9): 1268-1288.
- Heinze, S., Bode, M., Kubetzka, A., Pietzsch, O., Nie, X., Blügel, S. and Wiesendanger, R. (2000). Real-space imaging of two-dimensional antiferromagnetism on the atomic scale. **Science** 288(5472): 1805-1808.
- Hermans, A. and Wightman, R. M. (2006). Conical tungsten tips as substrates for the preparation of ultramicroelectrodes. **Langmuir** 22(25): 10348-10353.
- Howell, J. O. and Wightman, R. M. (1984). Ultrafast voltammetry and voltammetry in highly resistive solutions with microvoltammetric electrodes. **Analytical Chemistry** 56(3): 524-529.
- Hübner, B., Koops, H. W. P., Pagnia, H., Sotnik, N., Urban, J., and Weber, M. (1992). Tips for scanning tunneling microscopy produced by electron-beam-induced deposition. **Ultramicroscopy** 42: 1519-1525.
- Hudrová, L. and Štulík, K. (1972). A contribution to the problem of increasing the sensitivity of anodic-stripping voltammetry. **Talanta** 19(11): 1285-1293.
- Joost, F. (2004). **Principle of scanning probe microscopy** [On-line]. Available: <http://www.physics.leidenuniv.nl/sections/cm/ip/group/PrincipleofSPM.htm>.
- Julian, C. (1993). **Introduction to scanning tunneling microscopy**. New York: Oxford university press.
- Karolczak, M., Dreiling, R., Adams, R., Felice, L. and Kissinger, P. (1976). Electrochemical techniques for study of phenolic natural products and drugs in microliter volumes. **Analytical Letters** 9(9): 783-793.

- Kashyap, R. and Gratzl, M. (1998). Electrochemistry in microscopic domains. 1. The electrochemical cell and its voltammetric and amperometric response. **Analytical Chemistry** 70(8): 1468-1476.
- Kawagoe, K. T., Zimmerman, J. B. and Wightman, R. M. (1993). Principles of voltammetry and microelectrode surface states. **Journal of Neuroscience Methods** 48(3): 225-240.
- Kelly, R. S. and Wightman, R. M. (1986). Bevelled carbon-fiber ultramicroelectrodes. **Analytica Chimica Acta** 187: 79-87.
- Kim, P., Kim, J. H., Jeong, M. S., Ko, D. K., Lee, J., and Jeong, S. (2006). Efficient electrochemical etching method to fabricate sharp metallic tips for scanning probe microscopes. **Review of Scientific Instruments** 77(10): 103706.
- Koh, D. S. and Hille, B. (1999). Rapid fabrication of plastic-insulated carbon-fiber electrodes for micro-amperometry. **Journal of Neuroscience Methods** 88(1): 83-91.
- Kolb, D., Engelmann, G. and Ziegler, J. (2000). Nanoscale decoration of electrode surfaces with an STM. **Solid State Ionics** 131(1): 69-78.
- Koudelka-Hep, M. and van der Wal, P. D. (2000). Microelectrode sensors for biomedical and environmental applications. **Electrochimica Acta** 45(15): 2437-2441.
- Li, J., Schneider, W. D., Crampin, S. and Berndt, R. (1999). Tunneling spectroscopy of surface state scattering and confinement. **Surface Science** 422(1): 95-106.
- Li, Q. and White, H. S. (1995). Interferometric measurement of depletion layer structure and voltammetric data in concentrated organic redox solutions. **Analytical Chemistry** 67(3): 561-569.

- Li, T. and Hu, W. (2011). Electrochemistry in nanoscopic volumes. **Nanoscale** 3(1): 166-176.
- Li, X., Geng, Q., Wang, Y., Si, Z., Jiang, W., Zhang, X., and Jin, W. (2007). Micropatterning of active enzyme with a high-resolution by scanning electrochemical microscopy coupled with a nanometer-sized carbon fiber disk tip. **Electrochimica Acta** 53(4): 2016-2024.
- Lion, N., Rohner, T. C., Dayon, L., Arnaud, I. L., Damoc, E., Youhnovski, N., Wu, Z. Y., Roussel, C., Josserand, J. and Jensen, H. (2003). Microfluidic systems in proteomics. **Electrophoresis** 24(21): 3533-3562.
- Liu, Y., He, R., Zhang, Q. and Chen, S. (2010). Theory of electrochemistry for nanometer-sized disk electrodes. **The Journal of Physical Chemistry C** 114(24): 10812-10822.
- Loeb, G., Peck, R. and Martyniuk, J. (1995). Toward the ultimate metal microelectrode. **Journal of Neuroscience Methods** 63(1): 175-183.
- Malmsten, R. A. and White, H. S. (1986). Voltammetric studies beyond the solvent limits with microelectrodes. **Journal of the Electrochemical Society** 133(5): 1067-1068.
- Malmsten, R. A., Smith, C. P. and White, H. S. (1986). Electrochemistry of concentrated organic redox solutions. **Journal of Electroanalytical Chemistry and Interfacial Electrochemistry** 215(1): 223-235.
- Math, F. and Marianneau, G. (1994). A new method for manufacturing carbon-fibre microelectrodes. **Journal of Neuroscience Methods** 52(2): 149-151.

- McNally, M. and Wong, D. K. (2001). An in vivo probe based on mechanically strong but structurally small carbon electrodes with an appreciable surface area. **Analytical Chemistry** 73(20): 4793-4800.
- Mellander, L., Cans, A. S., and Ewing, A. G. (2010). Electrochemical probes for detection and analysis of exocytosis and vesicles. **ChemPhysChem** 11(13): 2756-2763.
- Messner, J. L. and Engstrom, R. C. (1981). Capillary packed-bed electrodes for microanalysis. **Analytical Chemistry** 53(1): 128-130.
- Meulemans, A., Poulain, B., Baux, G., Tauc, L., and Henzel, D. (1986). Micro carbon electrode for intracellular voltammetry. **Analytical Chemistry** 58(9): 2088-2091.
- Michael, A. and Wightman, R. (1996). **Laboratory Techniques in Electroanalytical Chemistry**: New York: Marcel Dekker, Inc.
- Millar, J. and Pelling, C. W. A. (2001). Improved methods for construction of carbon fibre electrodes for extracellular spike recording. **Journal of Neuroscience Methods** 110(1): 1-8.
- Miller, B. and Bruckenstein, S. (1974). Rotating disk electrode voltammetry using small sample volumes. **Analytical Chemistry** 46(13): 2033-2035.
- Mirkin, M. V., Fan, F. R. F. and Bard, A. J. (1992). Scanning electrochemical microscopy part 13. Evaluation of the tip shapes of nanometer size microelectrodes. **Journal of Electroanalytical Chemistry** 328(1): 47-62.
- Mirkin, M. V., Liu, B., and Rotenberg S. A. (2002). Probing redox activity of human breast cells by scanning electrochemical microscopy. In C. K. Sen and L. Packer (eds.). **Redox Cell Biology and Genetics Part A** 352(A): 112-122.

- Morris, R. B., Fischer, K. F. and White, H. S. (1988). Electrochemistry of organic redox liquids. Reduction of 4-cyanopyridine. **The Journal of Physical Chemistry** 92(18): 5306-5313.
- Morris, R. B., Franta, D. J. and White, H. S. (1987). Electrochemistry at platinum bane electrodes of width approaching molecular dimensions: breakdown of transport equations at very small electrodes. **The Journal of Physical Chemistry** 91(13): 3559-3564.
- Mousa, M. S. (1996). Electron emission from carbon fibre tips. **Applied Surface Science** 94: 129-135.
- Myland, J. C. and Oldham, K. B. (1993). General theory of steady-state voltammetry. **Journal of Electroanalytical Chemistry** 347(1-2): 49-91.
- Nagahara, L. A., Thundat, T., and Lindsay, S. M. (1989). Preparation and characterization of STM tips for electrochemical studies. **Review of Scientific Instruments** 60(10): 3128-3130.
- Nakamura, Y., Mera, Y., & Maeda, K. (1999). A reproducible method to fabricate atomically sharp tips for scanning tunneling microscopy. **Review of Scientific Instruments**, 70(8): 3373-3376.
- Nirmaier, H. P., & Henze, G. (1997). Characteristic behavior of macro-, semimicro- and microelectrodes in voltammetric and chronoamperometric measurements. **Electroanalysis** 9(8): 619-624.
- Norton, J. D., White, H. S. and Feldberg, S. W. (1990). Effect of the electrical double layer on voltammetry at microelectrodes. **The Journal of Physical Chemistry** 94(17): 6772-6780.

- Nyholm, L. and Wikmark, G. (1993). Anodic stripping voltammetry of copper at ex situ-formed mercury-coated carbon fibre microelectrodes in the presence of low concentrations of supporting. **Analytica Chimica Acta** 273(1): 41-51.
- Ohmori, T., Nagahara, L. A., Hashimoto, K. and Fujishima, A. (1993). Characterization of carbon material as a scanning tunneling microscopy tip for in situ electrochemical studies. **Review of Scientific Instruments** 65: 404-406.
- Ohmori, T., Nagahara, L. A., Hashimoto, K., and Fujishima, A. (1994). Characterization of carbon material as a scanning tunneling microscopy tip for in situ electrochemical studies. **Review of Scientific Instruments** 65(2): 404-406.
- Pałys, M. J., Sokolowska, H. and Stojek, Z. (2004). Voltammetric investigation of formation of complexes in low ionic strength environments: Theoretical description and modeling. **Electrochimica Acta** 49(22): 3765-3774.
- Pałys, M. J., Stojek, Z., Bos, M. and van der Linden, W. E. (1997). Voltammetric investigation of the complexation equilibria in the presence of a low level of supporting electrolyte Part 1: Steady-state current-potential curves for inert complexes. **Analytica Chimica Acta** 337(1): 5-28.
- Paredes, J. I., Martinez-Alonso, A. and Tascón, J. M. D. (2002). Scanning probe microscopies for the characterization of porous solids: strengths and limitations. **Surface Science and Catalysis** 144: 1-10
- Paulson, S. C., Okerlund, N. D. and White, H. S. (1996). Diffusion currents in concentrated redox solutions. **Analytical Chemistry** 68(4): 581-584.

- Penner, R. M., Heben, M. J. and Lewis, N. S. (1989). Preparation and electrochemical characterization of conical and hemispherical ultramicroelectrodes. **Analytical Chemistry** 61(15): 1630-1636.
- Pletcher, D. (1991). Why microelectrodes?. In M. I. Montenegro, M. A. Queiros, and J. L. Daschbach (eds.). **Microelectrodes: Theory and Application**. Boston: Kluver Academic Publisher.
- Pons, S. and Fleischmann, M. (1987). The Behavior of Microelectrodes. **Analytical Chemistry** 59(24): 1391A-1399.
- Qiu, X., Wang, C., Zeng, Q., Xu, B., Yin, S., Wang, H., Xu, S. and Bai, C. (2000). Alkane-assisted adsorption and assembly of phthalocyanines and porphyrins. **Journal of the American Chemical Society** 122(23): 5550-5556.
- Ragsdale, S. R. and White, H. S. (1997). Analysis of voltammetric currents in concentrated organic redox solutions using the Cullinan-Vignes equation and activity-corrected mutual diffusion coefficients. **Journal of Electroanalytical Chemistry** 432(1-2): 199-203.
- Rickart, M. and Bauer, M. (1998). An improved tip etch procedure for reproducible sharp STM tips. In B. Hillebrands (ed.). **Annual Report 1998** (pp. 53-55) Kaiserstautern: Fachbereich Physik Universität Kaiserstautern.
- Rievaj, M., Dovalovská, Z. and Bustin, D. (2006). Trace analysis of lead by anodic stripping voltammetry with collection at interdigitated microelectrodes in small-volume samples. **Chemical Papers** 60(2): 111-115.
- Rohlfing, D. F. and Kuhn, A. (2007). Scanning tunneling microscopy of electrode surfaces using carbon composite tips. **Electroanalysis** 19(2-3):, 121-128.

- Rohlfing, D. F. and Kuhn, A. (2007). Scanning tunneling microscopy of electrode surfaces using carbon composite tips. **Electroanalysis** 19(2-3): 121-128.
- Rohrer, G. (1993). The preparation of tip and sample surfaces for STM experiments. In A. B. Dawn (ed.), **Scanning Tunneling Microscopy and Spectroscopy Theory, Techniques, and Applications**. New York: VCH publisher, Inc.
- Rucki, R. J. (1980). Electrochemical detectors for flowing liquid systems. **Talanta** 27(2): 147-156.
- Schindler, W., Hofmann, D. and Kirschner, J. (2001). Localized electrodeposition using a scanning tunneling microscope tip as a nanoelectrode. **Journal of the Electrochemical Society** 148(2): C124-C130.
- Schulte, A. (1994). **Preparation and characterization of different types of ultramicro-electrodes: A contribution to the development of novel microsensors for electro-chemical bio- and trace analysis and various methods of scanning probe microscopy**. Ph.D. Thesis, University of Muenster, Germany.
- Schulte, A. and Chow, R. H. (1996). A simple method for insulating carbon-fiber microelectrodes using anodic electrophoretic deposition of paint. **Analytical Chemistry** 68(17): 3054-3058.
- Schulte, A. and Chow, R. H. (1998). Cylindrically etched carbon-fiber microelectrodes for low-noise amperometric recording of cellular secretion. **Analytical Chemistry** 70(5): 985-990.
- Schulte, A., Nebel, M., and Schuhmann, W. (2010). Scanning electrochemical microscopy in neuroscience. **Annual Reviews of Analytical Chemistry** 3: 299-318.

- Siegenthaler, H. (1999). STM in electrochemistry. In R. Wiesendanger and H-J. Günterodt (eds.). **Scanning Tunneling Microscopy II**. Berlin: Springer-Verlag.
- Slevin, C. J., Gray, N. J., Macpherson, J. V., Webb, M. A. and Unwin, P. R. (1999). Fabrication and characterisation of nanometre-sized platinum electrodes for voltammetric analysis and imaging. **Electrochemistry Communications** 1(7): 282-288.
- Smith, P., Haydon, P., Hengstenberg, A. and Jung, S. K. (2001). Analysis of cellular boundary layers: application of electrochemical microsensors. **Electrochimica Acta** 47(1): 283-292.
- Sonnenfeld, R., and Hansma, P. K. (1986). Atomic-resolution microscopy in water. **Science** 232(4747): 211-213.
- Stamford, J. A. (1986). Effect of electrocatalytic and nucleophilic reactions on fast voltammetric measurements of dopamine at carbon fiber microelectrodes. **Analytical Chemistry** 58(6): 1033-1036.
- Stevenson, K. J. and White, H. S. (1996). Electrochemistry of Organic Redox Liquids at Elevated Pressures. **The Journal of Physical Chemistry** 100(48): 18818-18822.
- Strein, T. G. and Ewing, A. G. (1992). Characterization of submicron-sized carbon electrodes insulated with a phenol-allylphenol copolymer. **Analytical Chemistry** 64(13): 1368-1373.
- Strein, T. G. and Ewing, A. G. (1992). Characterization of submicron-sized carbon electrodes insulated with a phenol-allylphenol copolymer. **Analytical Chemistry** 64(13): 1368-1373.

- Stulik, K., Amatoe, C., Holab, K., Marecek, V. and Kutner, W. (2000). Microelectrodes, definitions, characterization, and applications. **Pure and Applied Chemistry** 72(8): 1483-1492.
- Swiergiel, A. H., Palamarchouk, V. S., and Dunn, A. J. (1997). A new design of carbon fiber microelectrode for in vivo voltammetry using fused silica. **Journal of Neuroscience Methods** 73(1): 29-33.
- Tel-Vered, R., Walsh, D. A., Mehrgardi, M. A., and Bard, A. J. (2006). Carbon nanofiber electrodes and controlled nanogaps for scanning electrochemical microscopy experiments. **Analytical Chemistry** 78(19): 6959-6966.
- Tercier, M. L. and Buffle, J. (1993). In situ voltammetric measurements in natural waters: Future prospects and challenges. **Electroanalysis** 5(3): 187-200.
- Tersoff, J. and Lang, N. D. (1993). Theory of Scanning Tunneling Microscopy. In J. A. Stroscio and W. J. Kaiser (eds.), **Scanning Tunneling Microscopy**. SanDiego, CA: Academic Press.
- Troyer, K. P. and Wightman, R. M. (2002). Dopamine Transport into a Single Cell in a Picoliter Vial. **Analytical Chemistry** 74(20): 5370-5375.
- Walter, R., Vandaveer, I. and Fritsch, I. (2002). Measurement of ultrasmall volumes using anodic stripping voltammetry. **Analytical Chemistry** 74(14): 3575-3578.
- Wang, C. L., Creasy, K. E., and Shaw, B. R. (1991). Ring-modified carbon fiber microelectrodes and multi-microelectrode devices. **Journal of Electroanalytical Chemistry and Interfacial Electrochemistry** 300(1): 365-375.
- Wang, J. and Freiha, B. A. (1982). Microelectrolytic cell for voltammetric analysis. **Analytical Chemistry** 54(2): 334-336.

- Wang, J. and Zadeii, J. M. (1988). Anodic stripping voltammetry at ultramicroelectrodes for metal speciation studies in aqueous solutions of low ionic strength. **Journal of Electroanalytical Chemistry and Interfacial Electrochemistry** 246(2): 297-305.
- Wang, W., Zhang, S. H., Li, L. M., Wang, Z. L., Cheng, J. K., and Huang, W. H. (2009). Monitoring of vesicular exocytosis from single cells using micrometer and nanometer-sized electrochemical sensors. **Analytical and Bioanalytical Chemistry** 394(1): 17-32.
- Widera, J., Steinecker, W., Pacey, G. and Cox, J. (2003). Voltammetry in electrolyte-free liquids using a three-electrode probe with a sol-gel matrix. **Journal of Applied Electrochemistry** 33(1): 121-124.
- Wiesendanger, R. and Güntherodt, H. J. (1994). **Introduction Scanning Tunneling Microscopy I** (2nd ed.). Berlin, Germany: Springer-Verlag.
- Wightman, R. M. (1981). Microvoltammetric electrodes. **Analytical Chemistry** 53(9): 1125A-1134A.
- Wightman, R. M. (1981). Microvoltammetric Electrodes. **Analytical Chemistry** 53: 1125A-1134A.
- Wightman, R. M. and Wipf, D. O. (1989). Voltammetry at ultramicroelectrodes. In A. J. Bard (Ed.), **Electroanalytical Chemistry** (Vol. 15, pp. 268-353). New York: Marcel Dekker, Inc.
- Wightman, R. M., Runnels, P. and Troyer, K. (1999). Analysis of chemical dynamics in microenvironments. **Analytica Chimica Acta** 400(1): 5-12.

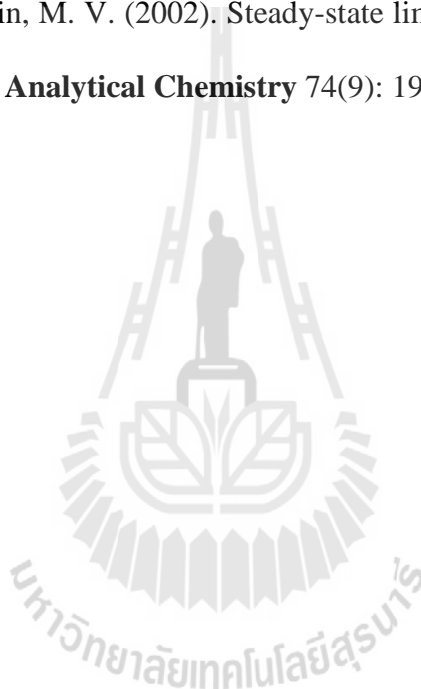
- Wipf, D. O., Kristensen, E. W., Deakin, M. R. and Wightman, R. M. (1988). Fast-scan cyclic voltammetry as a method to measure rapid heterogeneous electron-transfer kinetics. **Analytical Chemistry** 60(4): 306-310.
- Wong, D. K. and Xu, L. Y. (1995). Voltammetric studies of carbon disk electrodes with submicrometer-sized structural diameters. **Analytical Chemistry** 67(22): 4086-4090.
- Wong, D. K. Y. and Ewing, A. G. (1990). Anodic stripping voltammetry at mercury films deposited on ultrasmall carbon-ring electrodes. **Analytical Chemistry** 62(24): 2697-2702.
- Xin, Q. and Wightman, R. M. (1998). Simultaneous detection of catecholamine exocytosis and Ca^{2+} release from single bovine chromaffin cells using a dual microsensor. **Analytical Chemistry** 70(9): 1677-1681.
- Yum, K., Cho, H. N., Hu, J. and Yu, M. F. (2007). Individual nanotube-based needle nanoprobe for electrochemical studies in picoliter microenvironments. **ACS Nano** 1(5): 440-448.
- Zhang, X. G. and Stimming, U. (1990). Scanning tunneling microscopy of copper corrosion in aqueous perchloric acid. **Corrosion Science** 30(8): 951-954.
- Zhang, X., Zhang, W., Zhou, X., and Ogorevc, B. (1996). Fabrication, characterization, and potential application of carbon fiber cone nanometer-size electrodes. **Analytical Chemistry** 68(19): 3338-3343.
- Zhao, G., Giolando, D. M., and Kirchoff, J. R. (1995). Chemical vapor deposition fabrication and characterization of silica-coated carbon fiber ultramicroelectrodes. **Analytical Chemistry** 67(15): 2592-2598.

Zoski, C. and Vanysek, P. (1996). Modern techniques in electroanalysis. **Chemical Analysis Series** 139: 241.

Zoski, C. G. (2002). Ultramicroelectrodes: design, fabrication, and characterization. **Electroanalysis** 14(15-16): 1041-1051.

Zoski, C. G. (2002). Ultramicroelectrodes: design, fabrication, and characterization. **Electroanalysis** 14(15-16): 1041-1051.

Zoski, C. G. and Mirkin, M. V. (2002). Steady-state limiting currents at finite conical microelectrodes. **Analytical Chemistry** 74(9): 1986-1992.



CHAPTER III

CONICAL CARBON FIBER

ULTRAMICROELECTRODES AS IMAGING TOOL FOR

SCANNING TUNNELING MICROSCOPY AND

SENSORS FOR VOLTAMMETRY

Abstract

Microscopically small electrodes with electroactive dimensions in the micro- and nanometer range are nowadays routinely used tools for modern electroanalysis and surface science with electrochemical probe microscopes. Within this project novel procedures for the preparation of needle-type carbon UMEs with conical geometry of the exposed conductive carbon surface have been developed. A simple DC etching procedure in NaOH solution provided in a first step narrowed single carbon fibers with well-formed nanocones at their bottom. Coating the carbon fiber stems but not the end of the tips of the carbon cones effectively with electrodeposition paint (EDP) layers limited the bare carbon to the foremost end and restricted the faradaic current response due to interfacial redox activity to exactly this area. The established conical carbon micro- and nanoelectodes adequately displayed the expected sigmoidal voltammograms of the dissolved redox mediator ruthenium hexamine chloride and proved their quality in terms of insulation stability. As probes in ambient and ultrahigh vacuum (UHV) scanning tunneling microscopy (STM)

devices insulation-free carbon tips allowed high quality STM imaging. The Si(111) surface, for instance, was imaged in UHV with clear atomic resolution. Carbon tips for electrochemical (“in situ”) STM studies in electrolytes (EC-STM tips), prepared via electrochemical etching of carbon fibers and subsequent tip-sparing insulation, were electrochemically stable in acidic electrolyte and allowed high resolution in situ imaging of both the bare Au (111) electrode surface and of Au (111) that was covered with a monolayer of the organic molecule octyl-triazatriangulenium. The inherent simplicity of the production of the CF-based voltammetry and probe microscopy sensors of this study is a clear advantages over published other options, in particular over those handling carbon nanotubes, which are especially hard to work with even in an optical microscope setting. More important positive feature of the novel carbon EC-STM tips is their wide potential window which allows them to be used at so far not assessable combinations of tip and substrate working potentials. All assets together give the accomplished CF-based sensors the potential to be used by the community of users as probes for interesting new STM-based imaging, spectroscopy and surface modification experiments. Positive tip potentials, for instance, can be reached that are impossible with the most frequently used tungsten tips because of surface oxide formation and related loss of good enough conductivity for the electron tunneling process. It is thus feasible to expect that the carbon probes will facilitate a number of exciting new STM studies at conductor/electrolyte interfaces.

3.1 Introduction

As discussed in Chapter II, the conical geometry of UMEs can be useful for many electrochemical applications, one of which is the use as scanned probe tip for in situ STM-based surface inspection with up to atomic resolution. Here, the focus was the preparation of carbon fiber-based conical carbon UMEs and then the exploration of their suitability to act as probe tip for STM experiments under various conditions, including measurements in air, UHV and the electrochemical environment. A first requisite on the road to success was the access to conical carbon tips that are sharp enough to support the flow of a tunneling current between the terminating carbon atom and a neighboring atom on the conducting sample surface. Important first step was thus also tapered carbon fiber preparation. The prepared tip structure had to be rigid enough not to suffer from mechanical or thermal vibration to an extent prohibiting in the later STM application formation of a stable tunneling contact to the conducting sample of choice. Also important is the cleanness of the produced tip structures since presence of contaminants like insulating oxides or etching byproducts could alter tip conductivity and/or geometry and again work against good STM performance (Bonnell, 1993; Chen, 1993; Joost, 2004; Julian, 1993; Rohrer, 1993; Tersoff and Lang, 1993; Wiesendanger and Güntherodt, 1995).

The carbon fiber-based novel STM probes should be considered as complementary not replacing alternatives to the metallic options that are already available since long. In particular platinum tips suffer at higher working potentials from the onset of cathodic or anodic gas evolution (H_2/O_2) from water reduction/oxidation, also known as water electrolysis. The related faradaic currents are disturbing factors in the accurate acquisition of the tunneling current through the

tip-substrate gap and, if too large, STM measurements are not possible at all. Carbon is known to have large overpotentials for the electrolysis of water and STM tips made of that material should thus be beneficial in terms of a disturbance of the tunneling current by redox contributions.

In the following a detailed explanation of the procedures used for tapered CF tip preparation, CF tip insulation will be provided. Also, the characterization of freshly prepared CF tips by SEM and voltammetry is part of this chapter and finally the results of a CF tip employment as bare and insulated STM tips for imaging experiments in air, UHV, and in electrolytes will be reported and discussed in terms of quality.

3.2 Experimental and methods

3.2.1 Conical CF UMEs: Fabrication and characterization

3.2.1.1 Electrochemical carbon fiber tip etching

Four different kinds of CFs were used as precursors for the electrochemical etching procedure that was meant to produce the desired tapered CF structures with nanometric tip apertures, namely the P100 (Union Carbide, Houston, USA), M40 (Cytec, New Jersey, USA), T300 (Cytec, New Jersey, USA) and E/XAS (SGL TECHNIK GmbH, Meitingen, Germany). The diameter of the P100, a pitch-based carbon fiber, is about 10 μm while the M40, T300 are 3.5 - 5, and the E/XAS is 5 - 7 μm in diameter, respectively. Prior to use, all carbon fibers were kept in acetone (99.8%, Carlo Erba, Italy) for 5 days to remove the thin polymer coating (“sizing”) which is usually applied in the last step of the carbon fiber manufacture as protection against damage during handling and processing (e.g. weaving) into intermediate

forms. Bundles of cleaned CFs were rinsed with deionized (DI) water and then gently mopped by soft tissue paper and left at room temperature for a few hours to dry. A sharp needle was used to pick up a single filament of a CF from the fiber bundle using a small drop of conductive carbon paint (SPI supplies, West Chester, PA, USA) as gluing material. The CF was then cut to the desired length (e.g. 3 mm long) before it was transferred to one end of a few cm long copper (Cu) or tungsten (W) wire (0.25 mm diameter, 99.99% purity, Goodfellow, England) that served as holding wire. Again, conductive carbon paint was the sticking glue to make an electrical contact between the wire and the fiber. Figure 3.1 displays a schematic representation of the established CF/Cu wire structure.

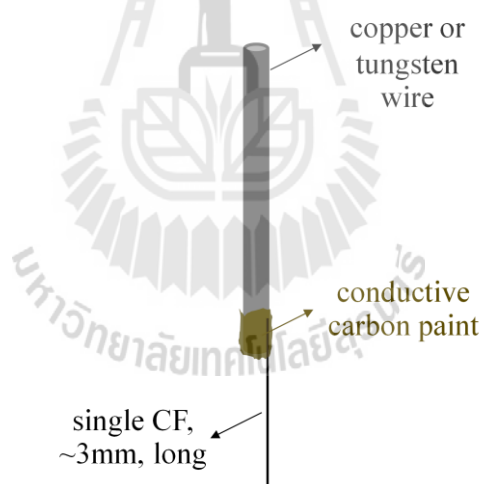


Figure 3.1 Illustration of a single carbon fiber/tungsten wire assembly as used as precursor for conical CF UME fabrication.

Following published CF etching recipes (Mousa, 1996; Schulte, 1993), a 0.1 M sodium hydroxide (NaOH, anhydrous pellet, 97% purity, Carlo Erba, Italy) was selected as preferred electrochemical etching electrolyte.

Pointed carbon fibers were formed by an electrochemical etching procedure that was executed in a one-compartment cell at room temperature by applying the desired voltage for etching in the directing current (DC) mode from a function generator (Agilent® 3322A 20Hz function/arbitrary wave form generator, USA).

Actually, the single carbon fiber at the copper wire acted as working electrode. Counter electrode (CE) was a platinum (Pt) wire of ring shape that saw the CF to be etched placed in its center and thus uniformly exposed all around by the electrical field. The two-electrode configuration for etching is shown in the two photographs of Figure 3.2. After etching, the resulting tapered carbon fibers were rinsed with water and stored in a safe container for the later characterization by means of a scanning electron microscopy (SEM) (e.g. see, for instance, Figure 3.4).

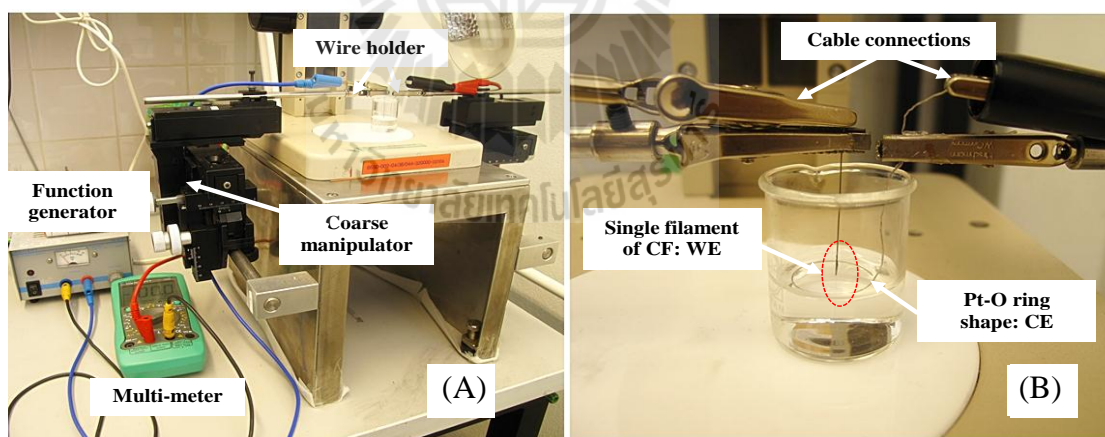


Figure 3.2 Setup used for the electrochemical etching of carbon fibers with the aim of tip formation.

The setup that was used for the electrochemical etching of carbon fibers with DC voltage with the aim of conical tip formation. A single filament of CF was immersed into the etching solution with the aid of a coarse micromanipulating device.

3.2.1.2 Cathodic electrodeposition paint application to etched carbon fiber tips

The cathodic electrophoretic paint (EDP) Clearclad[®] HRS C/F (L/D) (LHV Coating Limited, Birmingham, England) supplied an electrochemical polymer deposition system that was suitable for coating carbon fibers with a uniform and thin insulation layer that did not make the fiber structure significantly thicker.

Etched CFs from the electrochemical etching step were coated with cathodic electrophoretic deposition paint in a one-compartment cell at room temperature by applying the desired deposition voltage with a function generator (Agilent[®] 3322A 20Hz function/Arbitrary wave form generator) operated in the DC mode. Counter electrode (CE) and EDP paint container at the same time was in the procedure a rolled-up piece of Pt foil with a “o”-shaped cross section. The length of the Pt trough was about 4 mm long and the diameter about 2 mm (refer to Figure 3.3).

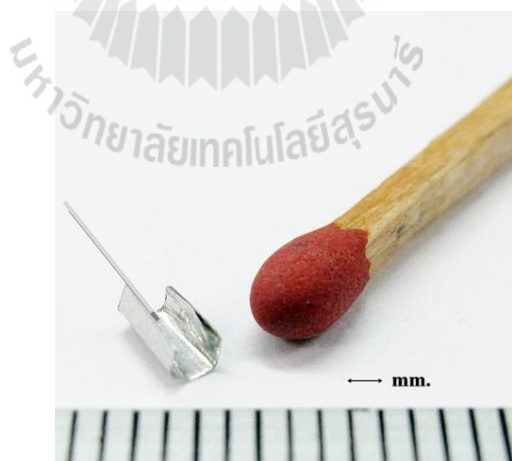


Figure 3.3 Photograph of the rolled up Pt foil with a “o” shaped cross section that was used as counter electrode and trough for the EDP paint application to CFs.

A “u” shaped cross section that was used as counter electrode and trough for the EDP paint insulation of CFs. To allow a size estimation the end of a match stick and a mm scale are shown, too.

Working electrode (cathode) was the etched CF to be EDP paint insulated all along the cylindrical face but not at the tip front to keep a tiny conical carbon surface exposed as UME structure. A heat-treatment in a universal laboratory oven (Model UFB 400) operated at elevated temperature (190 – 195 °C) transferred the fresh and thus still wet electrodeposition paint into a tightly adhering uniform coating that was found to be pore-free, well insulating and chemically resistant to common aqueous electrolytes.

3.2.1.3 Silicone insulation of the CF/holding wire junction

The cathodic paint insulated well the CF but because it was thin on the low micrometer scale it was not effective for protecting the CF/metal wire junction with its sharp edges from contact with electrolytes. This critical region of the structure was thus sealed additionally into a thicker layer of a two-component silicone elastomer (Sylgard[®] 184 silicone elastomer kit, Dow Corning, USA). The simple procedure used to apply the silicon rubber coating to the CF/wire junction is described in the “3.4. Results and Discussion” section; needed were a coarse manipulator that supported movement of the CF/wire assembly in 3 dimensions (x, y, z), and a plastic tube which was cut into half to form a small trough for the liquid mixture of the two components forming the silicone rubber upon heat treatment. Heat-curing into a silicone rubber was actually facilitated by the hot air stream of heat gun and formed a

transparent polymer encapsulant with good electrical resistance. To ensure definite insulation of the junction the silicone application was repeated three times.

3.2.1.4 Optical and electrochemical characterization of CF tips

Etched carbon fibers and completed conical CFUMEs were inspected with respect to tip dimension and integrity of insulation with a scanning electron microscope (SEM) (either a “JEOL JSM-840A scanning microscope” or a “GEMINI Leo 1530” (Figure 3.4).

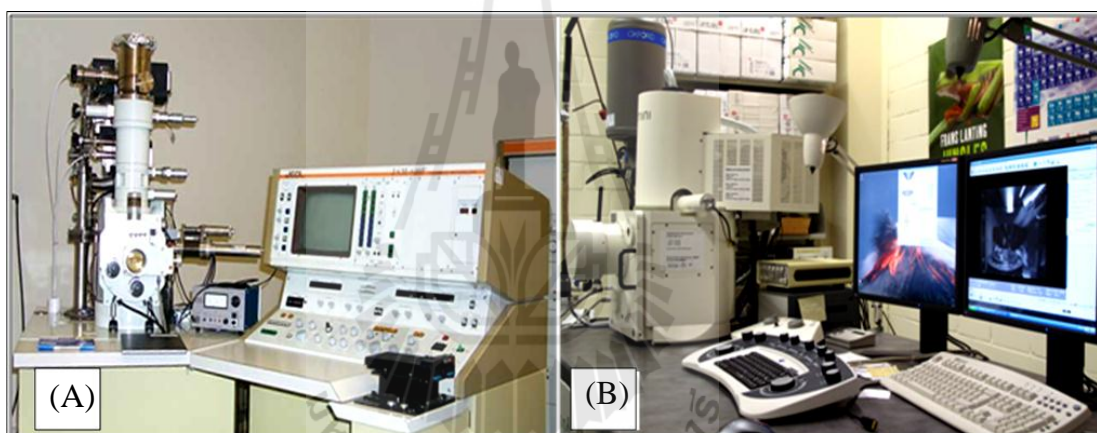


Figure 3.4 The two models of SEM instruments for tip characterization.

(A) “JEOL JSM-840A scanning microscope” and (B) “GEMINI Leo 1530”.

The solutions/reagents used for voltammetric quality checks of completed insulated CF UMEs were; 0.1 M potassium chloride (KCl, 99-100.5% purity, Carlo Erba) as supporting electrolyte spiked with either 1 mM hexamine-rutheniumtrichloride ($(\text{Ru}(\text{NH}_3)_6)\text{Cl}_3$, 98% purity, Sigma-Aldrich) as reversible and kinetically unproblematic redox mediator. Voltammetric experiments, if not otherwise mentioned, were carried out at room temperature with a computer-controlled

potentiostat (model Reference 300[®], Gamry Instruments, Warminster, PA USA). A normal three-electrode cell configuration suitable for work with microelectrodes was used with the CF UME as the working electrode, a Pt spiral or foil as counter and a Ag/AgCl wire as reference electrode.

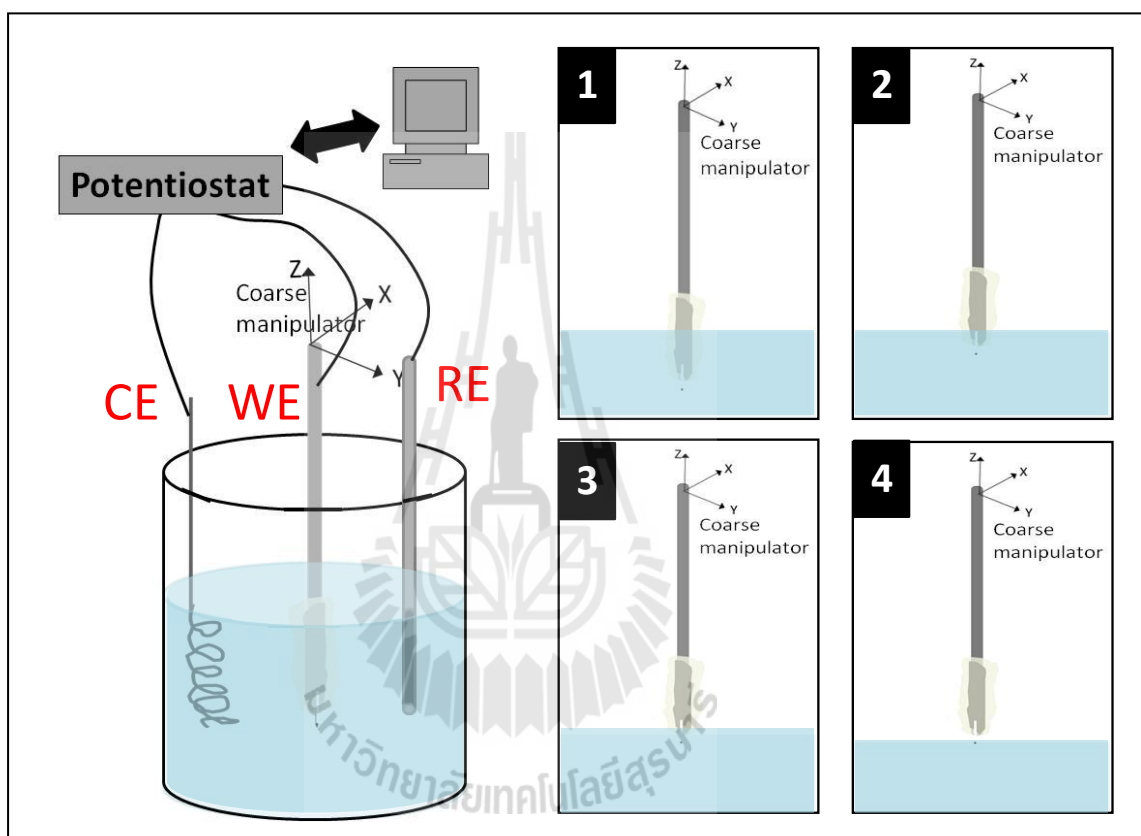


Figure 3.5 Scheme of voltammetric CF tip characterization in 1 mM $\text{Ru}(\text{NH}_3)_6\text{Cl}_3$ in 0.1 M KCl.

Scheme of tip characterization by electroanalytical technique. Three-electrodes are immersed into 1 mM $\text{Ru}(\text{NH}_3)_6\text{Cl}_3$ in 0.1 M KCl, the working electrode is completely insulated CF tip which is movable by coarse manipulator; to prove the insulating profile, tip is moved in z direction to demonstrate each position (subfigure 1 to 4).

3.2.2 Tapered CFs as probe tip for atomic resolution STM in the UHV and electrolyte environments.

3.2.2.1 STM in ultra-high vacuum (UHV) atmosphere

To proof the suitability of electrochemically etched carbon fiber tips to serve as STM probes with atomic resolution capability, they were tested in a special UHV-STM device for their imaging performance on a Si (111) single crystal surface with a 7×7 surface reconstruction. This work was carried out in collaboration with a Surface Science group from the Ruhr-University of Bochum, Bochum, Germany (Group leader: Professor Koehler). Figure 3.6 displays a schematic of the Si sample structure together with a representative published example of an STM image of the specimen (Duke, 2003; Takayanagi and et al, 1985) that would be expected in case of success. Si(111) is a semiconductive substrate and the atomic structure shows as large shaded circles the adatoms in the top layer of the structure (Figure 3.6(A)). The side view (Figure 3.6(B)) visualizes the nearest neighbor bonding in a plane normal to the surface containing the long diagonal of the surface unit cell.

Before used for imaging trials, the Si (111) substrate had to be pretreated with a vacuum degassing procedure (12 h at 600 °C, a 1 h treatment at 800 °C, and flash-annealing at 1250 °C). Also etched CF/W wire assemblies had to be heat-cleaned at 650 °C for five minutes in high vacuum chamber specially made for the heat annealing of W or Pt STM tips, in order to remove any residual liquefier of the conductive carbon paint that otherwise could later in the STM device contaminate the Si sample, even when present at ultra-trace levels.

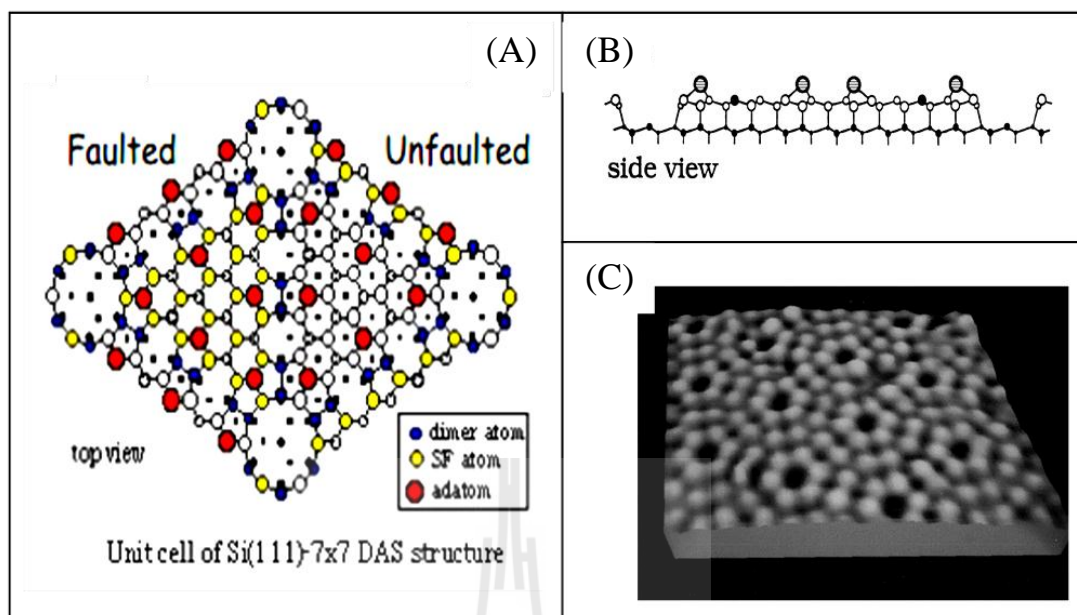


Figure 3.6 The (7×7) structure of the (111) surface of silicon.

(A) Schematic top view. (B) Schematic side plan view. (C) STM micrograph (Duke, 2003; Takayanagi and et al, 1985).

3.2.2.2 In situ STM in electrolytic environments (EC-STM)

The most attractive probe microscopy application of tapered and CF tips is their use in electrolytic environments where the carbon material has the advantage of high overpotentials for water electrolysis over noble metal alternatives and does not as easy contaminate with anodically formed insulating oxide films as tungsten tips. A requisite is of course the tip-sparing insulation of the carbon cones at the end of etched CFs; this was described earlier. One set of EC-STM trials with etched and insulated CF tips were performed on disk-shaped atomically flat Au (111) single crystals with a diameters of 10 mm, which were oriented within 0.3° and a commercial product of MaTecK GmbH, Julich, Germany. Before imaging, then Au (111) single crystal surface in electrolyte was annealed by electropolishing in 0.1

M H₂SO₄ (96%, RPE, Carlo Erba, Italy) under constant potential application 4 V. for 20 sec. After the treated Au surface was rinsed with DI water, it was soaked in 0.1 M HCl for 4 min. The Au sample surface was then further flame annealed with butane torch for 4 min. STM imaging experiment took place in 0.1 M perchloric acid (HClO₄) (Merge, Germany). Another set of STM imaging trials used Au(111) surfaces as described above but with triazatriangulenium (TATA) molecules present as an adsorbate surface modification. The molecular structure of the TATA molecules is shown in Figure 3.7. TATA was synthesized following a procedure described in a report of the Magnussen Laboratory (Baisch et al., 2009). For all in situ STM measurements a PicoPlus SPM (Agilent, Inc., Santa Clara, USA) was employed, if not otherwise mentioned in the constant current mode of operation. Lateral drifts in the STM images were software corrected to produce high quality STM images of the target substrates. Optionally, the conductive Au(111) surface has been operated as an active working electrode, while two-Pt spirals were employed as auxiliary and pseudo-reference electrodes, respectively.

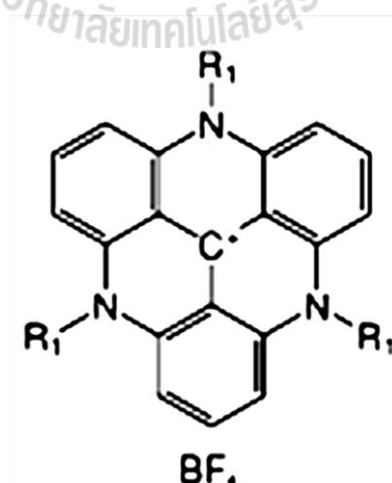


Figure 3.7 Chemical structure of self-assembled monolayer of the octyl-TATA molecule on the Au(111) substrate.

The octyl-TATA molecule which was used for preparation of self-assembled monolayers of an organic compound on the Au(111) substrate (Baisch et al., 2009).

3.3 Results and discussion

3.3.1 The formation of tapered carbon fiber tips with nanometric tip radii

High quality nanometric CF tips were needed as the precursors for the preparation of the targeted conical carbon UMEs/EC-STM probes. Tapering CF etching is possible via electrical spark, ion beam, flame and electrochemical etching. All procedures have been reviewed in the introductory section of this thesis. Most promising from the available methods for conical CF etching, because simple and reproducible, was an electrochemical procedure reported by Mousa in 1996 for the preparation of tapered carbon fiber-based electron emitters (Mousa, 1996). Mousa accomplished the electrochemical etching of single CF in alkaline solution and, as evidenced in Figure 3.8, obtained at a few mm long CF stems short and mechanically stable tapered tips with clearly submicron tip radii.

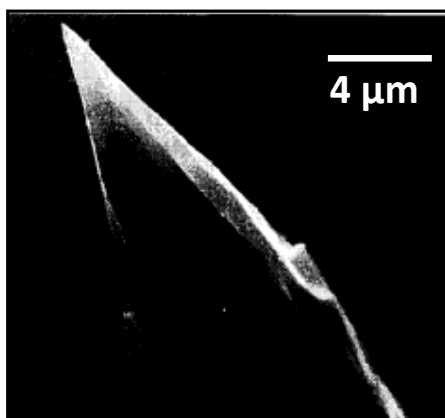


Figure 3.8 A scanning electron micrograph of a 7 μm diameter electrochemically etched carbon fiber electron emitter.

A scanning electron micrograph of a 7 μm diameter electrochemically etched carbon fiber electron emitter after operation for 96 h (Mousa, 1996).

Moreover, Schulte achieved a similar quality of an electrochemically CF etching in alkaline solution, however, instead with an individual CF for of a bundle of hundreds of CFs (Schulte, 1994; Besenhard, Schulte, Schur, and Jannakoudakis, 1991). SEM micrographs of bundle-etched carbon fibers are shown in Figure 3.9(A) and Figure 3.9 (B), and again evident are the well-pronounced conical tip geometry of the tapered CFs and a high ratio of successfully sharpened CFs. Because etching was obtained in bundles of CF, individual fibers with good tips had to be selected in a subsequent preparation step in order to get them connected to a holding wire (Figure 3.9 (C₁₋₄)) (Schulte, 1994).

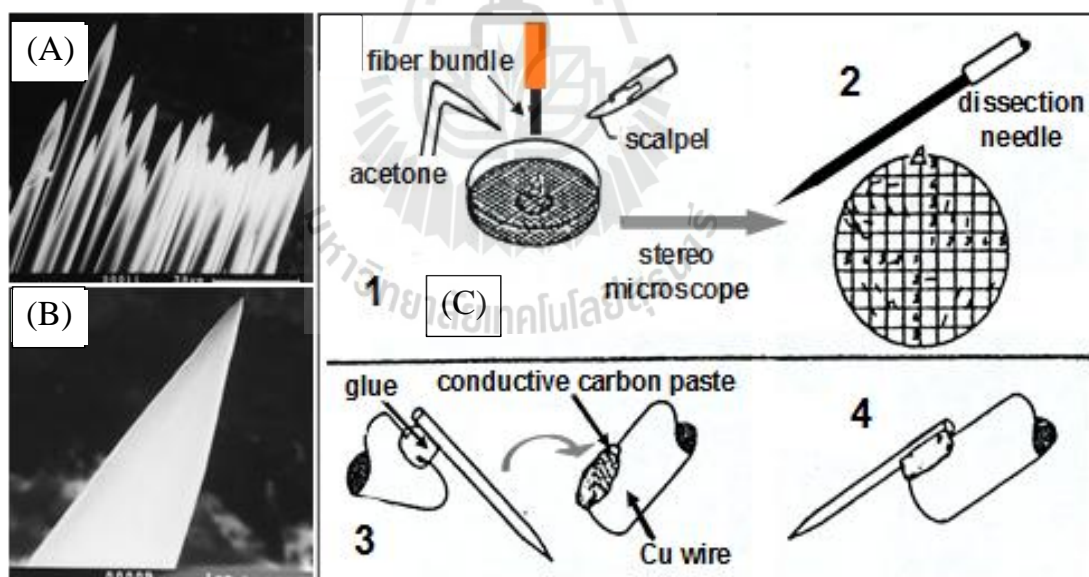


Figure 3.9 Scanning electron micrographs of electrochemically etched CFs and a schematic of the selection procedure of high quality.

SEM images of electrochemical etching of a bundle of CFs and single CF and schematic of the separation procedure of a single-shaped CF. (A) and (B) are low and high resolution scanning electron micrographs of electrochemical etching of CF that

were electrochemically etched in a bundle and a zoom of single tip, respectively. (C₁₋₄) is a schematic of the separation procedure of CFs with high quality tips and the attachment to a holding metal wire (Besenhard, Schulte, Schur, and Jannakoudakis, 1991).

With respect to the tip geometry and dimensions both the Mousa and the Schulte type of electrochemically etched carbon fibers would have been promising for an exploration as scanning probe for STM. However, the length of the carbon fiber extending from the end of the holding metal wire was in both cases several millimeters and the structure thus far too wobbly during the targeted scanning procedure for stable acquisition of a tunneling current without the influence of vibrations likely to be induced in course of the probe tip movement disturbing seriously STM imaging. Desai et al. reported for a 520 μm long CF that was attached to a metal wire oscillation at resonance frequency of 33.4 kHz (Desai, Netravali, and Thompson, 2006). The bending of the fiber is clearly visible in the high-speed flash photographs of Figure 3.10 and such an effect obviously would be against success with applications of CFs as well-imaging scanning probes. Fortunately, the usual scanning frequency in a probe microscope is much less than the kHz range and routine are 0 to about 100 Hz for conventional STM imaging purposes. A length of a protruding tapered CF of a maximum of about a few hundred micrometer was thus expected to be suitable for the construction of functional STM probes. As bundle etching with subsequent selection and metal wire-anchoring of tapered CFs with submicron tips was considered too tricky, the pathway towards the desired structures – a metal wire with an individual $\leq 500 \mu\text{m}$ long tapered CF attached – involved the Mousa strategy for the electrochemical etching of single carbon fibers, however, with

a modification favoring the desired length of the protruding fiber. The details of the developed procedure are schematically illustrated in Figure 3.11 and will be explained below.

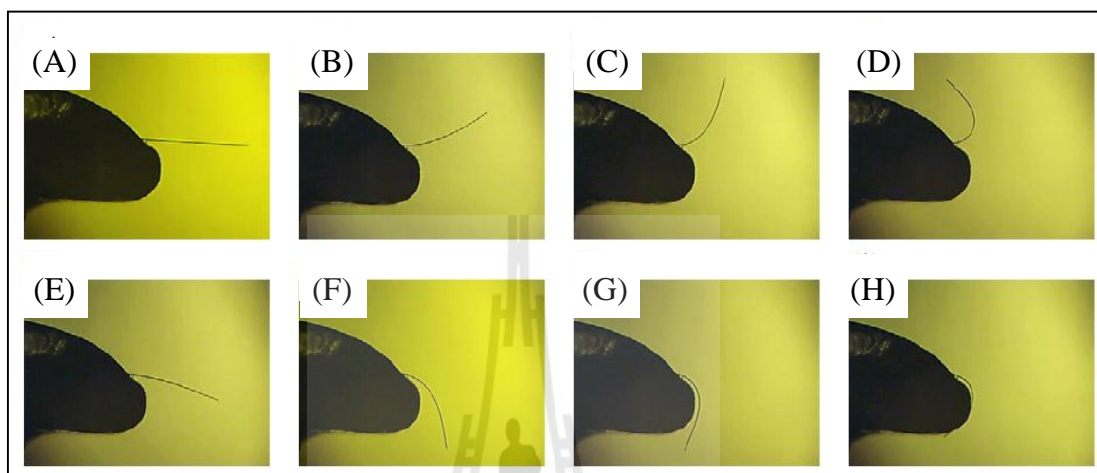


Figure 3.10 High-speed flash photographs of an oscillating 520 μm -long and 5- μm -diameter CF.

High-speed flash photographs of a single 520 μm long, 5 μm diameter graphite fiber cantilever oscillating at a 33.4 kHz resonance (Desai et al., 2006).

As suggested in the original work the electrolytically etching of the carbon fibers was done in 0.1 M NaOH. To accomplish as short as possible protruding etched CF, a CF/wire assembly (see Figure 3.11 (A)) was fully immersed into the NaOH, with a simple manual manipulator in use for downward placement, and then carefully lifted again. Through surface tension and NaOH adherence, the wire end pulled solution above normal level until a height d_1 in Figure 3.11 (C) the NaOH slipped off the wire. The wire was next brought down as much as possible, however, without getting in touch with solution again and etching was started with this minimal wire-to-liquid separation, raising the voltage until a desired etching current of 30–40

μA was observed. Anodic carbon fiber etching took place mainly at the air/liquid interface and, consistent with the earlier published Mousa observation, the current decreased slowly in the beginning and more rapidly later, as the fiber structure became thinner and thinner (see Figure 3.11 (D)). At the end point of etching the fiber got fully etched through leading to a complete loss of contact to the solution, and current drop to zero. At this stage a sharp cone was formed at the tip of the etched CF and the power supply was immediately switched off to avoid tip damage. Freshly etched fibers were removed from the etching setup and cleaned with streams of clean DI water. At the end, completed tips and CFs were inspected with a stereomicroscope and, for better quality judgments, in a scanning electron microscope (SEM) at higher resolution.

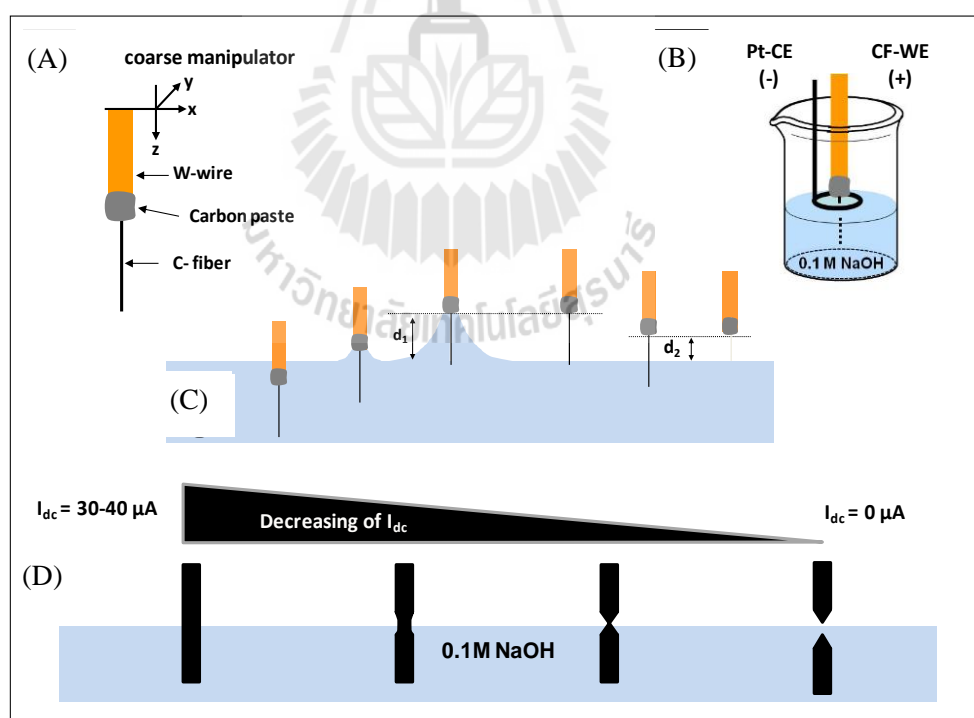


Figure 3.11 Procedure for controlled carbon fiber etching and establishment of an etched CF/metal holding wire assembly.

Procedure for controlled carbon fiber etching and establishment of an etched CF/metal holding wire assembly that finally has only a few hundred micron of the etched fiber extending from the wire end. (Sripirom, Noor, Köhler and Schulte, 2011). (A) Schematic of a tungsten wire holding a single CF and attached to a manual manipulator for controlled positioning in x, y and z directions. (B) Electrochemical cell arrangement for the CF etching in NaOH solution. (C) Strategy for keeping the protruding length of the etched CF at minimal length. (D) Current decrease during electrochemical CF etching and principle of the related tip formation.

Figure 3.12 shows SEM micrographs of four different kinds of carbon fibers that have been treated with the above described electrochemical etching procedure, namely the pitch-based carbon fiber P100 and the PAN-based fibers M40, T300 and E/XAS. Reproducibly, the etched carbon fiber extended from its anchor point at the holding wire by about a few hundred micrometers, which was about the desired length supposed to be good for an application as STM scanning probe.

Tapered tips were produced via the electrochemical etching for all tested CFs. However, the quality of the tip geometry and dimension was not very good for the pitch-based P100 (Figure 3.12(A)) and the PAN-based M40 (Figure 3.12(B)) fibers. In marked contrast the PAN-based T300 (Figure 3.12(C)) and E/XAS (Figure 3.12(D)) fibers formed well-shaped, short nanometric carbon cones that were mechanically stable and as sharp as common metallic STM tips.

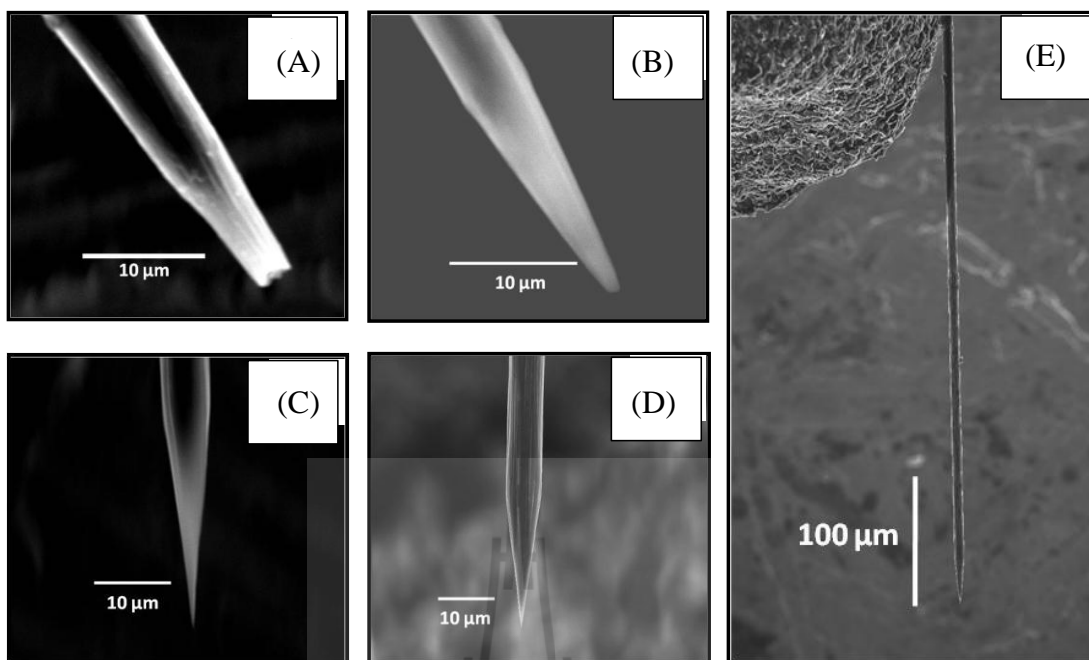


Figure 3.12 Scanning electron micrographs of electrochemically etched CFs.

Scanning electron micrographs of CFs that were electrochemically etched in 0.1 M NaOH, following the procedure illustrated in Figure 3.11. The close-up images (A-D) show the etching results for four different precursor fibers: (A) P100, (B) M40, (C) T300 and (D) E/XAS, respectively. (E) Overview of an electrochemically etched E/XAS fiber with about 400 μm extending from the anchor point at the holding wire.

In terms of reproducibility of the etching procedure, the fiber which performed best was the E/XAS-fiber for which 8 out of 10 fibers were successfully etched into structures as shown in Figure 3.12(D) and Figure 3.12(E). Hence, the E/XAS-fiber was used for the further experiment on route towards probe tip preparation for EC-STM. The quality of chosen E/XAS carbon fiber tips is once more highlighted in Figure 3.13, which shows SEM images of a typical case at different spatial resolution. Both the conical tip shape and the tip surface smoothness are as

well confirmed as a tip radius of $\sim 30\text{nm}$. This tip quality competes well with the Pt and W tips that are almost entirely used by the community of STM users for atomic resolution imaging. After success was gained with the first step of carbon fiber etching, the further attempts focused on the exploration of the functioning of STM tips as sensing probes for STM, first in UHV and in electrolytes.

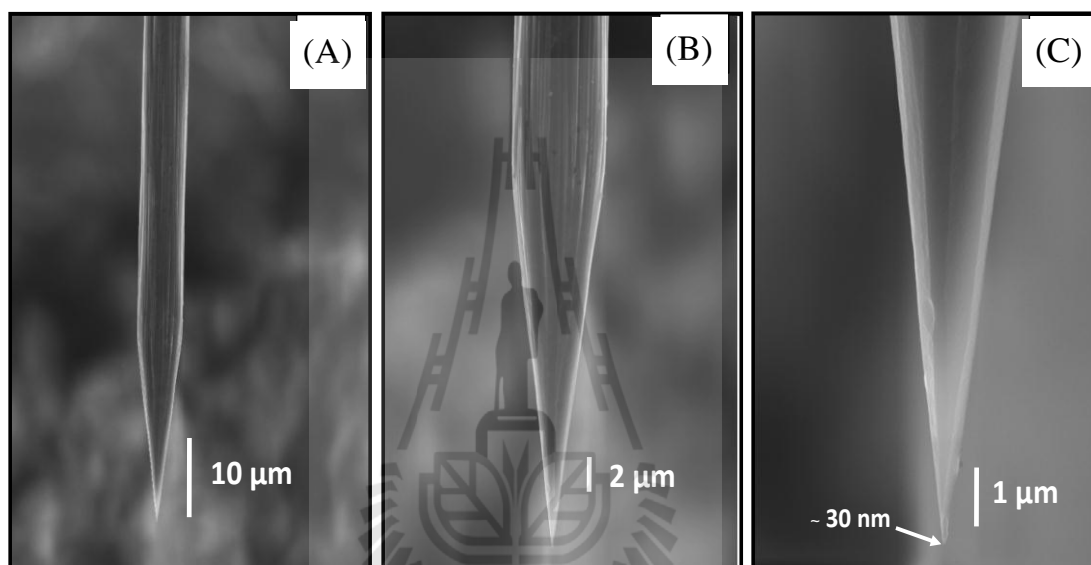


Figure 3.13 Scanning electron micrograph of electrochemically etched CFs (E/XAS). Scanning electron micrograph of an electrochemically etched carbon fiber (E/XAS) in 0.1 M NaOH. The low magnification image (A) shows an overview of the resulting tapered CF tip, the medium magnification image (B) is a close up of the same CF tip, and (C) is a zoom into the very end of the tip in (A) and (B).

3.3.2 STM imaging with etched carbon fiber tips

– Atomic resolution STM imaging in UHV

Starting point for the own STM trials was the knowledge in the group that electrochemically etched carbon fiber tips, when at reduced length straight in

place on a holding metal wire, were able to acquire STM images of a gold-coated optical grating in the constant current mode (Schulte, 2008). Figure 3.14(A) and Figure 3.14(B) are examples of STM images of the nanoscopic gold device at two different scan ranges. The STM topography image with the larger scan range (Figure 3.14(A)) revealed the nanoline pattern of the grating with some tens of nm height variations, straight line appearance and the expected density of 2.5 grooves per μm . Evaporated Au placed on holographic structures tends to form crystallites with nm grains sizes and these apparently came up as visible surface irregularities in the magnified adjacent lines of the sample that are imaged in Figure 3.14(B)) which is a layer STM zoom. Repetitive tip approaches and withdrawals did not harm the imaging capability of CF tips and topographic STM imaging on the Au nanoline patterns was also not affected by waiting times of a few days after tip preparation, which was a sign of reasonable tip stability. Not proven at the early stage of the carbon STM probe development was, however, the milestone of a capability for atomic resolution imaging of solid sample surfaces. This was thus a major task of own attempts and was addressed first with imaging trials in an UHV-STM machine of a collaborator from the Ruhr –University of Bochum, Germany.

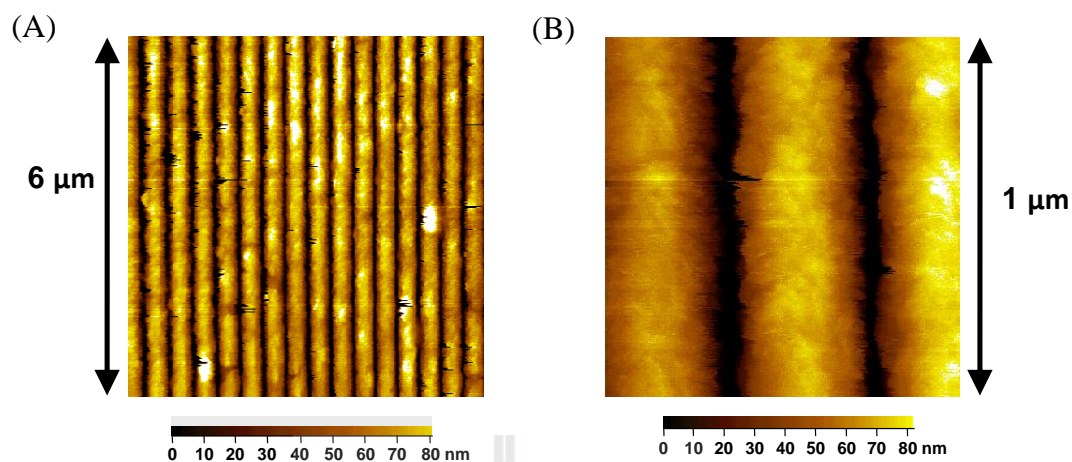


Figure 3.14 Constant-current scanning tunneling microscopy images of a thinly gold-coated optical grating.

Constant-current scanning tunneling microscopy images (bias voltage 0.25 V, tunneling current 0.5 nA) of a thinly gold-coated optical grating with 2500 grooves/mm at two different spatial resolutions. The side lengths of the squares in (A) and (B) are 6 and 1 μm, respectively. Darker regions in the birds-eye-view plots correspond to positions above grooves in the grating and the associated color scales permit a topography weighting.

Test sample surface for own UHV-STM trials was a Si(111) substrate exposing the standard 7×7 -surface reconstruction. Prior to the incorporation into the UHV-STM device, freshly prepared tapered CF tips were annealed at a temperature of 650 °C for five minutes in a high vacuum chamber. The exclusion of oxygen hindered the carbon fiber to be burned and usually tips went through the treatment without cause of any damage to their functional carbon nanocone tips. The heat treatment was a requisite to degas the carbon paint was suspended in an organic solvent. After the heat pretreatment, CF tips were introduced into the tip holder of the UHV-STM and in

the machine challenged with efforts to establish the atomic resolution imaging of the Si(111) 7×7 -surface reconstruction.

Figure 3.15(A) shows an atomically resolved image of the Si surface scanned with the tip shown in Figure 3.15(C) and Figure 3.15(D), the lateral resolution being confirmed by the periodic arrangement of the 7×7 -construction, with some missing adatoms. STM scanning of the clean sample was possible over several hours, proving that tip outgassing either did not take place at all or not to an extent that badly affected the quality of imaging. The line profile through the unit cell sketched in Figure 3.15(B) shows that the resolution perpendicular to the surface is comparable to that of standard W-tips (Figure 3.16) (Kobayashi, Yamada, Horiuchi and Matsushige, 1999). Optical inspection of probes before and after scanning established that imaging was through the CF tip, rather than the supporting W-wire. Figure 3.15(C) shows a micrograph of the CF tip and the supporting wire directly after the degassing procedure but before transfer into the UHV chamber with a base pressure of 2×10^{-10} mbar. The micrograph in Figure 3.15(D), taken after successful employment of the tip UHV-STM imaging, proves that the CF probe survived the scanning experiment and transfer processes.

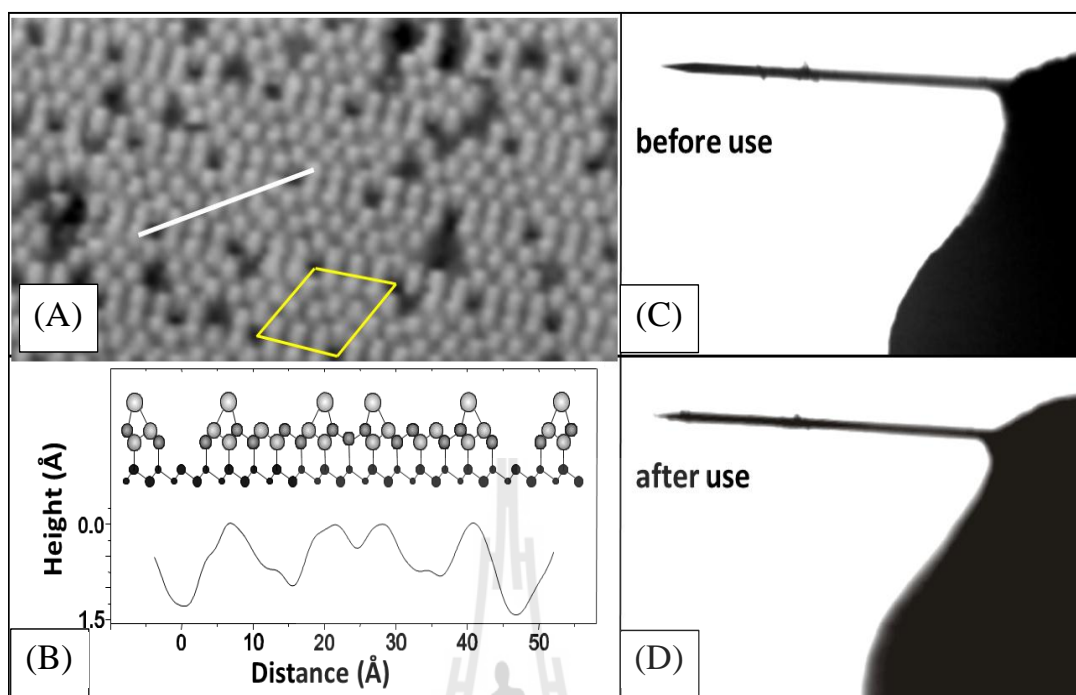


Figure 3.15 Test of a CF tip in a UHV scanning tunneling microscope for Si(111)-7x7 surface imaging.

(A) Empty states STM image (bias voltage + 2.0 V, tunneling current 0.4 nA) of the Si(111)-7x7 surface scanned in UHV (size 190 Å x 95 Å); the unit cell is marked by the yellow box. (B) Lower part: line profile diagonally through the unit cell along the white line in (A); upper part: ball model of the atomic arrangement along the line profile. (C) and (D) show optical micrographs of the W-wire with the attached carbon tip before and after use in UHV.

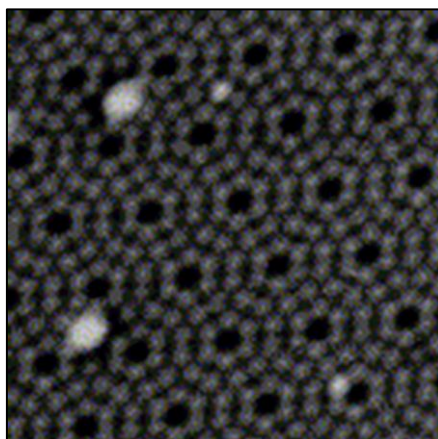


Figure 3.16 A representative published example of an atomically resolved STM image of a Si(111), 7×7 -reconstructed surface obtained by a tungsten STM tip in UHV-STM.

A representative published example of an atomically resolved STM image of a Si(111), 7×7 -reconstructed surface obtained by a tungsten STM tip in UHV-STM. The scan size of these images is $5.5\text{ nm} \times 5.5\text{ nm}$., $V_{\text{bias}} = 2\text{ V}$., $I_t = 100\text{ pA}$ (Kobayashi et al., 1999).

The demonstration of the atomic resolution imaging capacity of etched CF STM probes was a significant achievement in context of the theme of this thesis. However, in order to make the next step and progress further to the finally desired successful application for in situ STM in electrolyte solutions the conductive surface of the CF tips had to be minimized as otherwise the faradaic current (I_F) would cover the tunneling current and hinder imaging. The related scenario is schematically depicted in Figure 3.17 which also suggests the solution for the problem. All except the very end of the tapered carbon tip has to be insulated with an appropriate coating to keep the faradaic current component much smaller than the tunneling one. The realization of the strategy proposed in Figure 3.17 will be subject of the next section.

of course, can produced partially insulated carbon fiber tips not only be functional EC-STM tip but also be used as voltammetric ultramicroelectrodes with a conical sensor geometry, which still is a rare since special electrode form

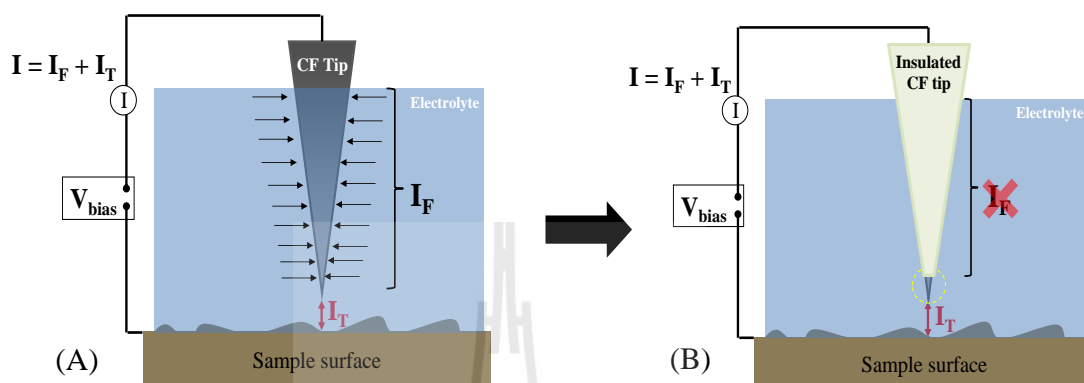


Figure 3.17 Principle of the operation of STM tips in electrolytes.

The problem of the operation of STM tips in electrolytes (A) and a possible solution. The biased STM tip acts as an electrode and a faradaic current (I_F) may be induced that disturb the tunneling current (I_T). Insulation of all but not the very end of STM tips is reducing the electroactive area of the STM tip, keep I_F at minimum (B).

3.3.3 Etched carbon fiber tip insulation - Fabrication of conical carbon UMEs/EC-STM tips

Important task to be completed for reaching etched carbon fiber-based conical carbon UMEs that optionally could work as EC-STM tips was the tip-sparing application of an electrically well insulating polymer layer to tapered CFs with nanometric tip apertures as obtained via controlled electrochemical etching. Only then faradaic redox reactions and current flow is limited to the outermost tip region and thus kept small enough not to bury the tiny tunneling current and make application for STM imaging purposes possible. The principle of the novel procedure that was

developed here for the completion of the desired sensor architecture is schematically illustrated in Figure 3.18. Chosen as insulating polymer was a cathodic electrodeposition paint (EDP) that was known from the original industrial use as well corrosion-protective layer on car bodies as a chemically resistive and superbly insulating material. For tip-protected EDP coating, an etched CF at the holding wire was made the cathode and a piece of platinum foil that was partially rolled to give a Ω -shaped cross section served as the anode and a container for the EDP solution at the same time. Both the fiber and the Pt electrode were attached to two x, y, and z micromanipulators for precise maneuvering and the Ω -trough was filled with the EDP solution. Under optical control by the stereomicroscope of the working platform, an etched CF was gently lowered into the EDP solution, taking good care not to drag the very front of the fiber tip into the paint emulsion. A constant potential (5 V) was then applied between the two electrodes for 240 s. This caused water electrolysis and cathodic hydroxide evolution. The local pH shift in the vicinity of the CF cathode caused EDP precipitation on the immersed CF surface but of course not on its protruding part. Curing fresh deposits at 195 °C for 5 minutes dried the paint and established the desired good electrical insulation. To eliminate any residual porosity in the thin polymer coating, the steps of EDP deposition and heat curing were repeated once.

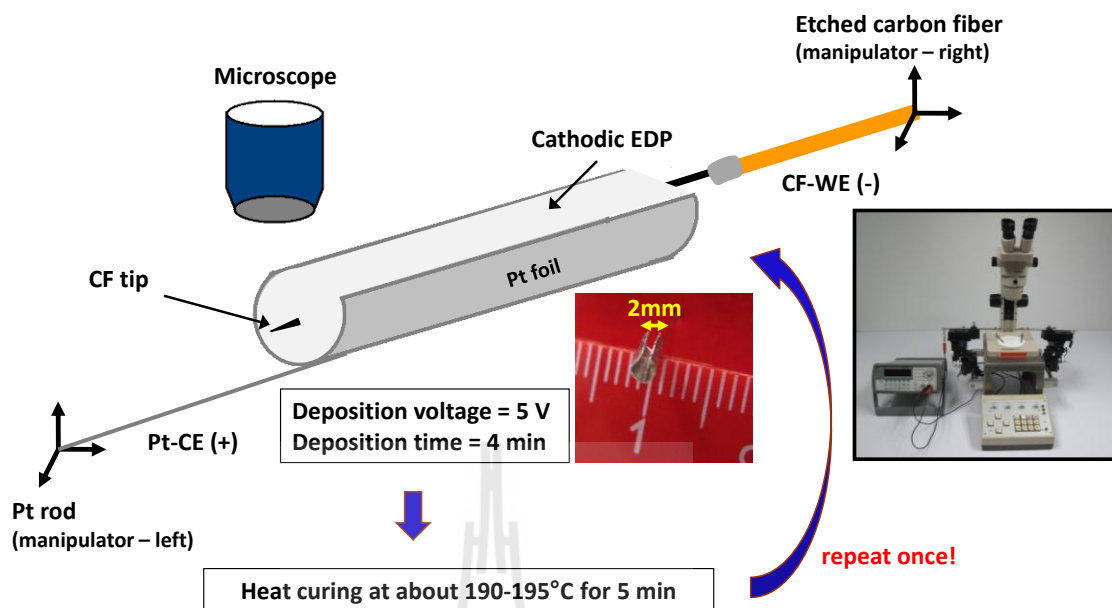


Figure 3.18 Schematic of CF tip insulation by electrodeposition paint solution in a Ω -shaped Pt trough.

Use of the simple stereomicroscope/micromanipulation platform that was built within the frame of this thesis for convenient carbon fiber maneuver for easily performed tip-sparing polymer insulation of etched carbon fiber tips. A Ω -shaped Pt trough and the etched carbon fiber are movable in x, y, z direction by two micromanipulators, with fine-positioning possible in the sub- μm range. A stereomicroscope assisted proper tip placement into the electrodeposition paint solution; to leave a conical carbon tip exposed, only the very ends of etched fibers should not be immersed. Thin-film paint precipitation at the immersed part of etched carbon fibers was induced by DC voltage application (5 V, 240 s). A following heat treatment of fresh paint deposits transformed them into insulating coatings and produced hemispherical carbon microelectrodes. The inset in Figure 3.19 is a photograph of the manipulator platform for simple CF tip insulation.

Figure 3.19(C) is displaying the end part of a carbon fiber tip that was insulated with the described procedure of tip-protected deposition of the cathodic paint, namely Clearclad Coatings (LHV Coating Limited, Birmingham, England). For comparison also shown are cylindrical (Figure 3.19(A)) and disk-shaped (Figure 3.19(B)) versions of carbon fiber microelectrodes. Reproducibly, the heat-cured EDP coating appeared uniform and pinhole-free and aligned well to the shape of the underlying carbon structures, regardless of their shape. Uncritical thickenings of the EDP layer often appeared in the case of insulated etched CFs (refer to Figure 3.19(C)), but these were always distant from the tip, and did not disturb the voltammetric tip response and STM imaging ability.

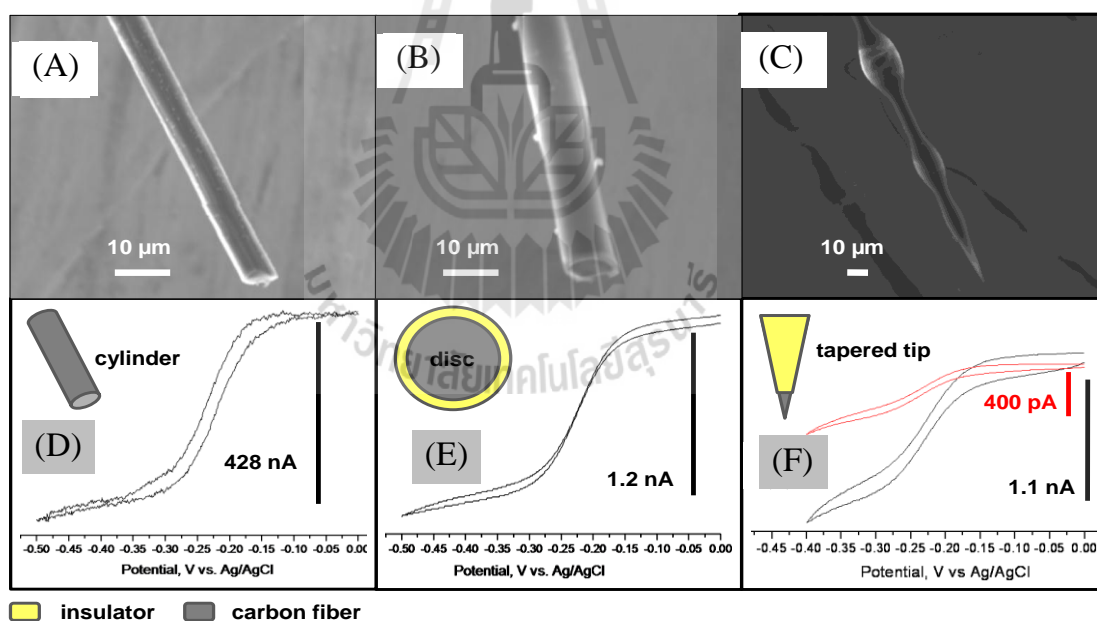


Figure 3.19 Scanning electron micrographs of carbon fiber microelectrode of various geometry. And cyclic voltammograms of then in 1 mM $\text{Ru}(\text{NH}_3)_6\text{Cl}_3$ in 0.1 M KCl.

The top row shows scanning electron micrographs of (A) a cylindrical, (B) a disk-shaped, and (C) a conical carbon fiber microelectrode. In the bottom row are the cyclic voltammograms of 1 mM $\text{Ru}(\text{NH}_3)_6\text{Cl}_3$ in 0.1 M KCl at (D) a cylindrical

carbon fiber microelectrode, (E) a disk-shaped carbon fiber microelectrode, and (F) two needle-type carbon fiber microelectrode of different size. Scan speed for all recordings was 50 mV/s, and the reference electrode was a Ag/AgCl wire and the counter electrode a coiled Pt wire.

Etched carbon fibers and their polymeric EDP coating shared carbon atoms as the main source of the secondary electrons used for SEM image formation, and the polymer film in the tip region was of gauzy appearance, so that the electron microscope could not distinguish coated and bare regions of the tip (refer to Figure 3.19). Characterization of the exposed carbon surface therefore had to be made by comparative electrochemical measurements with sensors of known geometry (the cylindrical and a disk-shaped CF microelectrode, in this case, in Figure 3.19(A) and Figure 3.19(B)). Cyclic voltammetry was carried out in an 1 mM $\text{Ru}(\text{NH}_3)_6\text{Cl}_3$ in 0.1 M KCl electrolyte solution with a Ag/AgCl wire as pseudo reference, a coiled Pt wire as counter-electrode, and one of the CF microelectrode configurations as the working electrode. Both the cylindrical and the disk-shaped CF microelectrode displayed the typical steady-state cyclic voltammogram (CV) with the well-pronounced current plateau that is expected for the reduction of Ru^{3+} at sensors of the particular size. The diffusion-limited current, i_{lim} , of the microdisk carbon electrode (refer to Figure 3.19(E)) was almost 400 times smaller than the one of the cylindrical equivalent (refer to Figure 3.19(D)), which reflects the effectiveness of the EDP coverage in restricting the electroactive area to the disc face at the very end of the conductive filament. Figure 3.19(F) shows two representative CVs of needle-type CF microelectrodes that

were prepared by tip-sparing EDP insulation, but with more or less of the etched tips left out of the EDP solution during electrochemically triggered deposition. From a comparison of the CVs in Figure 3.19(E) and Figure 3.19(F) it is evident that the measured currents for the needle-like CF microelectrodes (1.1 and 0.4 nA) were, under otherwise same conditions, comparable to that observed for the disk CF microelectrode (1.2 nA). The sigmoidal shape and low plateau values of the two I/E traces indicated good electrical insulation and limitation of electroactivity to the tips of the tapered structures, as expected for a conical microelectrode.

Furthermore, the diffusion-limited current (i_{lim}) of the three voltammograms (refer to Figure 3.19(D)-(F)) can be used to calculate the equivalent effective radius (r_{eff}) of the exposed electroactive carbon surface according to the following equation:

$$i_{lim} = 2\pi n F D C r_{eff} \quad \text{Equation 3.1}$$

Where n is the number of electrons transferred during the electrochemical reaction at the UME surface (here; $n = 1$), F is Faraday's constant (96,485 C/mol), D is diffusion coefficient (here; $D = 7.2 \times 10^{-6} \text{ cm}^2/\text{s}$ (Zoski, Yang, He, Berdondini and Koudelka-Hep, 2007)), C is concentration of electroactive species (here; $C = 0.001 \text{ M}$), and r_{eff} is effective radius of experimental UME (detailed calculation see in the Appendix).

The effective radii for the conical-CF UMEs in Figure 3.19 (F) were calculated as 2.52 μm and 920 nm, respectively. Both were just different in how much the carbon surface was pulled into EDP solution. Thus, the EDP insulation method

allowed indeed the manufacture of voltammetric CF electrodes with dimensions in the micrometer to nanometer range.

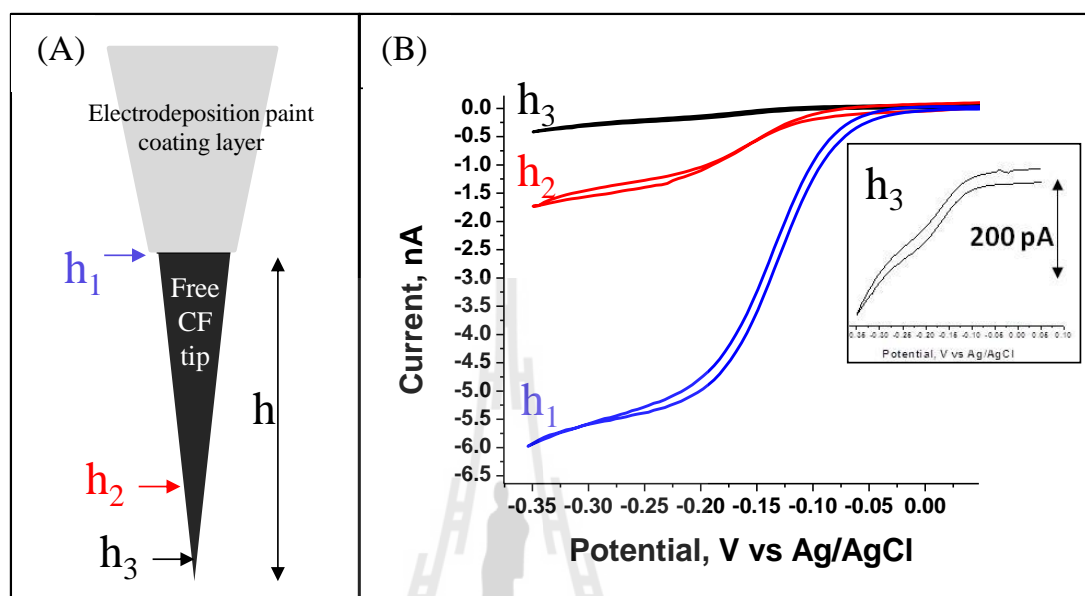


Figure 3.20 Etched carbon fibers shielded with electrodeposition paint except at the top of the taper.

(A) An etched carbon fiber that is shielded with electrodeposition paint but not at the top. h_1 , h_2 , and h_3 denote the variable height of the free carbon cone. (B) Cyclic voltammograms of 1 mM $\text{Ru}(\text{NH}_3)_6\text{Cl}_3$ at carbon cones with the sizes as to the left.

With a comparably easy strategy the effective insulation of all but not the topmost part of the nanometric carbon fiber cones (Figure 3.20 (A)) can be achieved and the voltammetric performance of the resulting tapered electrode structures was in accordance with the micro- and nanoelectrode theory (Figure 3.20 (B)). The effective radii for the conical CF-UMEs that led to the cyclic voltammograms in Figure 3.20 were calculated from the experimentally limiting currents (i_{lim} of $h_{1, 2, 3} \approx 5, 1, \text{ and } 0.2 \text{ nA}$, respectively) by using equation 3.1 as

11.45, 2.29 μm and 458 nm, respectively. Compared to literature-known other pathways towards conical carbon fiber micro- and nanoelectrodes a major strength of the fabrication method developed in this thesis is its simplicity, both in the required instrumentation and in the execution of the procedure. These assets are expected helping to make the tiny EDP-coated conical carbon sensors a common analytical tool in electrochemistry and surface science laboratories.

3.3.4 The insulation of the etched carbon fiber/metal wire junction with a silicone elastomer

Though the tip-sparing EDP paint insulation sealed the carbon fiber electrically very well all around and ensured that the electrochemical redox activity was limited to the front of the tapered carbon tips it did not protect the sharp edges of the holding copper or tungsten wire reliably from contact to electrolyte. Leakage currents thus occurred often from this critical area and additional protection had to be applied here before STM trials in electrolyte solution could be attempted in order to ensure that the tiny tunneling current through a carbon fiber tip was not buried in too large intrinsic current noise signals. The simple procedure schematically illustrated in Figure 3.21(A) was consequently developed and offered good success rates for covering CF/metal wire junction with a clear and safely insulating layer of a rubber-like material that well separated the edges and flat regions of the conductive joint from any contact with the aqueous salt solution. In brief, an about 10 mm long U-shaped plastic container of a few mm diameter was mounted on a holder and filled with a mixture of the two components of the silicone elastomer Sylgard. Similarly to the application of the cathodic EDP insulation in the earlier step but without involving

exposure to voltage, the already EDP coated etched CF tip was positioned just above this tubular basin using an x, y, z micromanipulator and stereomicroscope for careful placement. Then the structure was lowered gently and slowly introduced into the liquid Sylgard precursor mixture while initially carefully avoiding an immersion of the polymer-insulated fiber and its connection to the wire. The entire carbon fiber carrying wire including the junction to the filament was then horizontally dragged into the Sylgard but not the protruding CF or its tip. A slow vertical movement allowed to lift the fiber/wire assembly and the junction between the imperfectly EDP insulated contact point between the metal wire and the carbon fiber was left with a layer of the viscous rubber precursor, which was in a final step of heat-curing converted into an electrically insulating silicone rubber coating by exposure to the gentle warm stream of air from a heat gun. Figure 3.21(B) shows a drawing of the resulting conical CF UME with improved electrical insulation of the fiber/wire junction and the expected electroactivity limited to just the tip. Imaging by SEM (Figure 3.21(C) and Figure 3.21(D)) confirmed the relatively thick covering of Sylgard on the end of the holding wire as well as the integrity of the EDP paint-coated CF, with no sign of unwanted contamination with the silicone material.

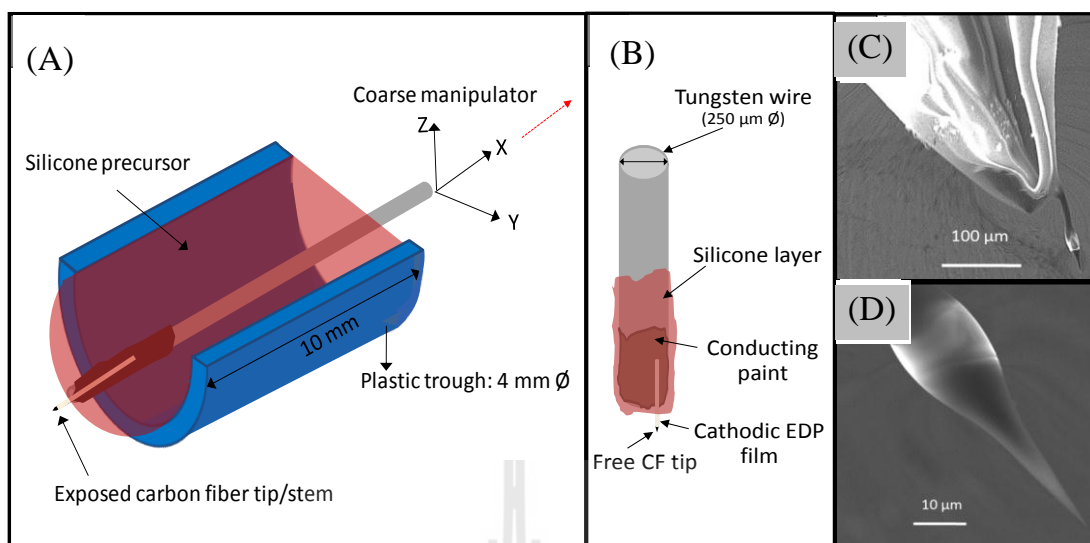


Figure 3.21 Application of an insulating silicone rubber coating to the carbon fiber/metal wire junction of EDP insulated CF UMEs.

(A) A drawing displaying the method for applying an insulating silicone rubber coating to the carbon fiber/metal wire junction of EDP insulated CF UMEs. With help of a simple manipulator, the thinly EDP-coated carbon fiber is pulled into a liquid silicone rubber precursor, which is held in a tiny U-shaped plastic container. At the beginning only the tungsten wire is immersed and then the entire stem apart from the extreme tip of the insulated fiber is placed. A careful lift of the carbon fiber/metal wire leaves the UME metal junction behind with an adherent Sylgard surface film that by gentle heat-curing with a hot air gun is transferred into a solid, insulating silicone polymer. (B) Drawing of resulting CF-UME after the application of a protecting silicone layer to the carbon-tungsten junction. (C) Scanning electron microscope image (low magnification) of a structure as drawn in part B. (D) Scanning electron microscope image (high resolution) of the front part of the EDP coated CF UME in part C that has EDP paint all over and an invisible area of bare graphitic carbon exposed at the end as a functional tunneling tip.

Whether the silicone application to the CF/wire junction indeed protected against the appearance of leakage currents and unwanted noise was tested via voltammetric inspection. Completed conical CF UME with the extra silicone in place at the holding wire/carbon paste/carbon fiber junction were partially (fiber only, with increasing immersion depth) or fully immersed into a solution of 1 mM $(\text{Ru}(\text{NH}_3)_6)\text{Cl}_3$ in 0.1 M KCl and cyclic voltammograms were then acquired. Figure 3.22 displays the typical outcome of such a CV test with the microelectrode configuration as presented in Figure 3.21. Actually, the perfect overlay of the CVs valid for tip-only and full structure immersion is clear evidence for the effectiveness of the Sylgard protection of the CF/wire junction. Whether only the tip was exposed to electrolyte or the whole CF UME including its metal wire stem was dipped into the redox mediator solution did not make a difference in the voltammetric response anymore and this behavior was the fundamental requisite for the ability to successfully execute EC-STM with the novel CF UMEs in use as the scanning probes.

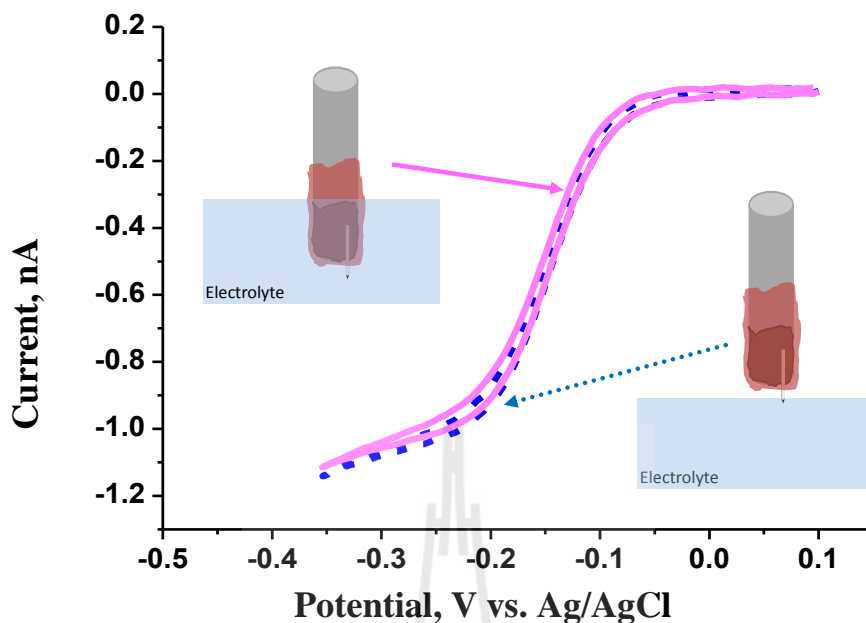


Figure 3.22 Cyclic voltammograms (CVs) of a conical CF-based UME.

Cyclic voltammograms (CVs) of a completed conical CF UME with the extra silicone in place at the holding wire/carbon paste/carbon fiber junction were partially or fully immersed into a solution of 1 mM $(\text{Ru}(\text{NH}_3)_6)\text{Cl}_3$ in 0.1 M KCl. Cyclic voltammograms (CVs) of a well-insulated CF that fully immersed into electrolyte (pink solid line) or only dipped with the tip of the smoothly insulated tapered carbon fiber into the solution (blue dash line). The almost perfect overlap of the two sigmoidal curves is a clear sign of efficient insulation of the entire wire/fiber structure.

During practical EC-STM experiments insulated CF tip may be immersed into electrolyte solutions for several hours. Therefore, the stability of CF UME insulation had to be confirmed via voltammetric inspection over that period of time and a comparison of the diffusion-limiting currents acquired in course of the

measurement. Representative voltammograms of the stability tests in 1 mM $(\text{Ru}(\text{NH}_3)_6)\text{Cl}_3$ in 0.1 M HClO_4 (a typical electrolyte for in situ STM studies) are shown in Figure 3.23(A) while Figure 3.23(B) displays a plot of the extracted diffusion limiting faradaic UME currents (ΔI) as function of time of electrolyte exposure. As evidenced in the I/t plot the faradaic response of a conical CF-based UME that was fully immersed into acidic electrolyte did not change significantly for the tested length of 180 min of HClO_4 electrolyte exposure, which is nicely demonstrating the integrity of the insulating layer on both the CF surface and the CF/holding wire junction during exposure to the acidic solution. Conclusion at this stage thus was that CF UMEs with the potential to be used as scanning probes for electrolytic STM were successfully constructed and ready for suitability test trials in an appropriate STM device.

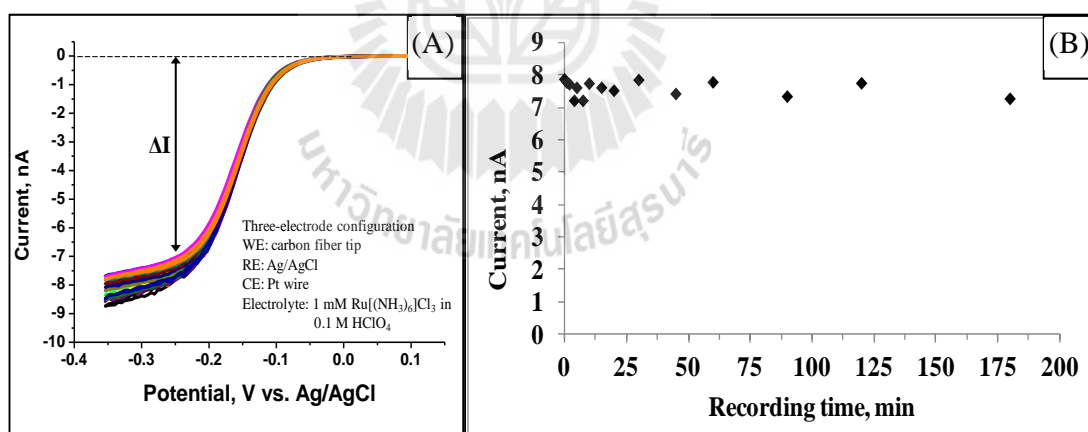


Figure 3.23 Insulation stability test for an EDP-insulated conical CF-UME.

(A) Superimposed cyclic voltammograms of a CF UME as shown in the Figures 3.22 (B) and 3.23 in 1 mM $[\text{Ru}(\text{NH}_3)_6]\text{Cl}_3$ in 0.1 M HClO_4 . One CV was recorded at 0, 1, 2, 3, 4, 5, 10, 20, 30, 45, 60, 90, 120, 180 min. (B) Plot of the diffusion limiting

current (ΔI) extracted from the CVs in (A) at the same potential (0.25 V vs. Ag/AgCl) versus recording time (0-180 min).

3.3.5 Proof of the beneficial potential window of CF-UME for the target application “EC-STM”

In Chapter II it was claimed that carbon has the advantage of a wider electrochemical potential window over noble metal-based alternatives as electrode material for voltammetric experiments. To demonstrate this property for CF UMEs that, when conical electrode geometry was established, were supposed to be advanced EC-STM scanning probes, their current-voltage response was inspected in various types of electrolytes including neutral 0.1 M KCl (pH 7), alkaline 0.1 M NaOH (pH 13) and acidic 1 M H₂SO₄, (pH 0). The cyclic voltammetry trials were carried out with a scan speed of 50mV/s in a beaker-type electrochemical cell and three electrode configuration. A conical CF UME or, for comparison, a disk-shaped Pt UME were the working electrodes, while a coiled Pt wire was counter and a Ag/AgCl wire the reference electrode. Figure 3.24 displays the observed set of three voltammograms. In all CVs the onset of water electrolysis and related hydrogen and oxygen evolution is visible through the appearance of large cathodic and anodic currents at the left and right side of the potential axes. The potential window, defined as the region of low microelectrode current, was in all electrolytes wider for the carbon than for the Pt disk sensors. At pH 0, pH 7, and pH 13, for instance, the potential ranges with very low background currents were respectively 3.7, 2.0, and 3.6 V of disk-shaped carbon UME and 1.85, 1.65, and 2.0 V for disk-Pt UME. Positive interpretation of this observation is that CF-based UMEs indeed have a wider potential window when

compared with noble metal analogues and they thus very likely will offer an improved performance level for both voltammetry and EC-STM studies.

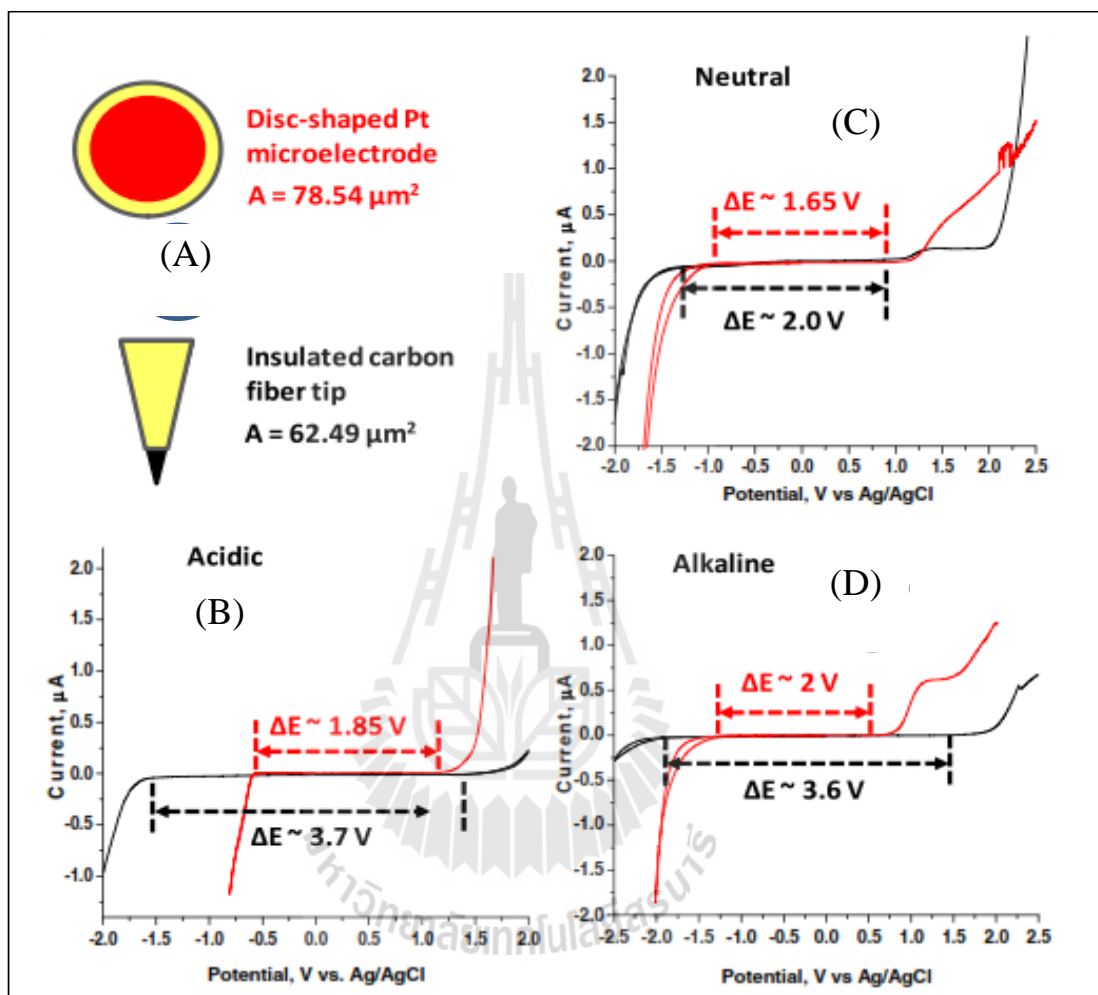


Figure 3.24 Potential window assessment for a EDP insulated conical CF-UME.

Comparison of the potential windows of carbon and Pt working electrode. (A) A conical carbon and a Pt disk UMEs were used for a comparative assessment of the potential window. The electroactive area of the sensors was determined electrochemically by voltammetry in 1 mM $[\text{Ru}(\text{NH}_3)_6]\text{Cl}_3$ in 0.1 M KCl. (B–D) Cyclic voltammograms as obtained with a conical carbon (black) and a Pt disk (red) UME at an acidic (B: pH 0), neutral (C: pH 7) or alkaline (D: pH 13) aqueous

electrolyte without redox mediators. In all cases, the onset of cathodic hydrogen and anodic oxygen evolution causes significant current flow at suitably high working electrode potentials. The practical potential window is the range of potential with no significant current and is marked in the voltammograms by colored dashed lines and arrows.

The application of EDP/Sylgard-insulated conical CF UME as probes for EC-STM in mind, their potential window was also directly measured in the electrochemical cell of an in situ STM device. Figure 3.25 displays two superimposed cyclic voltammograms, one of which is from the CF-based (black trace) and the other from a traditional tungsten (red trace) EC-STM tip as acquired in the EC-STM setup with 0.1M HClO₄ as electrolyte. When scanning in the positive (anodic) direction, starting at about +0.7 V vs. Ag/AgCl, a small, gradually increasing anodic current is visible for the CF-based STM tip (black trace), which is probably produced by slow oxidation of the carbon fiber surface. Then at about 1.4 V vs. Ag/AgCl a more drastic current is observed, which corresponds to water electrolysis and oxygen evolution. In the negative (cathodic) direction, a considerable rise in current happens at about - 0.3 V vs. Ag/AgCl. This potential is too low for the current to be related to cathodic water electrolysis and hydrogen evolution. More likely, it is due to the reduction of surface oxides formed during the anodic scan towards high anodic overpotentials. The potential range in the CV between - 0.25 and + 0.8 V vs. Ag/AgCl is for CF-based STM tips the tip potential window suitable for in situ STM in the perchloric acid electrolyte. The residual (leakage) current in this span was approximately 50 pA or less and, as later also confirmed by in situ STM imaging experiments, small enough in

magnitude not to hinder the STM imaging process with about 10-fold larger tunneling currents in the order of 500 pA or more. The CV of a common tungsten EC-STM tip (red trace) as routinely used for imaging experiments in perchloric acid electrolyte was quite different. During the anodic scan in the positive direction, an oxidation current came up already at about 0 V, slowly increased till about 0.5 V, and then strongly increased thereafter. This observation relates to a narrower potential window as true for the CF-STM tips and highlights the benefits of the choice of carbon as tip material. Furthermore, in contrast to graphitic carbon, which does not form passive surface oxides, tungsten is known to coat itself with an insulating oxide layer. This significant difference may explain why, as demonstrated below, carbon tips can achieve STM imaging at positive potentials that are not assessable with tungsten tips as scanning probes.

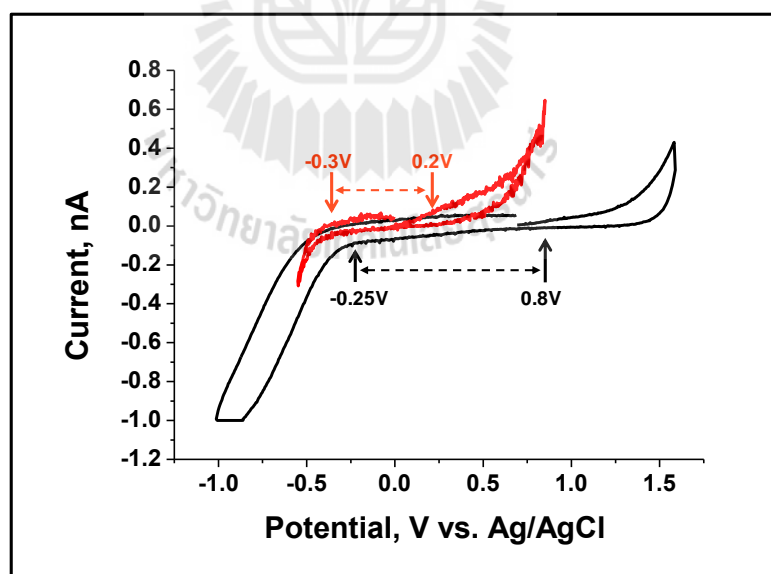


Figure 3.25 Cyclic voltammograms recorded for a conical CF-based UME and a tungsten EC-STM in the electrochemical cell of an EC-STM setup.

Cyclic voltammograms recorded with a conical CF-based in situ STM tip (black trace) and a tungsten in situ STM tip (red trace) in 0.1M HClO₄ in the electrochemical cell of an STM setup.

The regions in between the vertical black and red arrows represent the electrochemical potential window available for electrochemical STM studies for the different type of probes.

3.3.6 STM imaging with carbon fiber-based EC-STM tips

3.3.6.1 Imaging of bare Au(111) sample surfaces

The capability of CF-based STM tips for atomic resolution imaging in UHV was demonstrated earlier in experiments on Si(111) single crystal surfaces. Task was of course also to proof a similar quality of performance for the more challenging environment of electrolyte solution. CF-based STM tips have thus been challenged with attempts to resolve the structural fine details of a Au(111) surface in perchloric acid. Large-scale in situ STM images taken of a monocrystalline facet of Au(111) revealed a surface consisting of flat terraces separated by numerous steps (see Figure 3.26(A)). A cross section through one particular terrace step (Figure 3.26(B), blue trace) exposed a height difference of 700 pm, which corresponds well with what was observed by others with Pt or W in situ STM tips (Möller, Magnussen, & Behm, 1996) for the height of a single atomic step separating two Au(111) terraces. On the terraces of the Au(111) structure, on the other hand, the characteristic stripe pattern of the herringbone reconstruction with a vertical modulation of 0.02 nm (Figure 3.26(B), red trace) can be observed in the same manner as with common metallic STM tips. The observed outcome of the first set of imaging trials

demonstrated a good performance of the carbon tips for topographical imaging and promising application could be foreseen.

To see whether EDP/Sylgard-insulated CF-based in situ STM tips would work at exceptional tip potentials STM imaging on the Au(111) sample was carried out at various tip potentials in the range of 0 to +0.6 V. As can be seen in Figure 3.26(C)-(D), well resolved STM images of the Au surface could be obtained with tip potentials as low as 0 and as high as 0.6 V, whereas outside of this range STM imaging became unstable. Conclusion was that with carbon tips STM measurements can be performed at substantially more positive tip potentials than with metal tips, a property which may lead to novel applications, in particular for inspections of organic adsorbate layers and single molecule scanning tunneling spectroscopy.

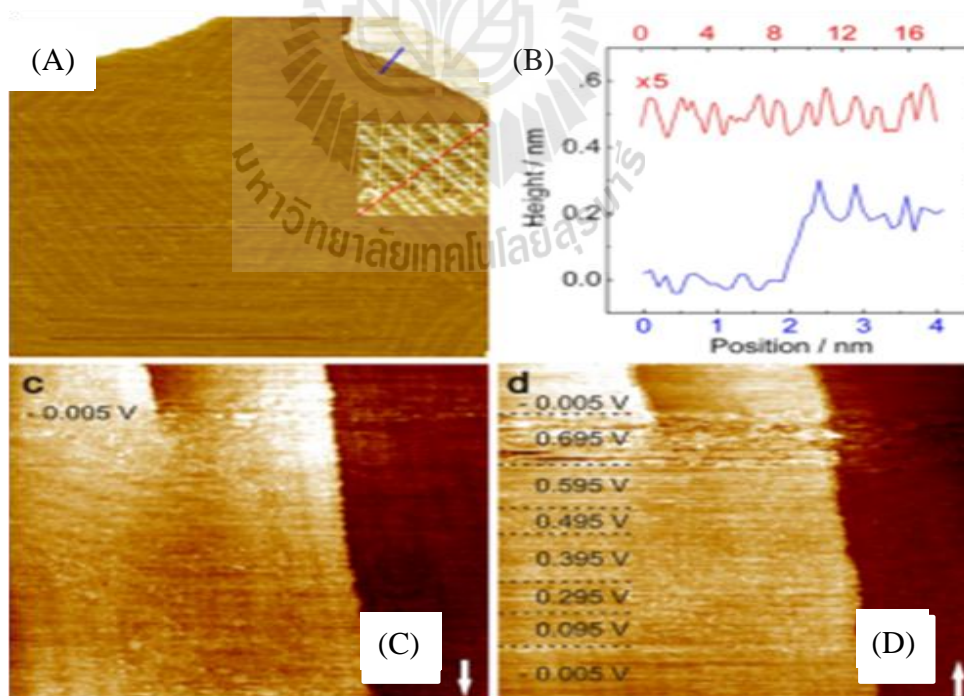


Figure 3.26 In situ STM images of a clean Au(111) electrode surface in 0.1 M HClO₄.

In situ STM images of a clean Au(111) electrode surface in 0.1 M HClO₄, showing (A) an image of characteristic surface topography, exhibiting monoatomic steps between terraces and the herringbone surface reconstruction within the terrace structure (69 x 69 nm², I_T = 0.5 nA, U_{sample} = 0.01 V, U_{tip} = -0.11 V), (B) cross sections along the red and blue lines indicated in (A), and (C, D) examples of images recorded at variable tip potential (95 x 95 nm², I_T = 0.6 nA, U_{sample} = 0.2 V, U_{tip} is displayed in the subfigures).

3.3.6.2 Molecular STM imaging with CF-based probe tips of organic adsorbate layers on gold surfaces

After it was proven that CG-based EC-STM tips indeed were good enough for obtaining atomic resolution imaging on Au(111) single crystal surface it was appealing to test whether also the molecular structural details could be resolved of adsorbate layers of organic molecules that self-assemble on e.g. specific noble metal surfaces. As model samples used were octyl-triazatriangulenium (TATA) adlayers on Au(111). TATA molecules form well-ordered hexagonal adlayers with a ($\sqrt{19} \times \sqrt{19}$) R23.4° superstructure on the Au (111) surface. This structure was clearly observed in the imaging experiments with the CF tips (see Figure 3.27(A)). Prior to an application for STM trials on TATA adlayers, CF STM tips were tested on bare Au(111) for atomic resolution imaging capacity to prove the tip quality and ensure the potential for molecular resolution on the chemically modified metal surface. Usually the detailed TATA structure could be resolved, when atomic resolution images were possible on bare Au(111). Typical tip currents for such molecular resolution images were 0.1 nA, which is about 3 times larger than those in STM studies employing

conventional tungsten tips. In some small-scale images even higher, sub-molecular resolution could be achieved, revealing the 3-fold symmetry of the TATA molecules (Figure 3.27(B)). The quality of the STM images is similar to those obtained with metal tips for this adsorbate system (Baisch et al., 2008; Jung et al., 2011; Kuhn et al., 2010).

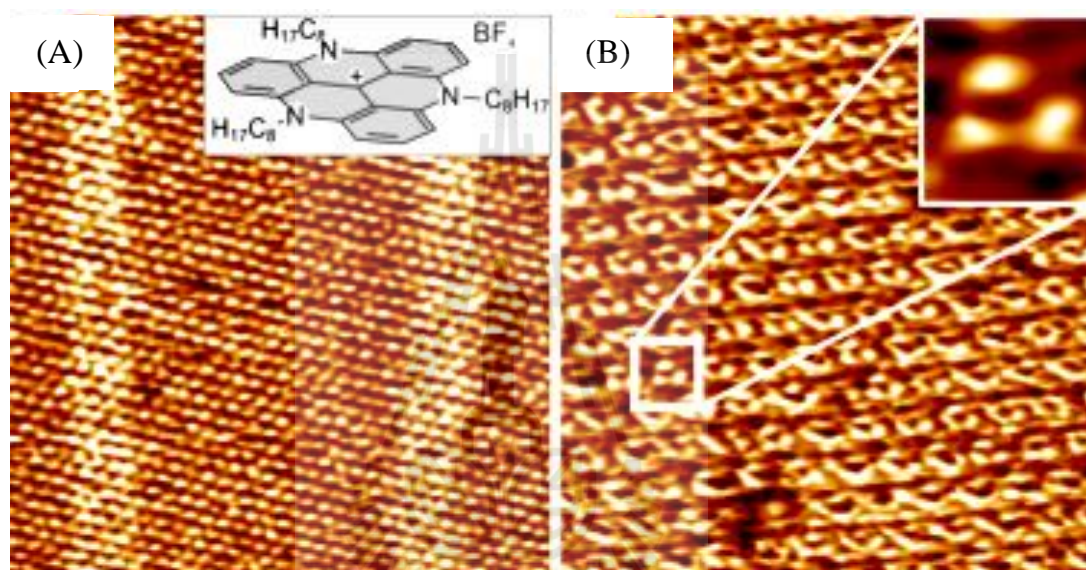


Figure 3.27 In situ STM images of an octyl-TATA adlayer on Au(111) in 0.1 M HClO₄.

In situ STM images of an octyl-TATA adlayer on Au(111) demonstrating high resolution imaging. (A) Long-range structural order ($35 \times 35 \text{ nm}^2$, $I_T = 0.1 \text{ nA}$, $U_{\text{sample}} = 0.4 \text{ V}$, $U_{\text{tip}} = -0.05 \text{ V}$). (B) submolecular resolution imaging of the TATA molecules ($12.5 \times 12.5 \text{ nm}^2$, $I_T = 0.1 \text{ nA}$, $U_{\text{sample}} = 0.3 \text{ V}$, $U_{\text{tip}} = -0.06 \text{ V}$). The inset in part a shows the structure of a TATA molecule and that in part B is a magnification of one of the many adsorbed TATA molecules (Baisch et al., 2008).

3.4 Conclusion

The potential of CF-based nanometric tips for atomic resolution STM imaging in ultrahigh vacuum, and, after appropriate insulation, in electrolyte environment has been demonstrated. The novel STM probe tips resolved, for instance, the atomic structure of a Si(111) single crystal surface as good as common metallic probe tips would do. In a typical electrolyte, EDP/Sylgard-insulated CF tips could be operated as EC-STM scanning probes and they demonstrated the ability to well resolve both the atomic fine structures of single crystal Au(111) surfaces and the molecular arrangement of self-assembled adlayers of organic molecules on a Au(111) substrate. As the material of the developed novel scanning probes is carbon and carbon is known to be related to an extended potential window compared to e.g. noble metal or tungsten, access to exciting STM experiments has been opened and future work will have to explore related opportunities.

3.5 References

- Baisch, B., Raffa, D., Jung, U., Magnussen, O. M., Nicolas, C., Lacour, J., Kubitschke, J. and Herges, R. (2008). Mounting freestanding molecular functions onto surfaces: the platform approach. **Journal of the American Chemical Society** 131(2): 442-443.
- Bonnell, D. A. (1993). Microscope Design and Operation. In B. Dawn (ed.), **Scanning Tunneling Microscopy and Spectroscopy Theory, Techniques, And Applications** (pp. 7-30). New York: VCH publisher, Inc.

- Chen, J. C. (1993). **Introduction to Scanning Tunneling Microscopy**. New York: Oxford University Press.
- Desai, S., Netravali, A. and Thompson, M. J. (2006). Carbon fibers as a novel material for high-performance microelectromechanical systems (MEMS). **Journal of Micromechanics and Microengineering** 16(7): 1403-1407.
- Duke, C. B. (2003). The birth and evolution of surface science: Child of the union of science and technology. **Proceedings of the National Academy of Sciences** 100(7): 3858–3864
- Joost, F. (2004). **Principle of scanning probe microscopy** [On-line]. Available: [http:// www.physics.leidenuniv.ml/sections/cm/ip/group/Principle of SPM.htm](http://www.physics.leidenuniv.nl/sections/cm/ip/group/Principle%20of%20SPM.htm).
- Julian, C. (1993). **Introduction to scanning tunneling microscopy**. New York: Oxford university press.
- Jung, U., Kuhn, S., Cornelissen, U., Tuzcek, F., Strunskus, T., Zaporojtchenko, V., Kubitschke, J., Herges, R. and Magnussen, O. (2011). Azobenzene-Containing Triazatriangulenium Adlayers on Au(111): Structural and Spectroscopic Characterization. **Langmuir** 27(10): 5899-5908.
- Kobayashi, K., Yamada, H., Horiuchi, T. and Matsushige, K. (1999). Investigations of C60 molecules deposited on Si(111) by noncontact atomic force microscopy. **Applied Surface Science** 140(3–4): 281-286.

- Kuhn, S., Baisch, B., Jung, U., Johannsen, T., Kubitschke, J., Herges, R. and Magnussen, O. (2010). Self-assembly of triazatriangulenium-based functional adlayers on Au (111) surfaces. **Physical Chemistry Chemical Physics** 12(17): 4481-4487.
- Möller, F. A., Magnussen, O. M. and Behm, R. J. (1996). Two-Dimensional Needle Growth of Electrodeposited Ni on Reconstructed Au(111). **Physical Review Letters** 77(15): 3165-3168.
- Mousa, M. S. (1996). Electron emission from carbon fibre tips. **Applied Surface Science** 94/95: 129-135.
- Rohrer, G. (1993). The preparation of tip and sample surfaces for STM experiments. In A. B. Dawn (Ed.), **Scanning Tunneling Microscopy and Spectroscopy Theory, Techniques, and Applications** (pp. 155-188). United States of America: Wiley, John & Sons, Incorporated.
- Schulte, A. (1994). **Preparation and characterization of different types of ultramicro-electrodes: A contribution to the development of novel microsensors for electro-chemical bio- and trace analysis and various methods of scanning probe microscopy**. Ph.D. Thesis, University of Muenster, Germany.

Sripirom, J., Noor, S., Köhler, U. and Schulte, A. (2011). Easily made and handle carbon nanocone for scanning tunneling microscopy and electroanalysis.

Carbon 48: 2402-2412.

Takayanagi, K., Tanishiro, Y., Takahashi, M., and Takahashi S. (1985). **Journal of**

Vacuum Science & Technology A3: 1502.

Tersoff, J. and Lang, N. D. (1993). Theory of Scanning Tunneling Microscopy. In J.

A. Stroscio and W. J. Kaiser (eds.), **Scanning Tunneling Microscopy**.

SanDiego, CA: Academic Press.

Wiesendanger, R. and Güntherodt, H. J. (1994). **Introduction Scanning Tunneling**

Microscopy I (2nd ed.). Berlin, Germany: Springer-Verlag.

Zoski, C. G., Yang, N., He, P., Berdondini, L. and Koudelka-Hep, M. (2007).

Addressable Nanoelectrode Membrane Arrays: Fabrication and Steady-State

Behavior. **Analytical Chemistry** 79: 1474-1484.

CHAPTER IV

A NOVEL SYSTEM FOR SIMPLE SMALL-VOLUME VOLTAMMETRY

Abstract

Clinical, environmental, forensic, toxicological, pharmaceutical and synthetic chemistry laboratories repeatedly face the challenging situation that only a very tiny amount of sample is accessible for inspection. Comprehensive qualitative and/or quantitative assessments aiming on complementary data from the various existing analytical methods is in this case problematic as the few micrograms- or liters of sample material have to be shared for multiple measurements in portions that are even smaller than the original low measures. In this context assay miniaturization is certainly a demanding requisite and a lot of efforts was and is spent on suitable solutions. Idea here was the realization of a miniaturized three-electrode electrochemical suitable for the execution of the full spectra of powerful voltammetric trace analysis, however, in just 15 μL volumes of the measuring electrolyte buffer. The design of the novel system involves a rolled piece of Pt foil of an inverted Ω shape that is electrolyte container and counter electrode at the same time. The limitation of the diameter and length of the tube to the low mm scale restricts the enclosed volume to the desired microliters. Working and reference electrodes of appropriate size are just incorporated from the left and right tube endings and kept

there stationary for the measurements. As shown later in detail such an arrangement is simple to put together, easy to use for repetitive measurements and rather rapid in an analytical trial, with only 10 minutes required for one acquisition of analyte quantification via voltammetry in the standard addition mode. The quality performance level of the 15 μ L electroanalysis was evaluated through pioneering test trials with the common analgesic paracetamol. The choice of paracetamol analysis made sense as in pharmacokinetics, for instance, aim usually is to keep the total amount of volunteer's blood to be collected for the construction of drug concentration-time profiles at minimum level and withdrawals of smallest feasible blood samples at a time are preferred. Such a case of sample volume restriction needs adapted analytical schemes for sensitive measurements in uncommonly small measuring containers. The results here illustrated that adjusted paracetamol levels in model samples were well recovered in the innovative 15 μ L electrochemical cell with the deviations from true values being not larger than $\pm 5\%$. The system also worked well for paracetamol detection in serum samples coming from a volunteer who ingested a dose of 1000 mg of the drug. Comparative differential pulse voltammetry in serum samples obtained before and 1 and 4 hours after paracetamol medication disclosed nicely the absence, appearance and clearance of the drug, respectively. Quantitative measurements on the 1 hour samples revealed on the other hand a blood paracetamol level that was in good accordance with published data. In conclusion a miniaturized electrochemical cell has been realized that can accurately handle 15 μ L sample volumes for voltammetric analyte quantification and thus can work with samples obtained by the finger prick blood collection method. In the following the principles of the proposed strategy will be introduced and information be provided

that is relevant to the utilization for the determination of the chosen test analyte paracetamol.

4.1 Introduction

Miniaturization of the tools for optical and electrical/electrochemical instrumental analysis has always been a focus of science and technology. Among other relevant issues, the minimization of detection volumes was emphasized in a quite a few reports of the past decades. One detection method amenable to an adaptation for small-volume (trace) analysis is optical fluorescence microscopy that has been demonstrated as feasible, for example, in small droplets on the microliter scale but also nano- to picoliter volumes at the end of a capillary electrophoresis system have been addressed with success. (Holland and Jorgenson, 1995; Larson, Ahlberg and Folestad, 1993; Mahoney and Hieftje, 1994). Nuclear magnetic resonance spectroscopy (NMR), another powerful detection method and traditionally a large-volume technique, recently was being adapted for the analysis of samples in the nanoliter range (Olson, Peck, Webb, Magin and Sweedler, 1995; Wu, Peck, Webb, Magin and Sweedler, 1994). Small-volume detection has been possible by electrochemical methods since the advent of microelectrodes a few decades ago. Currently, ultramicroelectrodes are, for instance, extensively in use as nano- to picometer tapered detectors for the pipette outlets of microbore liquid chromatography (Mayne and Dujardin, 2008) and capillary electrophoresis (Frisbie, 2003). Detection in sub-femtoliter volumes with ultramicroelectrodes has also been reported to measure the activity of single molecules trapped in an adherent solution at the tip of a SPM probe (Etienne, Anderson, Evans, Schuhmann and Fritsch, 2006;

Fan, Kwak and Bard, 1996). The detection of trace amount of chemical secretion from single living cell in small-volume-electrochemical cell has been reported, and measured, for instant, secretion or exocytosis of neurotransmitters (e.g. catecholamine, dopamine, serotonin, etc.) (Bond, 1994; Lin, Trouillon, Svensson, Keighron, Cans and Ewing, 2012; Troyer and Wightman, 2002; Wightman et al., 1991). Accurate measurements in small droplets, thin capillary outlets or individual living cells require of course the use of accurate manipulators, microscopes and probably software-assisted video microscopy.

First test trials of the 15- μ L three-electrode electrochemical cell that was proposed here were meant to involve voltammetric analysis of the analgesic acetaminophen (N-acetyl-p-aminophenol, ACMP), which is more commonly known as paracetamol. Paracetamol is active ingredient in many over-the-counter pharmaceuticals, e.g., Tylenol[®], Excedrin[®], Nyquil[®], and is frequently used as aspirin substitute. It is used against fever and to relieve mild to moderate pain, including instances of tension headache, migraine headache, muscular aches, neuralgia, backache, joint pain, rheumatic pain, general pain, toothache, teething pain, and period pain. It is suitable for most people, including the elderly and young children, because it reportedly has very few side effects the clinical suggestion for the maximal dose for an adult is 4,000 mg/day or 4 tablets with a 1,000 mg dose. Pharmacokinetic studies (Ward and Alexander-Williams, 1999) revealed that (1) for adults the peak blood level remains less than 20 mg/L after a standard 1,000 mg dose had been ingested and uptaken, (2) blood serum levels will normally peak between 30 and 120 minutes after ingestion and (3) the beneficial analgesic effect of paracetamol may last up to about four hours. ACMP is one of the most frequently used analgesic drugs. As long as therapeutic

dosage levels are not exceeded the drug is relatively non-toxic. Continuous ingestion for longer times and overdosing, however, is known to have very adverse health effect and serious intentional or unintentional too large doses may even be lethal. Because of its prominent therapeutic use and frequent clinical cases of people suffering from overdosing, effective ACMP assays are of vital importance for pharmaceutical companies and clinical laboratories. A number of methods, including titrimetry (Burgot, Auffret and Burgot, 1997; Kumar and Letha, 1997), high performance liquid chromatography (Alkharfy and Frye, 2001; Altun and Erk, 2001; Campanero, Calahorra, García-Quétglas, López-Ocáriz and Honorato, 1999; Shervington and Sakhnini, 2000), capillary electrophoresis (Kunkel, Günter and Wätzig, 1997; Kunkel and Wätzig, 1999), spectrophotometry (Erk, 1999; Hanaee, 1997; Mohamed, AbdAllah and Shammam, 1997; Ni, Liu and Kokot, 2000; Ramos, Tyson and Curran, 1998; Săndulescu, Mirel and Oprean, 2000), and electrochemistry (Săndulescu, Mirel and Oprean, 2000; Wangfuengkanagul and Chailapakul, 2002; Zen and Ting, 1997) are available for quantitative paracetamol determination and they have been used to study the drug's oxidation mechanisms, its redox metabolites and appearance in pharmaceuticals and body fluids.

The method that was developed here is based on literature-known detection schemes; however, it was designed to work in an easy and rapid reproducible manner in the small volumes of 15 μL -volumes of measuring solution. At the center of the novel type of ACMP detection is the miniaturized three-electrode electrochemical cell configuration that has a carbon-fiber ultramicroelectrodes (CF-UMEs) implemented as working electrode to gain additionally from earlier mentioned advantages of a reduction in active electrode dimension. Though the prime target for the application

of the novel scheme was ACMP, use is not limited to this analyte and basically the determination of any electroactive species can be addressed with the system, at least if working electrode optimization for the particular compound of interest has been undertaken. Introduced in the following will be the principles of the novel small-volume voltammetric cell and a demonstration of its well-working will be presented for the model analyte paracetamol.

4.2 Experimental and methods

4.2.1 Working electrode preparation procedures

One important step is the fabrication of the CF-UMEs. A bundle of PAN-based CFs, actually of the type E/XAS, 5-7 μm diameter (SGL TECHNIK GmbH, Meitingen, Germany), was soaked in acetone (99.8%, Carlo Erba, Italy) for 5 days to remove the thin polymer coating layer that is usually applied by the producers as protective surface finish. Then the bundle of CFs was rinsed with deionized (DI) water, dried by a gentle touch with soft tissue paper and finally left at room temperature for a few hours before to dry further use. A copper needle wire with a bit of conductive carbon paint (SPI supplies, West Chester, PA, USA) on end was used to pick up a single CF filament from the bundle. The individual CF was with the aid of a small drop of conductive carbon paint attached to the bottom end of a tungsten (W) wire (0.25 mm diameter, 99.99% purity, Goodfellow, England) that served as holding wire. After that, the CF-W wire assembly was inserted into a glass capillary with a tapered tip of an inner diameter of $\sim 20 \mu\text{m}$. A 1-cm length of the CF was allowed to protude from the glass tip opening. The CF-W assembly was in this position tightly sealed with respect to the glass capillary using a two-component silicon elastomer for

fixation. At last, the CF was trimmed with a scalpel to get the desired length of a conductive microcylinder of about 1 mm. A schematic of the resulting cylindrical CF UMEs is displayed in Figure 4.1.

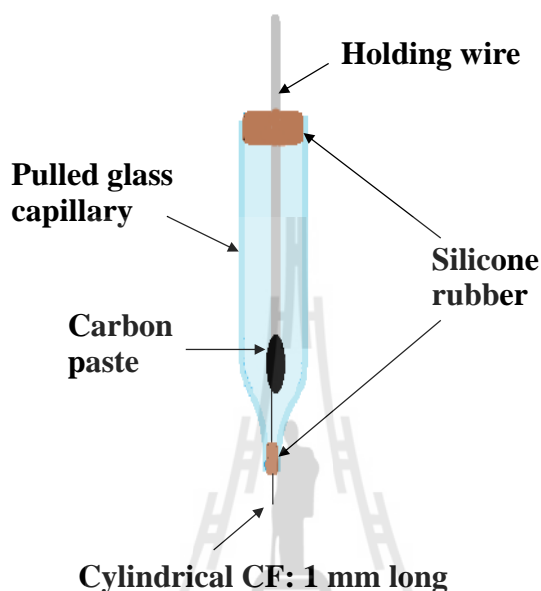


Figure 4.1 Schematic illustration of a cylindrical carbon fiber UME.

Schematic illustration of a cylindrical carbon fiber microelectrode as used for paracetamol voltammetry in a 15- μ l electrochemical cell.

Also used as working electrodes in test trials were carbon rods and disk-shaped gold and platinum microelectrodes. Carbon rods, actually used were common pencil leads (0.5 mm diameter, 2B, Paper Mate[®], Korea), which were electrochemically cleaned by the application of a cycling potential in H₂SO₄ (96%, Carlo Erba, Italy). Potential ramps from 0.0 to 0.8 V vs. Ag/AgCl at a scan rate of 100 mV/s were applied to the rods and repeated 50 times to achieve sufficient success with the pretreatment. After the electrochemical cleaning, was completed electrodes were rinsed by water and dried in air at room temperature, respectively.

The homemade glass-insulated disk-shaped metal microelectrodes were obtained by sealing gold and platinum microwires of 50 μm diameter (50 μm diameters, 99.99% purity, Goodfellow, England) into pulled glass pipettes and exposing the metal disk via careful polishing on emery paper of different grade. Before use the metal disk UMEs were always exposed to a final mechanical fine polishing with alumina paste (Gamma Micropolish[®] II, Buehler, USA) on a velvet cushion for 3 minutes, then rinsed with DI water, and finally allowed to dry in air at room temperature.

The counter electrode for all tests was a \cup -shaped Pt foil (details are provided below) and the reference electrode was a Ag/AgCl wire of 1 mm diameter. All potentials in the following work with the small-volume voltammetric cell are thus listed with respect to the Ag/AgCl pseudo reference electrode system.

4.2.2 Voltammetric measurements

4.2.2.1 Redox mediator voltammetry in the 15- μL electrochemical cell

To test the voltammetric performance and assess the evaporation effect on the 15- μL electrochemical cell, cyclic voltammograms were measured for the reversible redox mediator system $\text{Ru}^{3+}/\text{Ru}^{2+}$. Electrolyte for the trials was a 1 mM $(\text{Ru}(\text{NH}_3)_6)\text{Cl}_3$ solution in 0.1 M KCl, while the potential sweep was performed between -0.1 to -0.4 V vs. Ag/AgCl with a scan speed of 50 mV/s

4.2.2.2 Preparation of ACMP test solutions

A paracetamol tablet with a nominal content of 500 mg ACMP (Tylenol[®], USA) was dissolved in 0.10 M phosphate buffer pH 7.2. For comparison, a

standard solution of ACMP was prepared by dissolving commercial 4-Acetamidophenol (98% purity, Acros Organic, Belgium) in DI water as a stock solution and used without further purification. Diluted ACMP working solutions were prepared from the stock solution by appropriate dilutions with buffer.

4.2.2.3 ACMP voltammetry in beaker-type conventional or in small-volume electrochemical cells

All voltammetric measurements were carried out at room temperature with a computer-controlled potentiostat (model Reference 600[®], Gamry Instruments, Warminster, PA USA). A normal (beaker-type) three-electrode cell configuration suitable for work with microelectrodes was used to study the behavior of ACMP in voltammetric scans at the CF-UMEs of this study. Working electrode was the 1 mm long of cylindrical CF as obtained through the above mentioned fabrication procedure. Counter electrode (CE) in case of the beaker-type cell configuration was a coiled platinum (Pt) wire. And the reference electrode was a self-made Ag/AgCl wire. Cyclic voltammograms were recorded by scanning the potentials from 0.0 to +1.0 V vs. Ag/AgCl with a scan rate of 100 mV/s. When differential pulse voltammetry was chosen as analytical method the measured potential was swept from 0.2 to 0.8 V vs. Ag/AgCl, and the parameters for I/E curve acquisition were: step size 5 mV, sample period 1 s, pulse time 0.1 s, pulse size 50 mV. All experiments have been done in ambient condition without special preconcentration time adjusted.

4.2.2.4 Interference study

Ascorbic acid (AA) sodium salt (99%, Acros Organic, Belgium) was diluted in 0.1 M phosphate buffer pH 7.2 to prepare a stock solution of a compound that is known to be a main troubling interference for measurements in urine and blood samples. Diluted working solutions were prepared from the stock solution by appropriate dilutions with buffer.

4.2.2.5 Human blood serum (HBS) sample

5 ml blood samples were collected from a volunteer who had taken a medication of 1000 mg of paracetamol (2 tablets) at the preferred time (before, 1 h, and 4 h after medication). The collected blood was centrifuged at 2000 G for 15 min, by a high-speed micro centrifuge (model CF16RXII, Hitachi, Japan). After centrifugation, red blood cell precipitate and the serum HBS solution were separated. Then, the HBS was divided in portion, diluted into storage tubes and kept until use. HBS solution for voltammetric measurements were diluted in 1:1 ratio with 0.1 M phosphate buffer pH 7.2. The quantitative determination of ACMP level in HBS at the after 1 h medication was performed by the standard addition method. Three aliquots of this test solution were prepared by adding 10 μ M of ACMP standard solution increment.

4.3 Results and discussion

4.3.1 The 15- μ L-three-electrode cell design

Figure 4.2 shows a schematic of the simple stereomicroscope-micromanipulation platform that was adapted for electroanalysis in 15 μ L volume of samples. The Ag/AgCl wire reference and a working electrode of choice (e.g. a cylindrical CF electrode) are held by two micromanipulators and thus movable in x, y, z directions. The three-electrode configuration is completed by the tubular Pt trough that is meant to serve at the same time as electrolyte container and counter electrode. All three electrodes are connected to a computer-controlled potentiostat for voltammogram acquisition, storage and analysis.

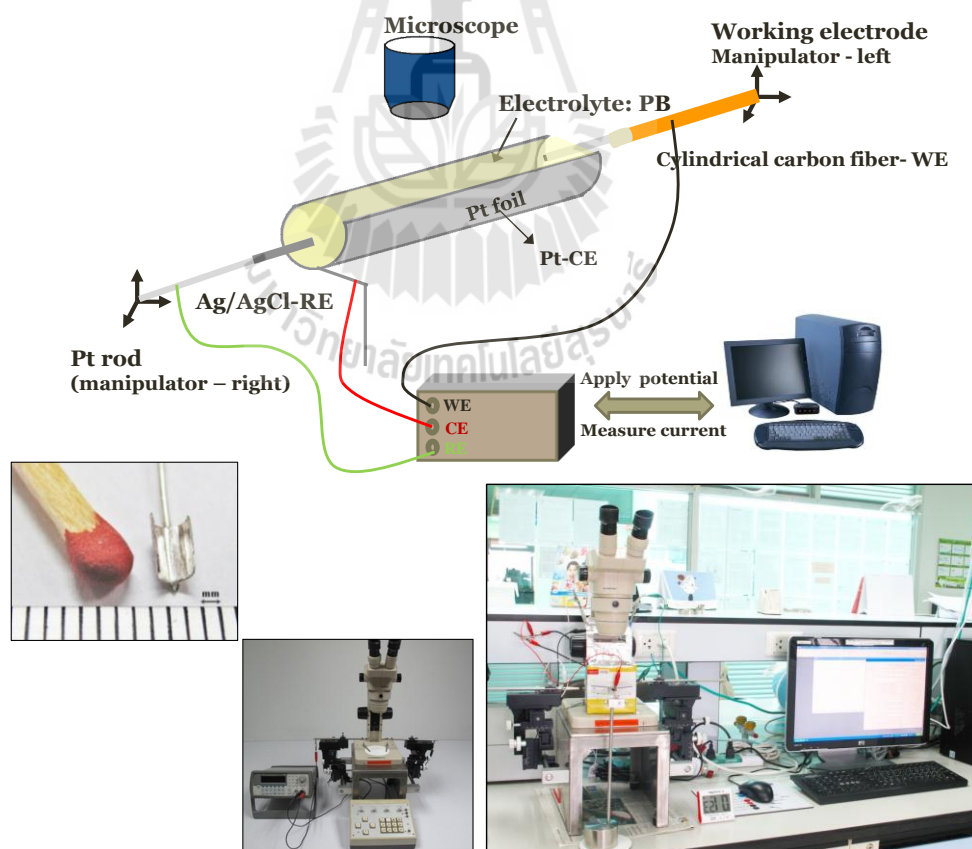


Figure 4.2 The stereomicroscope/micromanipulation platform for voltammetry in 15 μ L samples.

The three-electrode configuration consists of movable working (here: a cylindrical CF microelectrode) and a Ag/AgCl reference electrode (RE) and the \cup -shaped Pt trough as auxiliary electrode (CE). Note that the Pt trough is electrode and electrolyte container at the same time.

Important practical features of this developed small volume voltammetry cell are simple and quick handling, easy change of the working electrode type and a virtually unlimited recycling. One voltammetric analytical measurement cycle in the 15- μ L- three-electrode cell takes about 2 minutes in, for instance, the DPV mode with accumulation, and 10 minutes are thus needed for a the acquisition of the five voltammograms for analyte quantification by means of standard addition. The list of actions in such a trial with the system is as the following

- 1) Fixation of the Pt trough (CE) on the gripper and maneuvering into right position. Attachment of the other two electrodes (e.g. a CF-UME as WE and Ag/AgCl wire as RE) to the two micromanipulators (left and right) for controlled movement in x, y, z direction and placement of them into the tubular structure as shown in the schematic in Figure 4.2.
- 2) Electrolyte addition through careful pipetting of 15 μ L of measuring solution.
- 3) Execution of the electrochemical analysis.
- 4) Careful withdrawal of the WE and RE from the small tubular cell and electrolyte removal.

- 5) Cleaning of all three electrodes (WE, RE, and CE) by rinsing with DI water and quick drying via touch to soft tissue paper. Extra heat-cleaning of the Pt trough in an alcohol flame for a few seconds.
- 6) Repetition of steps 1) to 5) for next voltammogram acquisition.

To demonstrate the practicability of the above electrochemical analysis in the 15- μ L microliter Pt trough, cyclic voltammograms have been collected from different electrodes including a thin cylindrical carbon fiber microelectrode, a carbon pencil rod macroelectrode, and gold and a platinum disk microelectrode. All tested electrodes had an overall size smaller than the diameter of Pt trough, which was around 2 mm (Figure 4.2). The $\text{Ru}^{3+}/\text{Ru}^{2+}$ redox couple at 1 mM concentration has been used as test system for the small-volume voltammetry. The voltammograms in Figure 4.3 displayed reproducibly the expected appearance: For the carbon pencil rod WE with the largest diameter the typical peak-shaped voltammetric response of a macroelectrode was observed (Figure 4.3(A)) while a more or less well pronounced sigmoidal voltammetric response came up for the cylindrical CF and the Au and Pt microwire electrodes indicating that these worked as microelectrodes in the I/V experiment (Figure 4.3(B)-(D), respectively). This outcome offered first evidence that the established 15- μ L small volume electrochemical cell is capable of ordinary voltammetry measurements and may have the potential to be used for quantitative assessments.

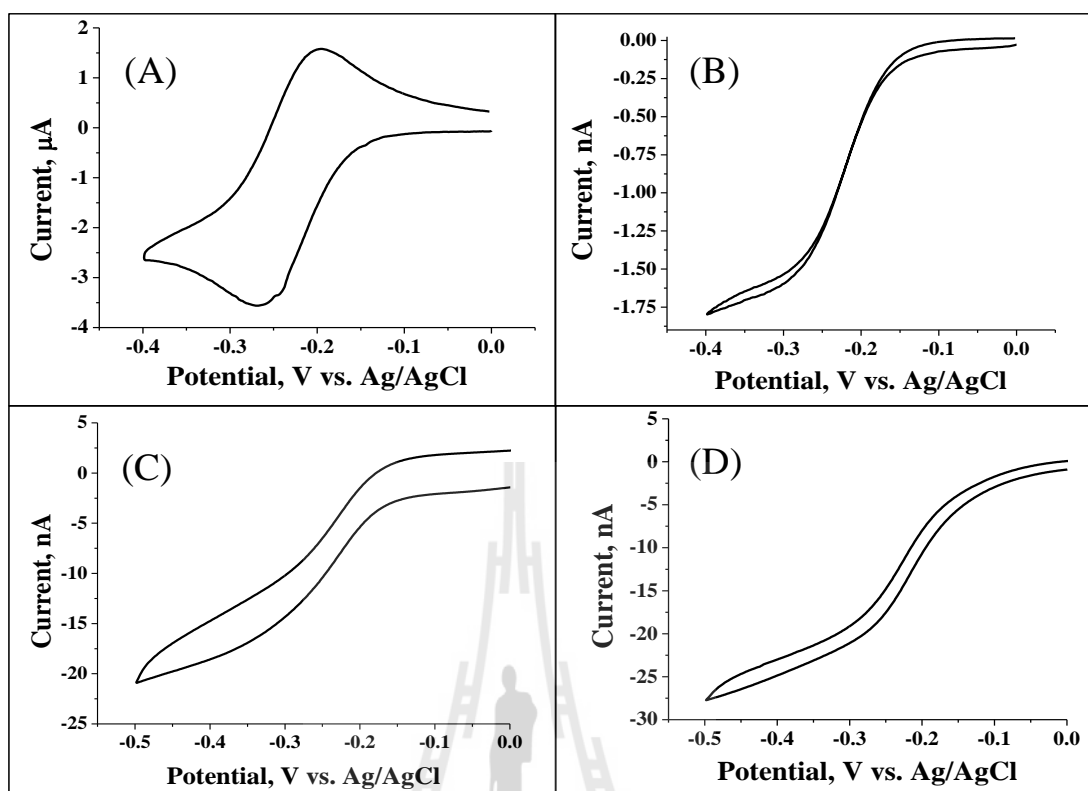


Figure 4.3 Cyclic voltammograms of 1 mM $\text{Ru}(\text{NH}_3)_6\text{Cl}_3$ in 0.1 M KCl at carbon and noble metal UMEs.

(A) carbon pencil rod electrode (0.5 mm \varnothing , 1 mm long), (B) cylindrical carbon fiber microelectrode (1 mm long), (C) disk-shaped Au microelectrode (50 μm \varnothing), and (D) disk-shaped Pt microelectrode (50 μm \varnothing). The potential sweep went from 0.0 to -0.4 or -0.5 V vs. Ag/AgCl at a scan rate of 50 mV/s.

Since above voltammetric test trial with the small-volume configuration was carried out in air room temperature, an important concern was evaporation of electrolyte solution, which could lead during the measurement of a critical change in analyte (mediator) concentration by the evaporation of water. A control experiment was thus performed addressing the response stability of the approach. Figure 4.4(A) and Figure 4.4(C) illustrate the cyclic voltammograms of 1

mM Ru^{3+} in the 15- μL Pt trough at Figure 4.4(A) a carbon pencil rod electrode (1 mm long, 0.5 mm \varnothing) and Figure 4.4(C) a single carbon fiber electrode (1 mm long, 5 μm \varnothing). CVs were measured every two minutes for a maximum of 10 minutes. For the two electrodes, the cathodic peak currents were extracted from the set of voltammograms and plotted as function of time (Figure 4.4(B) and Figure 4.4(D)). Interestingly, a significantly larger effect of solvent evaporation was observed over the inspected time period for the carbon pencil rod electrode as compared to the carbon fiber electrode. While the peak current went up from about 3.75 to 4.75 μA for the carbon rod electrode, the peak current was virtually stable for the carbon fiber electrode version. The better stability of the carbon fiber electrode may be explained by the relative proportion of the electrode structure and the electrolyte container itself. The larger carbon pencil rod electrode occupies by far more space in the small Pt trough than a microscopically thin carbon fiber electrode. This may help reducing the impact of the loss of a small amount of water through evaporation at the time-scale of the experiment. Because of the better performance in terms of response stability, all further experiments addressing quantitative voltammetric analyte determinations in the 15- μL three-electrode configuration have thus been done with cylindrical carbon fiber microelectrodes in use as sensors.

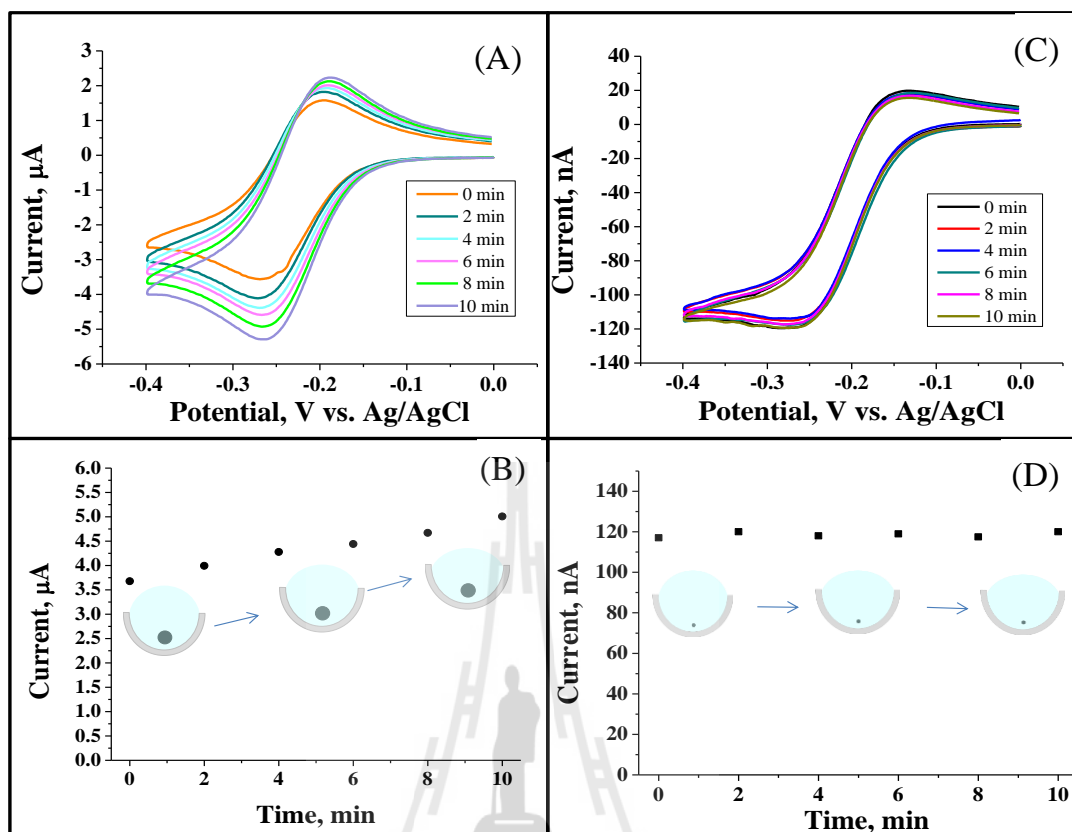


Figure 4.4 Influence of solvent evaporation on the voltammetry of in a 15- μL small-volume electrochemical cell.

Two cylindrical electrodes have been tested: (A and B) A carbon pencil rod electrode of 500 μm diameter and (C and D) a single carbon fiber electrode of 5 μm diameter. Scan speed for all voltammograms was 50 mV/s.

4.3.2 15- μL volume electroanalysis of acetaminophen (ACMP)

As mentioned above, acetaminophen or ACMP is well known as general drug used for pain relief, fever reduction, etc. With the aim to establish quantitative ACMP electroanalysis, the electrochemical behavior of 1mM ACMP was investigated here by CV at a CF electrode in 0.1M PB (pH 7.0). Figure 4.5 is displaying the current response of a CF working electrode that was obtained when its potential was

scanned from 0.0 V to 1.0 V and back. In the CV a clear anodic current appeared at +0.4 V vs. Ag/AgCl a constant plateau formed at potentials above about 0.6 V vs. Ag/AgCl. A well-shaped anodic ACMP peak also turned up when recording differential pulse voltammograms (not shown) and the concentrations dependence of this signal was employed for the further trials that aimed at analyte quantification.

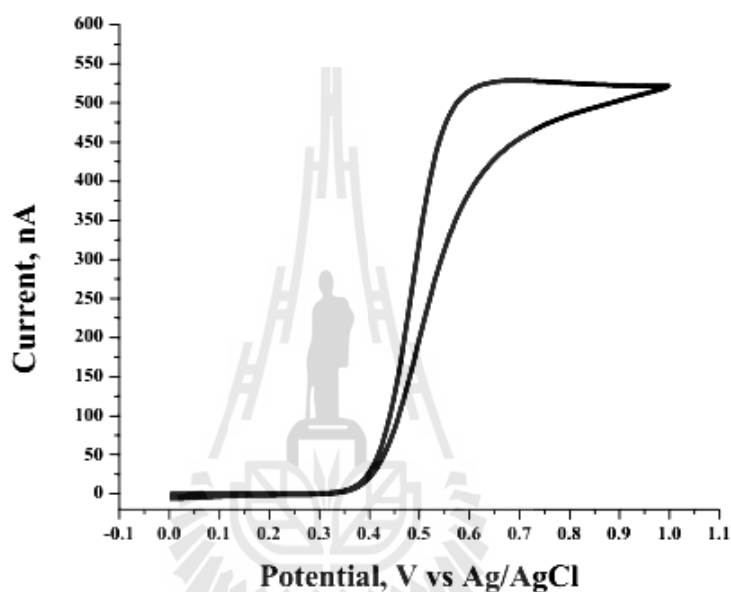


Figure 4.5 ACMP cyclic voltammogram at a cylindrical CF UME.

Analyte level was 1 mM in 0.1 M phosphate buffer (pH 7.2). The potential sweep rate was 100 mV/s from 0.0 to 1.0 V vs. Ag/AgCl.

A set of DPVs of ACMP at the cylindrical CF working electrodes is shown in Figure 4.6(A) with a variation of ACMP concentrations valid in the range 0.1–1500 μM (left panel). As expected, the values of the ACMP DPV peak current, I_p , increased with increased concentration of the analyte. Plots of I_p vs. [ACMP] (Figure 4.6(B)) were linear from 10 to 1500 μM . Lowest ACMP level that produced a pronounced DPV peak was about 0.25 μM .

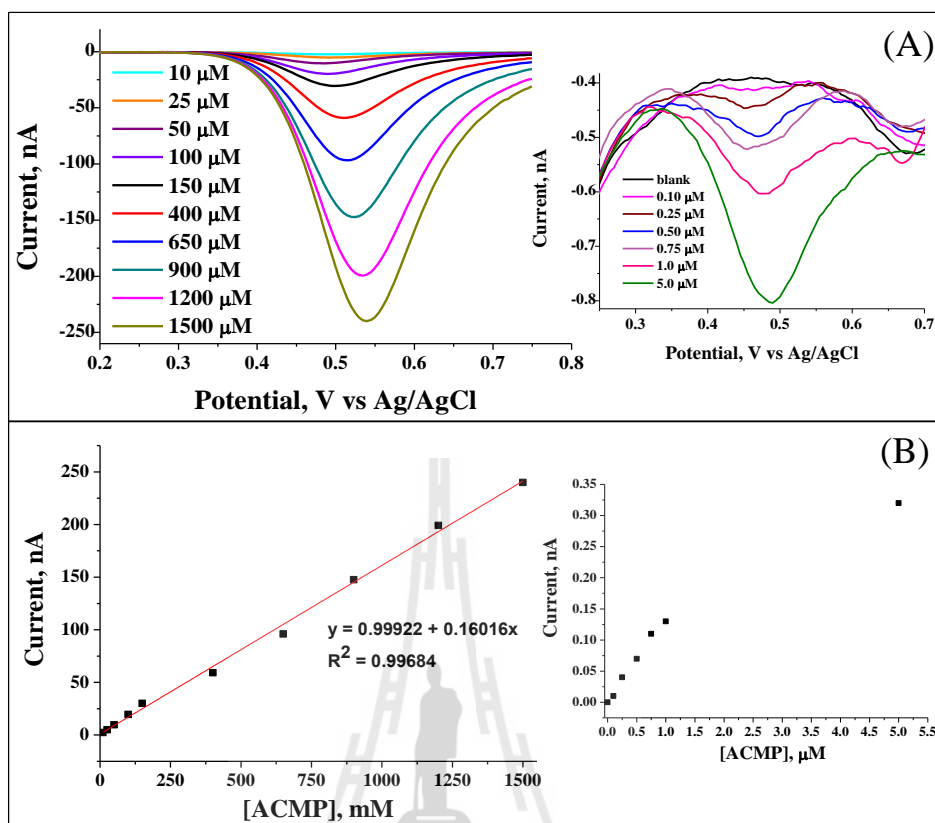


Figure 4.6 Acetaminophen calibration measurement in the 15- μL three electrode electrochemical cell.

(A) Collection of differential pulse voltammograms valid for 0.1 to 1500 μM ACMP. (DPV parameters were: step size of 5 mV, pulse time of 0.1 s and pulse size of 50 mV. (B) Plots of the DPV peak currents of the ACMP differential pulse voltammograms in (A) as a function of the analyte concentration. Linearity of the voltammetric response is observed from 10 to 1500 μM of the analyte.

Quantitative measurements of ACMP in the small-volume electrochemical cell were approached in the standard addition mode of DPV. Figure 4.7(A) shows four DPVs that were recorded sequentially in a test trial with the 15- μL three-electrode cell, handling first a 10 μM ACMP model sample and then the sample

with 20 μM , 40 μM , 60 μM and 80 μM standard additions of ACMP, respectively. Figure 4.7(B) is the plot of the ACMP peak current, I_p , vs. the concentration of added ACMP, [added ACMP]. The level of ACMP in the analyzed model samples was then obtained from the intersection of the extrapolation of the linear fit ($R^2 = 0.998$) with the x-axis. For the particular case shown the measured ACMP level was estimated to be 9.907 μM , and with 10 μM being the adjusted level, the measurement translates into a recovery rate of 99.07% (detail of calculation shows in appendix). In triplicate trials, the average concentration from assay for the voltammetric ACMP analysis was $10.36 \pm 0.75 \mu\text{M}$ ($n = 3$).

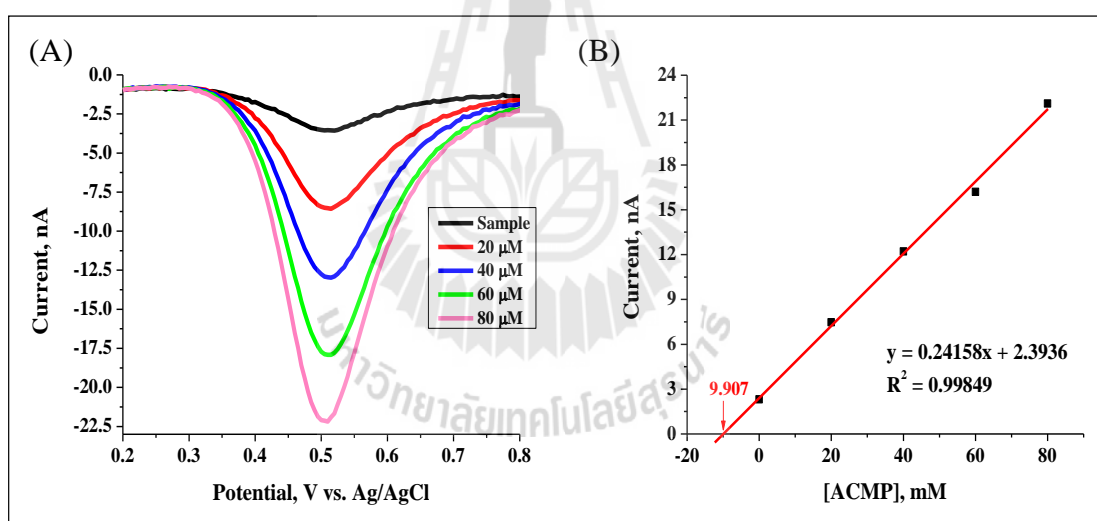


Figure 4.7 Voltammetric quantification of ACMP in the 15- μL three-electrode small-volume electrochemical cell by means of the standard addition method.

(A) Representative ACMP differential pulse voltammograms for a model sample with and without for ACMP supplementations of 20, 40, 60 and 80 μM . (B) Standard addition calibration curve constructed based on the data shown in (A) and the regression graph analysis leading to sample ACMP determination.

4.3.3 15- μ L volume electroanalysis of ACMP in drug tablets

The novel small-volume ACMP voltammetry procedure was further applied to the analysis of real samples and measurements were made with solutions gained by dissolving a commercial paracetamol tablet with 500 mg ACMP in measuring buffer. As representative example Figure 4.8 shows the DPV recordings of a typical standard addition voltammetry test with a 500 mg ACMP tablet sample inspected in a 15- μ L-three-electrode cell and, assuming ACMP as the main contributor to the electrochemical signal, a peak occurred at about 0.5 V vs. reference and increased linearly with the three equal additions of the ACMP stock solution. Taking dilution factors into account, the analysis of plots of the peak currents vs. the concentration of added ACMP allowed the calculation of the ACMP level in the paracetamol tablet for the particular sample as 500 mg, which reflects a recovery rate of 93.884 % ($n = 3$) or the average of the determined ACMP level in the inspected choice of tablet was 465.42 ± 3.93 mg ($n = 3$). The measured content was thus in an acceptable reach of the 500 mg list on the tablet package.

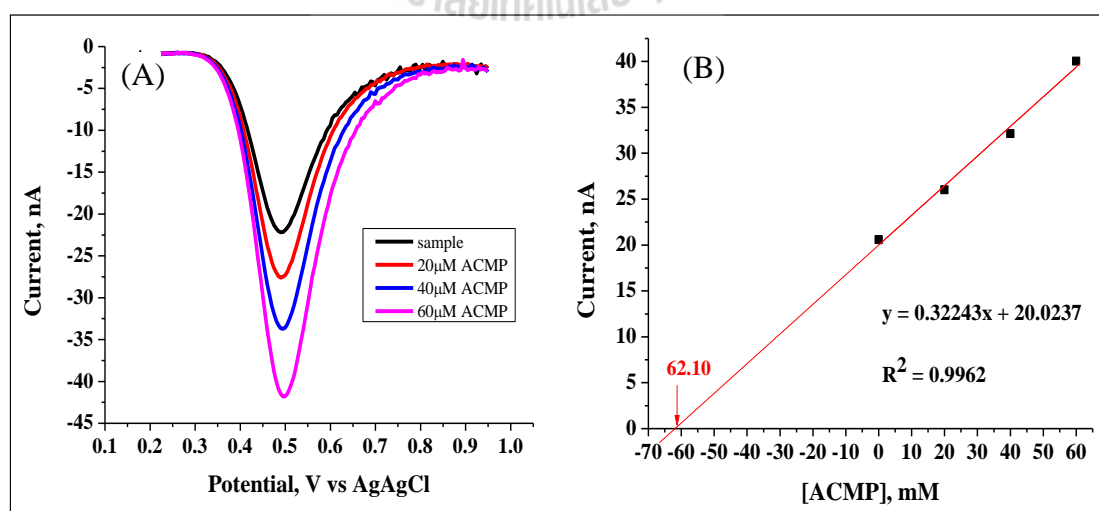


Figure 4.8 Voltammetric quantification of ACMP in a paracetamol tablet with a listed content of 500 mg active compound.

The sample was inspected in the 15- μL volume three-electrode electrochemical cell by means of the standard addition method. (A) Raw ACMP differential pulse voltammograms (DPV parameters: step size, 5 mV; pulse time, 0.1 s; pulse size, 50 mV) for a sample and the sample with 20, 40, and 60 μM additions of analyte. (B) Standard addition calibration curve and the corresponding regression graph analysis.

4.3.4 15- μL volume electroanalysis of ACMP in spiked human blood serum

For testing the suitability of the novel small-volume ACMP voltammetry procedure for ACMP assessments in human blood serum (HBS) samples, volunteer's blood was drawn and processed for analysis. For sample preparation the collected blood sample was centrifuged to separate the serum from the other blood contents such as the red blood cells etc. (details of the procedure: see Appendix). The volunteer's HBS samples were diluted with PB buffer (pH 7.2) 1:1 ratio prior to inspection, spiked with 10 μM ACMP and then voltammetrically approached without and with further addition of standard ACMP solution to get established quantitation via the standard addition method (Figure 4.9(A)). Figure 4.9(B) shows an example of a set of five DPV recordings as obtained in a typical standard addition voltammetry trial on the spiked HBS sample. A peak occurred at about 0.5 V vs. reference that increased well linearly with the three equal additions of the ACMP stock solution. The analysis of plots of the peak currents vs. the concentration of added ACMP allowed the calculation of the ACMP level of the spiked sample. As average of four measurements of a HBS sample with an adjusted 10 μM was thus measured $10.39 \pm 0.93 \mu\text{M}$ ($n = 4$). The recovery rate was thus in a good reach of ideal value and it

seemed that the small-volume ACMP voltammetry worked well even in samples that certainly had a more complex matrix as the dissolved ACMP powder model samples in a bare aqueous buffer.

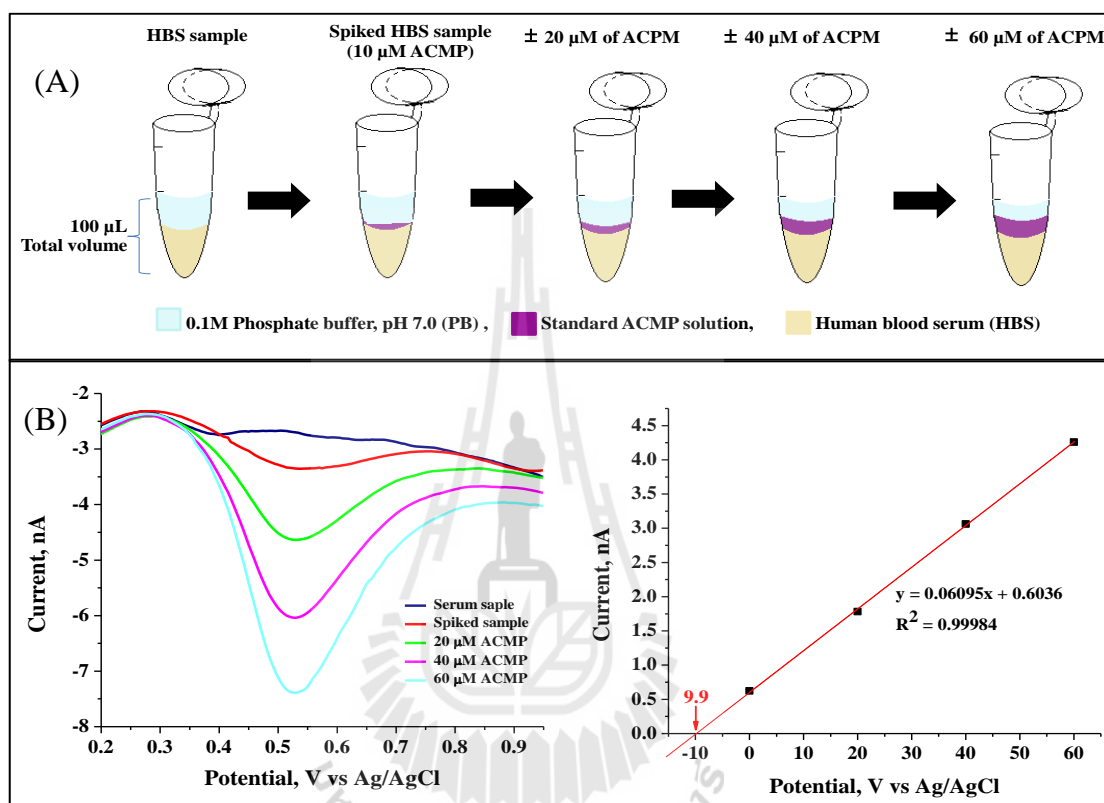


Figure 4.9 Small volume voltammetric quantification of ACMP in human blood serum (HBS).

Analysis took place in the 15- μL three-electrode electrochemical cell by means of the standard addition method. (A) Schematic of the preparation for spiked ACMP-HBS samples. (B) ACMP differential pulse voltammograms for a bare HBS sample, for a spiked HBS sample, and for the spiked sample with further 20, 40, and 60 μM additions of analyte and standard addition calibration curve and the regression graph analysis. (DPV parameters: step size, 5 mV; pulse time, 0.1 s; pulse size, 50 mV)

4.3.5 Detection of ACMP in human blood serum (HBS) sampled before and after oral medication.

As already mentioned earlier, paracetamol or ACMP is after uptake into the human body slowly internalized and channeled into the body fluids and then degraded via metabolization. Peak ACMP blood level is usually obtained about an hour after the time point of tablet ingestion and remains less than 20 mg/L after a normal adult took a 1,000 mg dose of the drug (Bannwarth, and Pehourcq, 2003). Here, the strategy of electroanalysis in the novel small-volume electrochemical cell has been used to reveal a replicate of the time-course of paracetamol appearance/disappearance in the blood serum of a volunteer that had been asked to ingest two 500 mg paracetamol tablets. Figure 4.10 illustrates the ACMP dynamics in human body in terms of the voltammograms taken at the different situations. The black curve represents the DPV response that is valid for HBS before oral medication and no relevant DPV peak showed up that might point towards the presence of ACMP. 1 h after paracetamol tablet ingestion a blood sample was collected and inspected by the small-volume voltammetry approach regarding the ACMP content. The expected ACMP peak appeared (Figure 4.10, red curve) and indicated the presence of the analyte as result of the drug uptake. Confirmation that the observed peak in the serum truly referred to ACMP came from a measurement on HBS samples with further addition of the standard ACMP solution. Supplementation with 50 μM ACMP lead to an increase of the native sample peak that prior to ACMP spiking was obtained at the same potential (blue curve). A blood sample that was collected 4 h after oral medication was also inspected for the ACMP content. As can be seen in Figure 4.10, the current trace for the “4 h”- sample overlapped well with the one

acquired before tablet uptake (green curve). As expected, the body of the blood donor had been metabolically cleared from the drug that was eaten and this clearance was properly reported by the analytical assessment in the small-volume electrochemical cell.

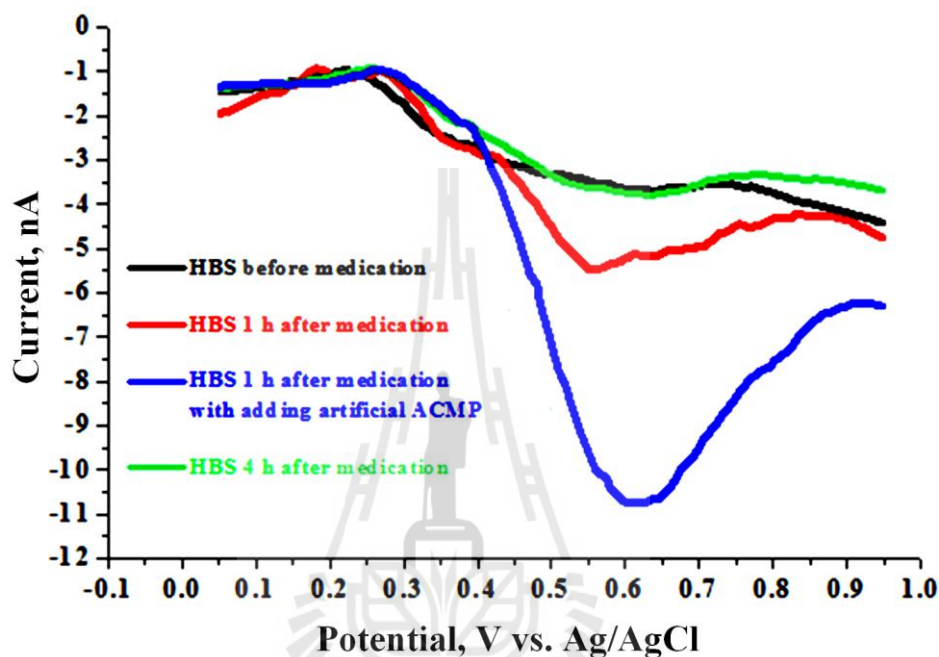
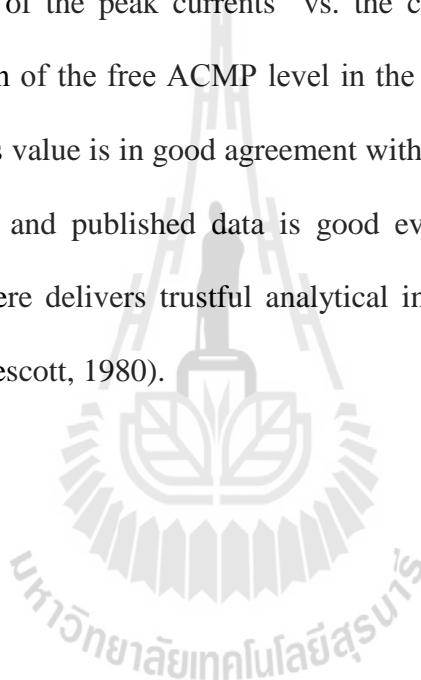


Figure 4.10 Application of the small-volume voltammetry for studying the pharmacokinetics of ACMP in HBS before and after paracetamol ingestion.

ACMP differential pulse voltammograms were recorded with a step size of 5 mV, a pulse time of 0.1 s and a pulse size of 50 mV for HBS samples taken before medication (black trace), 1 h after medication (red trace), 1 h after medication but instantly spiked with 50 μ M ACMP standard solution (blue trace), and 4 h after medication (green trace).

Also performed was a quantification of ACMP in the HBS samples that was taken 1 h after the tablet ingestion. The assessment used the small-volume

electrochemical cell and the standard addition method. In course of the trial, the HBS samples were diluted with PB buffer (pH 7.2) at a 1:1 ratio and supplemented with standard ACMP solution (Figure 4.11(A)). Figure 4.11(B) shows the DPV recordings of a typical standard addition voltammetry trial for the resulting four samples and, not surprisingly, the usual ACMP peak occurred at again in the I/E curves at about 0.5 V vs. reference and displayed an amplitude that was proportional to the ACMP level. The analysis of plots of the peak currents vs. the concentration of added ACMP allowed the calculation of the free ACMP level in the “1 h” HBS sample as $15.72 \pm 0.01 \text{ mg/L}$ ($n = 3$). This value is in good agreement with previous literature reports and the closeness of own and published data is good evidence that the small-volume approach suggested here delivers trustful analytical information (Forrest, Clements, and Prescott, 1982; Prescott, 1980).



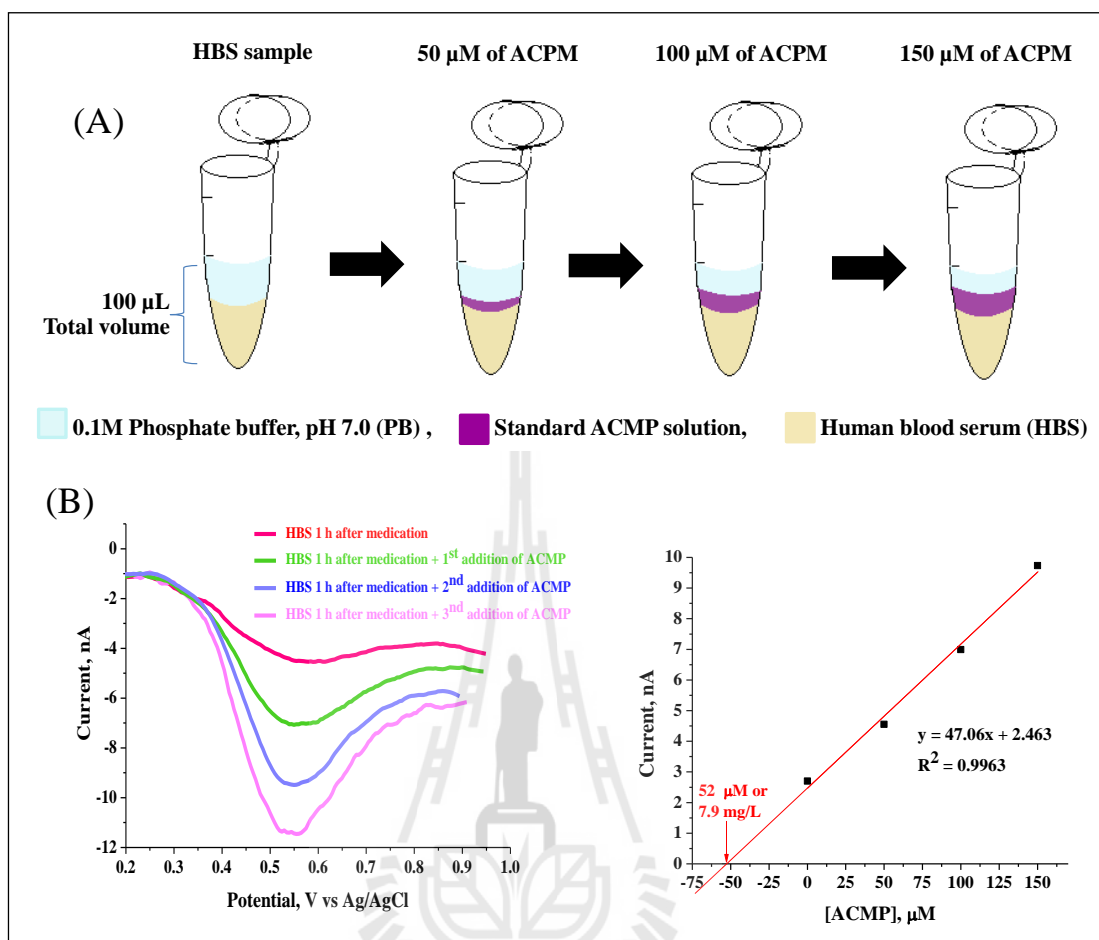


Figure 4.11 Determination of the ACMP quantity in HBS 1 h after ingestion of a paracetamol tablet.

Determination of the ACMP quantity in HBS 1 h after ingestion of 1000 mg of the compound via paracetamol tablet ingestion. Sample assessment used the small volume voltammetric cell of this thesis and the standard addition method for target analyte quantification. (A) Schematic of sample preparation. (B) ACMP differential pulse voltammograms (step size: 5 mV; pulse time: 0.1 s; pulse size: 50 mV) for the “1 h” sample and for the samples with 50, 100, and 150 μM additions of analyte and standard addition calibration curve and the regression graph analysis.

4.4 Conclusion

A novel three-electrode microcell has been presented for analytical voltammetry in about 15 μL measuring solutions. In the standard addition mode the use of the microcell is simple, accurate and reasonably fast. Successful proof-of-principle pharmacokinetic trials with the blood of a paracetamol consumer verified the functionality of the innovative microcell assay by revealing both drug appearance and in the blood serum clearance in a convincing manner. The methodology is thus suggested as an alternative option for small-volume electroanalysis in pharmaceutical, environmental and other chemical analysis laboratories.

4.5 References

- Alkharfy, K. M. and Frye, R. F. (2001). High-performance liquid chromatographic assay for acetaminophen glucuronide in human liver microsomes. **Journal of Chromatography B: Biomedical Sciences and Applications** 753(2): 303-308.
- Altun, M. L. and Erk, N. (2001). The rapid quantitative analysis of phenprobamate and acetaminophen by RP-LC and compensation technique. **Journal of Pharmaceutical and Biomedical Analysis** 25(1): 85-92.
- Bannwarth, B., and Pehourcq, F. (2003). Pharmacologic basis for using paracetamol: pharmacokinetic and pharmacodynamic issues. **Drugs** 63(2): 5-13.
- Bond, A. M. (1994). Past, present and future contributions of microelectrodes to analytical studies employing voltammetric detection. **Analyst** 119(11): 1R-21R.
- Burgot, G., Auffret, F. and Burgot, J. L. (1997). Determination of acetaminophen by thermometric titrimetry. **Analytica Chimica Acta** 343(1): 125-128.

- Campanero, M. A., Calahorra, B., García-Quétglas, E., López-Ocáriz, A. and Honorato, J. (1999). Rapid liquid chromatographic assay for the determination of acetaminophen in plasma after propacetamol administration: application to pharmacokinetic studies. **Journal of Pharmaceutical and Biomedical Analysis** 20(1–2): 327-334.
- Erk, N. (1999). Application of derivative-differential UV spectrophotometry and ratio derivative spectrophotometric determination of mephenoxalone and acetaminophen in combined tablet preparation. **Journal of Pharmaceutical and Biomedical Analysis** 21(2): 429-437.
- Etienne, M., Anderson, E. C., Evans, S. R., Schuhmann, W. and Fritsch, I. (2006). Feedback-Independent Pt Nanoelectrodes for Shear Force-Based Constant-Distance Mode Scanning Electrochemical Microscopy. **Analytical Chemistry** 78(20): 7317-7324.
- Fan, F. R. F., Kwak, J. and Bard, A. J. (1996). Single molecule electrochemistry. **Journal of the American Chemical Society** 118(40): 9669-9675.
- Frisbie, C. D. (2003). Scanning Probe Microscopy. In A. M. Robert (ed.), **Encyclopedia of Physical Science and Technology** (3rd ed., pp. 469-484). New York: Academic Press.
- Hanaee, J. (1997). Simultaneous determination of acetaminophen and codeine in pharmaceutical preparations by derivative spectrophotometry. **Pharmaceutica Acta Helveticae** 72(4): 239-241.
- Holland, L. and Jorgenson, J. (1995). Separation of nanoliter samples of biological amines by a comprehensive two-dimensional microcolumn liquid chromatography system. **Analytical Chemistry** 67(18): 3275-3283.

- Kumar, K. G. and Letha, R. (1997). Determination of paracetamol in pure form and in dosage forms using N, N-dibromo dimethylhydantoin. **Journal of Pharmaceutical and Biomedical Analysis** 15(11): 1725-1728.
- Kunkel, A., Günter, S. and Wätzig, H. (1997). Determination of pharmaceuticals in plasma by capillary electrophoresis without sample pretreatment reproducibility, limit of quantitation and limit of detection. **Electrophoresis** 18(10): 1882-1889.
- Kunkel, A. and Wätzig, H. (1999). Pharmacokinetic Investigations with Direct Injection of Plasma Samples: Possible Savings Using Capillary Electrophoresis (CE). **Archiv der Pharmazie** 332(5): 175-178.
- Larson, A. P., Ahlberg, H. and Folestad, S. (1993). Semiconductor laser-induced fluorescence detection in picoliter volume flow cells. **Applied Optics** 32(6): 794-805.
- Lin, Y., Trouillon, R., Svensson, M. I., Keighron, J. D., Cans, A. S. and Ewing, A. G. (2012). Carbon-Ring Microelectrode Arrays for Electrochemical Imaging of Single Cell Exocytosis: Fabrication and Characterization. **Analytical Chemistry** 84(6): 2949-2954.
- Mahoney, P. P. and Hieftje, G. M. (1994). Fluorimetric Analysis on Individual Nanoliter Sample Droplets. **Applied spectroscopy** 48(8): 956-958.
- Mayne, A. J. and Dujardin, G. (2008). Chapter 14 STM Manipulation and Dynamics. In E. Hasselbrink and B. I. Lundqvist (Eds.), **Handbook of Surface Science** (Vol. 3, pp. 681-759). North-Holland: Elsevier.

- Mohamed, F. A., Abdallah, M. A. and Shammat, S. M. (1997). Selective spectrophotometric determination of p-aminophenol and acetaminophen. **Talanta** 44(1): 61-68.
- Ni, Y., Liu, C. and Kokot, S. (2000). Simultaneous kinetic spectrophotometric determination of acetaminophen and phenobarbital by artificial neural networks and partial least squares. **Analytica Chimica Acta** 419(2): 185-196.
- Olson, D. L., Peck, T. L., Webb, A. G., Magin, R. L. and Sweedler, J. V. (1995). High-Resolution Microcoil ¹H-NMR for Mass-Limited, Nanoliter-Volume Samples. **Science** 270(5244): 1967-1970.
- Ramos, M. L., Tyson, J. F. and Curran, D. J. (1998). Determination of acetaminophen by flow injection with on-line chemical derivatization: Investigations using visible and FTIR spectrophotometry. **Analytica Chimica Acta** 364(1): 107-116.
- Săndulescu, R., Mirel, S. and Oprean, R. (2000). The development of spectrophotometric and electroanalytical methods for ascorbic acid and acetaminophen and their applications in the analysis of effervescent dosage forms. **Journal of Pharmaceutical and Biomedical Analysis** 23(1): 77-87.
- Shervington, L. A. and Sakhnini, N. (2000). A quantitative and qualitative high performance liquid chromatographic determination of acetaminophen and five of its para-substituted derivatives. **Journal of Pharmaceutical and Biomedical Analysis** 24(1): 43-49.
- Troyer, K. P. and Wightman, R. M. (2002). Dopamine transport into a single cell in a picoliter vial. **Analytical Chemistry** 74(20): 5370-5375.

- Wangfuengkanagul, N. and Chailapakul, O. (2002). Electrochemical analysis of acetaminophen using a boron-doped diamond thin film electrode applied to flow injection system. **Journal of Pharmaceutical and Biomedical Analysis** 28(5): 841-847.
- Ward, B. and Alexander-Williams, J. M. (1999). Paracetamol revisited: A review of the pharmacokinetics and pharmacodynamics. **Acute Pain** 2(3): 139-149.
- Wightman, R. M., Jankowski, J. A., Kennedy, R. T., Kawagoe, K. T., Schroeder, T. J., Leszczyszyn, D. J., Near, J. A., Diliberto, E. J. and Viveros, O. H. (1991). Temporally resolved catecholamine spikes correspond to single vesicle release from individual chromaffin cells. **Proceedings of the National Academy of Sciences** 88(23): 10754-10758.
- Wu, N., Peck, T. L., Webb, A. G., Magin, R. L. and Sweedler, J. V. (1994). ¹H-NMR spectroscopy on the nanoliter scale for static and online measurements. **Analytical Chemistry** 66(22): 3849-3857.
- Zen, J. M. and Ting, Y. S. (1997). Simultaneous determination of caffeine and acetaminophen in drug formulations by square-wave voltammetry using a chemically modified electrode. **Analytica Chimica Acta** 342(2): 175-180.

CHAPTER V

CONCLUSIONS AND RECOMMENDATIONS

5.1 Conical Carbon Fiber Ultramicroelectrodes as Imaging Tool for Scanning Tunneling Microscopy and Sensors for Voltammetry

5.1.1 Electrochemical tip etching

Graphite STM tips were prepared from PAN-based carbon fiber by novel procedure that uses a simple DC etching in NaOH solution to provide in a first step narrowed single carbon fibers with very well-formed nanocones at their bottom. The tip profile was usually sharp and smooth; the dimension of the tip apex was in 20-30 nm range. The length of the CF extending from the end of the holding wire had to be less than about half a millimeter and the etching procedure uses successfully adopted to accomplish this condition. Typical protruding structures were just a few hundred micrometers in length. The success rate of CF tip the process of etching was about 80% e.g. 8 out of 10 etched CFs had high quality carbon nanocones on their endings.

5.1.2 Carbon fiber tip insulation

Etched carbon fiber tips were insulated with electrodeposition paint (EDP) everywhere but not at the end of the tips apex of the carbon cones. This tip insulation effectively limited the bare carbon to the foremost end and restricted the

faradaic current response due to interfacial redox activity to exactly the front area. The CF/HW junction was coated with a transparent silicone-based encapsulant to ensure insulation at this critical area. Completed insulated etched CFs adequately displayed the expected sigmoidal voltammograms of dissolved ruthenium hexamine chloride and proved their quality in terms of insulation stability. Actually, they represent a novel type of conically-shaped carbon micro- and nanoelectrodes, which may find promising application in electroanalysis.

5.1.3 Application of tapered carbon fiber as novel scanned probe tips for STM

The potential of CF tips for imaging in STM has been demonstrated under various conditions; ambient condition at room temperature, ultrahigh vacuum, and in an electrolyte environment. CF tips could indeed observe the atomic arrangement of sample surface in both UHV and electrolyte solution. Moreover, CF tips revealed the molecular structure of a self-assembled monolayer of an organic triazatriangulenium platform on Au(111). The tip material carbon promises excellent advantages in terms of the accessible potential windows. However, experiments had a low success 10% rate of only about, that is one out of ten employed tip imaging provided satisfactory imaging properties. To make the developed CF tips a routine tool for in situ STM studies, the yield of good probes have to be improved, e.g. via better etching or functional tip modification.

5.2 A novel system for simple small-volume voltammetry

A novel three-electrode microcell has been accomplished for analytical voltammetry in 15 μL measuring solutions. The design of innovative microcell

supports simple and rapid are, with only 10 minutes required for one complete run of analyte quantification via voltammetry in the standard addition mode. Moreover, the 15- μL three-electrode cell design is able to excellently perform voltammetric experiments with various kinds and sizes of electrodes; disk-shaped carbon rod electrode (0.5 mm of diameter), possible are, for instant, disk-shaped carbon fiber electrode (7 μm of diameter), disk-shaped platinum microelectrode (50 μm of diameter), and disk-shaped gold microelectrode (50 μm of diameter).

5.2.1 15- μL -volume-electroanalysis of acetaminophen (ACMP)

The primary performance level of the 15 μL electroanalysis was evaluated through test trials with the common analgesic paracetamol. The inspection illustrated that adjusted paracetamol levels in model samples were well recovered with the deviations from true values being less than $\pm 5\%$. The system was also successfully applied to paracetamol detection in serum samples coming from a volunteer who ingested a dose of 1000 mg of the drug. Comparative differential pulse voltammetry in serum samples obtained before and 1 and 4 hours after paracetamol medication disclosed nicely the absence, appearance and clearance of the drug, respectively. Quantitative measurements on the 1 hour samples revealed a blood paracetamol level that was in good accordance published data. A miniaturized electrochemical cell has been realized that can accurately handle 15 μL sample volumes for analyte quantification and because of its simplicity and cost-effectiveness may become an accessory for laboratories dealing with sample of restricted volume.

APPENDICES



APPENDIX A

ELECTROCHEMICAL METHODS

Voltammetric techniques used in this thesis are cyclic voltammetry and pulse voltammetry. Usually, a potential is applied via a potentiostat to the working electrode (WE) and the faradic current response of the electrochemical cell is measured as a function of WE potential. Advice on the procedure of cyclic and pulse voltammetry can be found in “Electrochemical Methods: Fundamentals and Applications” (Bard and Faulkner, 2000).

A.1 Cyclic Voltammetry

A first choice of a voltammetric scheme is “cyclic voltammetry” (CV), which is the most widely used electrochemical technique for acquiring qualitative information on redox potential of redox couples and the reversibility of electrochemical charge transfer reaction of electrode surface. With CV, the applied potential is swept linearly between a starting (V_1) and a changing (V_2) potential (see Figure A.1 (A)). During such a potential sweep the potentiostat continuously measures the current as a function of time and applied potential, respectively. Obtained is a plot of current versus potential. Figure A.1 (B) shows the expected CV response for a measurement involving a reversible redox couple and a single potential cycle.

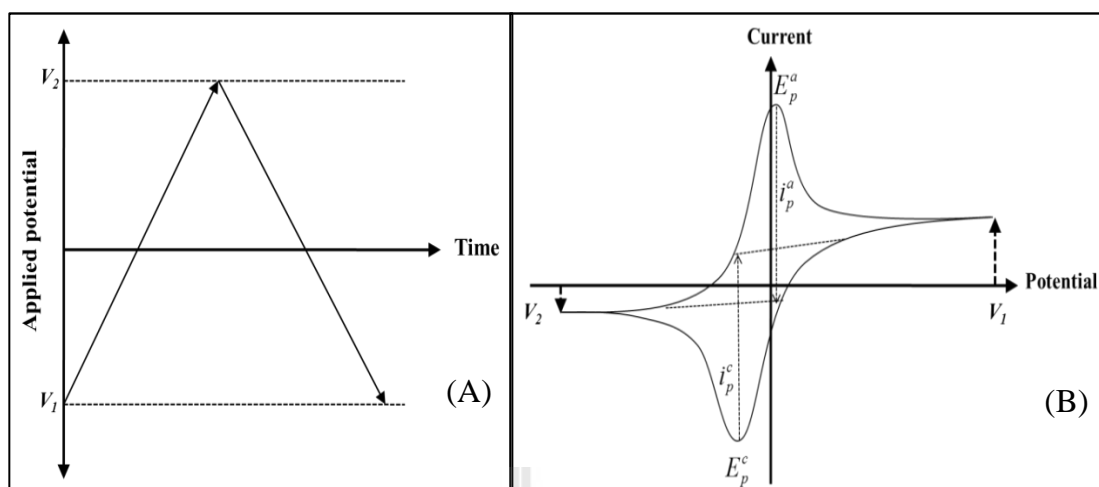


Figure A.1 The typical cyclic voltammogram for a reversible charge transfer reaction.

(A) is the cyclic voltammetry potential waveform and (B) the typical cyclic voltammogram for a reversible charge transfer reaction i_p^c and i_p^a are the cathodic and anodic peak currents, respectively.

As cyclic voltammetry is calling for a gradual change in electrode potential, there is always a superimposed capacitive current present that disturbs the analytically relevant faradaic current, which limits the performance of the method at low concentration of redox analyte.

A.2 Pulse voltammetry

To eliminate the negative influence of the unwanted capacitive current and to improve the signal-to-noise ratio, the methodology of pulse voltammetry was introduced. Pulse voltammetry takes advantage of the difference in the rate of the decay between the capacitive charging and faradaic charge transfer currents during a potential step (or "pulse"). While a charging current decays exponentially, a faradaic current (for the diffusion-controlled situation) decays as a function of the square root

of time that is the rate of decay of the charging current is considerably faster than the decay of the faradaic current. The charging current is negligible at a time of about $5R_uC_{dl}$ after the potential step (R_uC_{dl} is the time constant for the electrochemical cell, and ranges from μs to ms). Therefore, at the end of a short pulse, the measured current consists solely of the faradaic current. Measuring the total current at the end of a potential pulse thus allows discrimination between the faradaic and charging currents. Normal pulse voltammetry (NPV) consists of a series of pulses of increasing amplitude, with the potential returning to the initial value after each pulse (see Figure A.2(A)). Consider the electrochemically induced reduction of an oxidized species. If the initial potential is well positive of the redox potential of the species, the application of small amplitude pulses does not cause any faradaic reactions; hence there is no faradaic current response. When the pulse amplitude is high enough to bring potential close to the redox potential, then there is a faradaic reaction induced and response to the potential pulse. The current is measured, assuming moderately fast electron transfer kinetics. The magnitude of the current may depend on both the rate of diffusion of the electroactive species and the kinetics of electron transfer. At some level, the pulsed potentials are sufficiently negative of the redox potential and the electron transfer reaction occurs now rapidly enough to make the faradaic current depending merely on the rate of diffusion. A limiting current is attained, and visible as sigmoidal shaped normal pulse voltammogram.

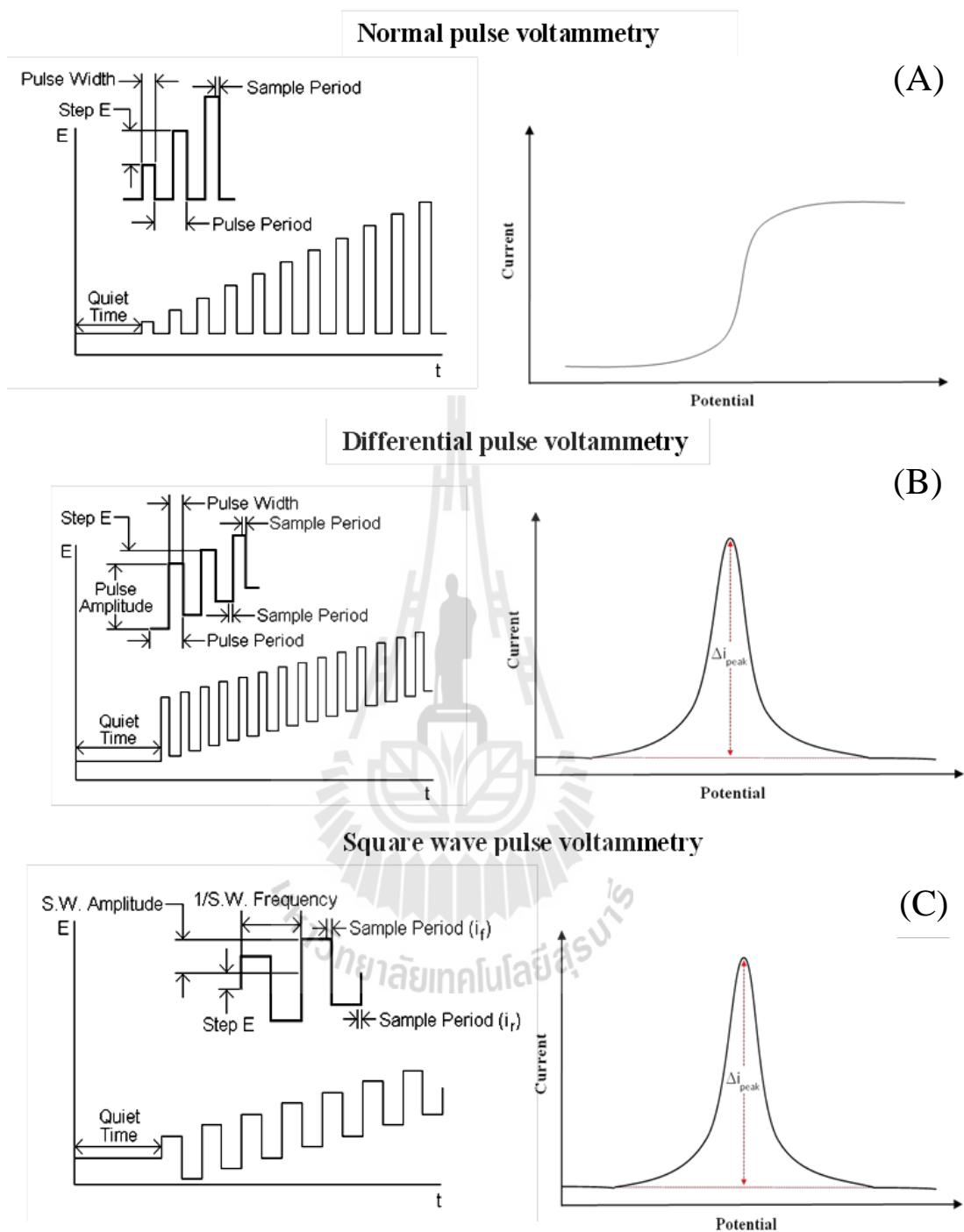


Figure A.2 Potential wave forms and voltammogram shape for normal pulse, differential pulse and square wave voltammetry.

(A), differential pulse voltammetry (B) and square wave pulse voltammetry (C).

Differential pulse voltammetry (DPV) is a further development of the pulse strategy and an extremely useful technique for measuring trace levels of organic and inorganic species. In DPV, the pulsed amplitude is fixed and superimposed on a linear potential ramp (see Figure A.2(B)). Again, consider a reduction at working electrode potentials around the redox potential, the difference between current sampled before and just the end of a pulse reaches a maximum, and is comparatively small for other electrode potentials. Result is a voltammogram with a symmetric peak. Square wave pulse voltammetry (SWV) is similar to DPV technique but the wave form is composed of a symmetrical square wave superimposed on a staircase wave form (see Figure A.2(C)). The current is measured on the reverse half-cycle (i_r) is subtracted from the current measured on forward half-cycle (i_f). The different current ($i_f - i_r$) is displayed as a function of the applied potential, and obtained are the typical bell-shaped SWV voltammogram.

APPENDIX B

ELECTROACTIVE AREA OF CONICAL ULTRAMICROELECTRODE

The voltammetric response of an UME provides an estimated information about both the conductor electroactive surface exposed to electrolyte and quality of the insulating sheath. The diffusion to a small conical electrode rapidly becomes hemispherical when the electrode is in the bulk solution. Effective radius can be calculated from the diffusion-limiting steady-state current assuming disk geometry:

$$i_{\text{lim}} = 2\pi \cdot n \cdot F \cdot D \cdot C \cdot r_{\text{eff}} \quad \text{equation (B.1)}$$

Where n is the number of electrons transferred during the electrochemical reaction at the UME surface (here; $n = 1$), F is Faraday's constant (96,485 C/mol), D is diffusion coefficient (here; $D = 7.2 \times 10^{-6} \text{ cm}^2/\text{s}$ (Zoski, Yang, He, Berdondini, & Koudelka-Hep, 2007)), C is concentration of electroactive species (here; $C = 0.001 \text{ M}$), and r_{eff} is effective radius of experimental UME.

Figure B.1 presents a drawing of conical CF electrode and an example of voltammetric response of such electrode. As can be seen, the limiting current (steady-state current (i_{lim}) response) for this example is about 1.7 nA.

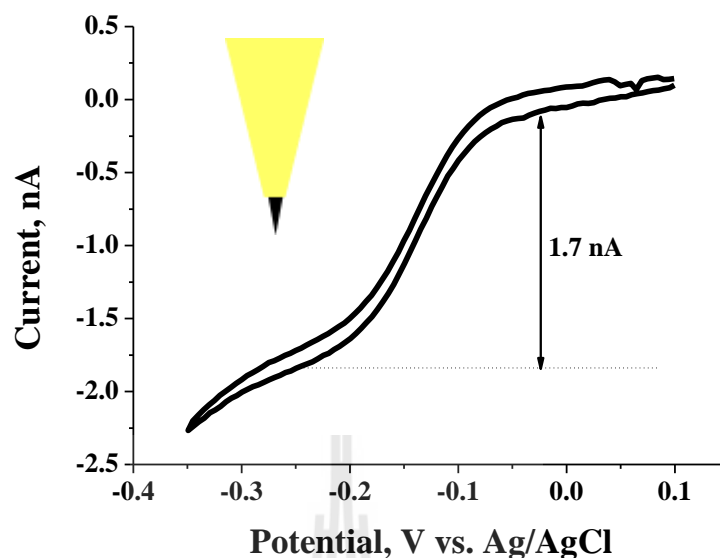


Figure B.1 Cyclic voltammograms of 1mM $\text{Ru}(\text{NH}_3)_6\text{Cl}_3$ in 0.1 M KCl at needle-type CF-UMEs of different size.

Scan speed for that recording was 50 mV/s; the reference electrode was a Ag/AgCl wire and the counter electrode a coiled Pt wire.

According to equation (B.1), the effective radius (r_{eff}) can be calculated as:

$$i_{\text{lim}} = 2\pi \cdot n \cdot F \cdot D \cdot C \cdot r_{\text{eff}}$$

$$1.7 \text{ nA} = 2\pi \times 1 \times 96485 \frac{\text{C}}{\text{mol}} \times 7.2 \times 10^{-6} \frac{\text{cm}^2}{\text{s}} \times 0.001 \frac{\text{mol}}{\text{L}} \times r_{\text{eff}}$$

$$r_{\text{eff}} = 3.661 \times 10^{-6} \text{ m}$$

$$r_{\text{eff}} = 3.66 \mu\text{m}.$$

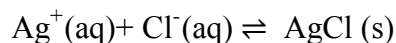
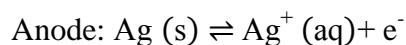
All radii of conical-shaped UMEs can be calculated from peak current of their cyclic voltammogram, as long as the diffusion coefficient and the mediator concentration and type are known.

APPENDIX C

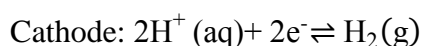
REFERENCE ELECTRODE FABRICATION

To fabricate Ag/AgCl/3M KCl reference electrodes, the following materials are needed: i) borosilicate Pasteur pipettes, ii) Ag wire (8 cm long piece length, 0.25 mm in diameter), iii) ceramic frits (2-3 mm long), iv) a mixture of 3 M KCl and 1 M HCl (5 ml).

A porous ceramic frit was inserted from the narrow end of the Pasteur pipette and the merger heated using a alcohol burner in order to tightly seal the frit into the molten end of the pipette glass. This step is very important since it determines the properties of the electrode such as leakage of internal electrolyte. Subsequently, the end containing the sealed ceramic frit was carefully mechanically polished to the desired length (Figure C.1(A)). The pipette was also cut from the wider end to adjust the length of the electrode. The Ag wire was chloridized in an electrolytic setup by immersing the Ag wire together with a Pt wire counter electrode in a mixture of 3 M KCl and 1 M HCl (5 mL). The electrodes were connected to power supply to apply constant potential at 5 V between the Pt wire acting as the cathode and the Ag as the anode for 10 minutes. The electroprecipitation of AgCl on the Ag wire was initiated by applying a potential of 5 V for 10 min. The corresponding equations for the redox process at the electrode during AgCl coating of the Ag wire are as follows:



or an overall reaction at anode: $\text{Ag(s)} + \text{Cl}^- \text{ (aq)} \rightleftharpoons \text{AgCl (s)} + \text{e}^-$



The reddish chloridized Ag wire was thoroughly rinsed with the DI water and inserted in the open of the end sealed glass pipette and fixed. The pipette with the chlorodized Ag wire inside was filled with 3 M KCl to stabilize the silver chloride concentration (figure C.1(B)) as needed for the establishment of a stable reference potential.

If needed, the reference electrode potential of the handmade Ag/AgCl-RE was measured versus a commercial Ag/AgCl-RE. The potential difference voltage was zero; vs. SHE (the standard hydrogen electrode), the potential was 0.230 ± 0.010 V.

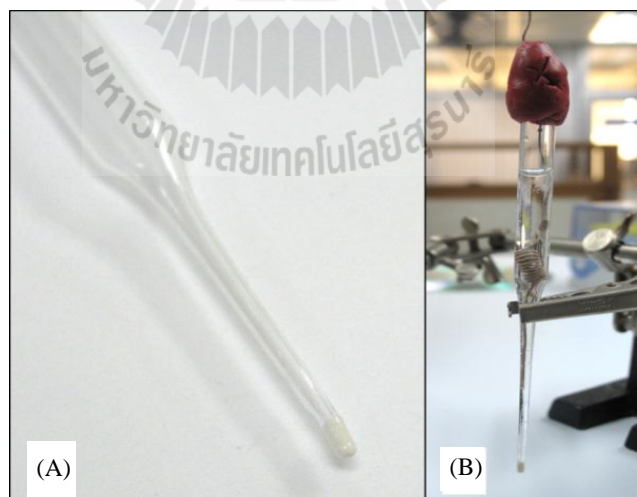


Figure C.2 Photographs of homemade Ag/AgCl reference electrode.

The tip of the glass pipette with the enclosed ceramic frit (A). A photographic image of the ready-to-use Ag/AgCl reference electrode (B).

APPENDIX D

QUANTITATIVE DETERMINATION OF

ACTAMINOPHEN

In this dissertation, the quantitative measurement of ACMP was performed by the standard addition technique. The standard additions method is commonly used to determine the concentration of an analyte that is in a complex matrix such as biological fluids, soil samples, etc. The reason for using the standard additions method is that the matrix may contain other components that interfere with the analyte signal causing an inaccuracy in the determined concentration. The idea is to add analyte (here is ACMP) to the sample ("spike" the sample) and monitor the change in instrument response. The change in instrument response between the sample and the spiked samples is assumed to be due only to change in analyte concentration. In course of a standard addition trial the sample has to be split equal into several aliquots in separate vials of the same volume. The first vial is then diluted to volume with the selected diluent (solvent, buffer). A standard containing the analyte at known concentration is then added in equal increment to the and the sample vials are then filled up to constant volume with the selected buffer. The instrument response is then measured for all of the diluted solutions and the data is plotted with the concentration of the standard addition on the x-axis and related peak current on the y-axis. Linear

regression is applied and the slope (m) and y-intercept (b) of the actual calibration curve are used to calculate the concentration of analyte in the sample:

$$y = mx + b \quad \text{equation (D.1)}$$

Where: y = instrument response (signal), x = concentration of standard, m = slope, and b = y-intercept

The assessment of the sample concentration is obtained from the x-interception (y = 0). Figure D.1 shows an example of the standard addition method for determining the ACMP level in HBS after the tablet consumption oral. The peak current from DPV increased with increasing ACMP concentration. The plot of peak current vs. ACMP concentration was constructed and the linear regression graph drawn ($y = 47.06x + 2.463$). According to the calibration plot, the x-interception (y = 0) of the measurement is about 52 μM or 7.9 mg/L of ACMP in HBS. However, the HBS original sample was diluted 2-fold into bare PBS buffer; therefore, the real level of ACMP in HBS is 104 μM or 15.8 mg/L.

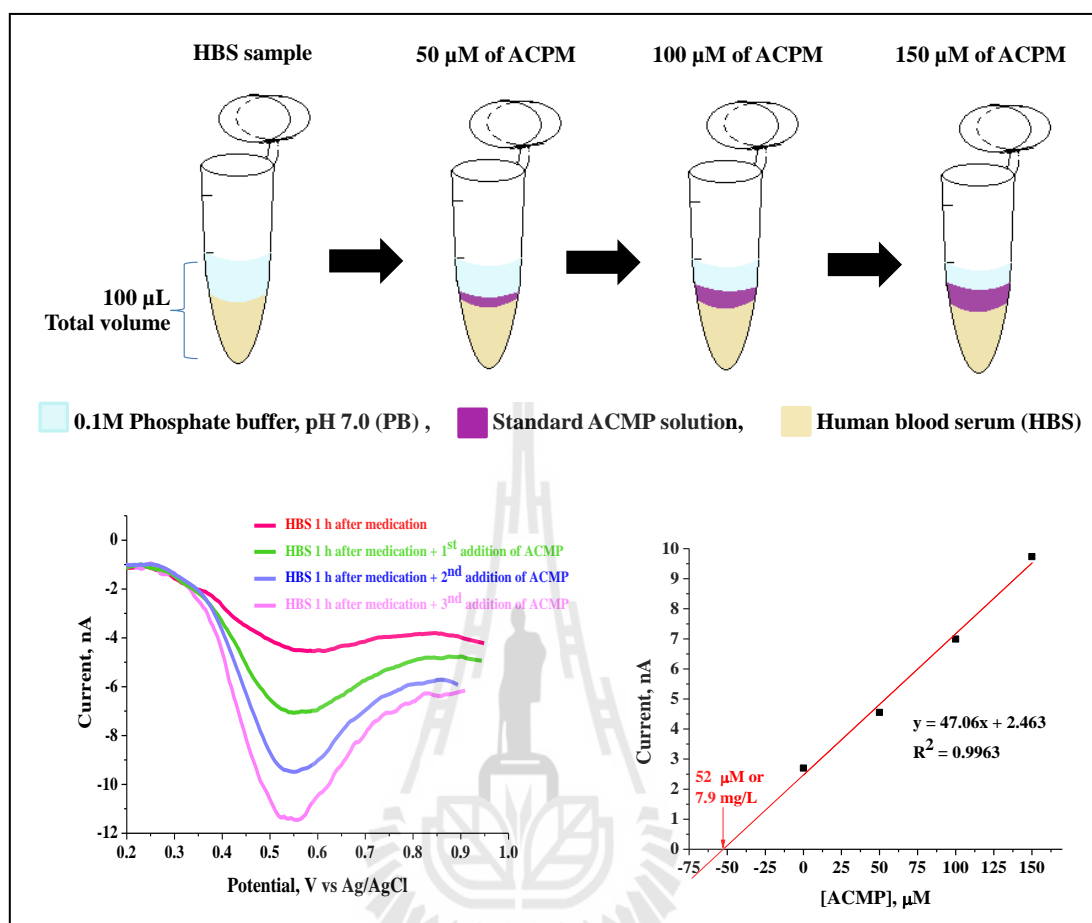


Figure D.1 Small volume voltammetric quantification of ACMP in HBS before and after ingestion of a paracetamol tablet and measured in 15-µL-three-electrode cell by means of the standard addition method.

(Top) Schematic of the solution preparation for ACMP determination in HBS sample.

(Bottom) ACMP differential pulse voltammograms (step size: 5 mV; pulse time: 0.1 s; pulse size: 50 mV) for a sample and the sample with 50, 100, and 150 µM additions of analyte and standard addition calibration curve and the regression graph analysis.

CURRICULUM VITEA

Name	Miss Jiyapa Sripirom
Date of Birth	2 September 1985
Place of Birth	Udon Thani, Thailand
Education	2003-2006, Bachelor of Engineering (Chemical Engineering), Ubon Rajathani University, Ubon Rajathani, Thailand 2007-2013, Ph. D. candidate (Chemistry), Suranaree University of Technology, Nakhon Ratchasima, Thailand
Grant and Fellowship	2007, Faculty Development Scholarship, Office of the Higher Education Commission, Ministry of Education, Thailand.
Publications	<u>Sripirom, J.</u> , Noor, S., Köhler, U., & Schulte, A. (2011). Carbon , 48, 2402-2412. <u>Sripirom, J.</u> , Kuhn, S., Jung, U., Magnussen, O., & Schulte, A. (2013). Analytical Chemistry , 85, 837-842.